THE TIME EVOLUTION OF GLOBAL BRAIN DYNAMICS IN THE HUMAN ELECTROENCEPHALOGRAM: INNOVATIONS IN QUANTITATIVE MULTI-VARIATE METHODS AND APPLICATIONS TO NEUROLOGICAL DISORDERS

A Dissertation

Presented to the Faculty of the Weill Cornell Graduate School

Of Medical Sciences

In Partial Fulfillment of the Requirements for the Degree of

Doctor of Philosophy

By

Tanya J. Nauvel

December 2017

THE TIME EVOLUTION OF GLOBAL BRAIN DYNAMICS IN THE HUMAN ELECTROENCEPHALOGRAM: INNOVATIONS IN QUANTITATIVE MULTI-VARIATE METHODS AND APPLICATIONS TO NEUROLOGICAL DISORDERS

Tanya J. Nauvel, Ph.D.

Cornell University 2017

Electroencephalography (EEG) is a complex multivariate signal measuring brain electrophysiology in real time. While very informative in neurological studies, the EEG presents serious challenges - it is often corrupted by noise, artifacts, and is inherently a high-dimensional, non-stationary process due to the intrinsic dynamics of underlying brain activity. Understanding how to interpret and analyze the EEG is therefore an ongoing effort employing a range of techniques. This dissertation aims to investigate novel approaches to quantitatively measure the inherent complexity of the EEG, and use these measures effectively to better understand and track the progress of recovery and treatment of complex neurological conditions in longitudinal studies through the use of three case studies. Specifically, novel EEG analyses utilizing graphical theoretical and spectral analytic measures are developed and applied to:

1) Studying the recovery of consciousness in patients with severe brain injuries;

2) Characterizing the effect of subcallosal deep brain stimulation in treatment resistant depression;

3) Validating the measures through the characterization of the test-retest stability of each measure in a set of healthy volunteers, tested at multiple time points.

The novel measures are shown to provide new insight in each patient study. In the context of disorders of consciousness, measures of spectral coherence show that the functional connectivity of the brain is closely linked to behavioral changes in consciousness, and specifically, that coherence network approaches may be used as markers of underlying functional and structural recovery of communication. In the case of treatment resistant depression and subcallosal DBS we find that spectral measures of the alpha band are predictors of the efficacy of treatment. Collectively, the studies carried out in this thesis show that our novel measures allow us to track global brain state changes that reflect inherent underlying neurological processes related to disorders of consciousness and neuropsychiatric disorders. Further development and use of these tools may to provide neurologists and psychiatrists with methods to track underlying functional brain changes in their patients, allowing for advances in treatment, prognosis, diagnosis and understanding of underlying mechanisms of disease.

BIOGRAPHICAL SKETCH

Tanya Jayne Nauvel was born in London, England. When Ms. Nauvel was two years old, the Nauvel Family returned to Pointe aux Canonniers, Mauritius, from where they had originally immigrated from. In 1999, Ms. Nauvel enrolled in Lycée La Bourdonnais in Curepipe, Mauritius. In 2002, Ms. Nauvel graduated with a Mention Bien on the French Baccalauréat Scientifique, specialization Mathématiques, and received a full scholarship to attend Bates College.

While at Bates College, Ms. Nauvel was recognized for her achievements by making the Dean's List, being nominated to the Sigma Xi Research Society, receiving the Albion Morse Scholar Award, and winning a Howard Hughes Medical Institute Fellowship to conduct neuroscience research with the Swartz Center at the University of California, San Diego and Mount Sinai Hospital. Less impressively, but no less meaningfully, Ms. Nauvel played classical piano, Quadrophonic Pans in the Steel Pan Orchestra, danced salsa with the Ballroom Society, and traveled to Berlin for her Junior Semester Abroad.

In 2006, Ms. Nauvel graduated from Bates College with a Bachelors of Science, majoring in Mathematics and minoring in German. Immediately after graduating, Ms. Nauvel worked as a research technician for Dr. Sheila Nirenberg at the Weill Cornell Medical College in New York City. Ms. Nauvel studied the visual sensory system and how neurons in the retina code for information. In 2008, Ms. Nauvel moved to Alexandria, Virginia, and joined Dr. Timothy Mhyre at Georgetown University where she studied the identification, validation, and peripheral biomarkers in Parkinson's and Alzheimer's disease.

In 2010, Ms. Nauvel enrolled in the Computational Biology and Medicine doctoral program at Weill Cornell Medical College. Ms. Nauvel completed one year of advanced classwork at the Cornell University campus in Ithaca, New York, and then, in 2011, began her thesis research under the mentorship of Dr. Nicholas Schiff, M.D. at the Brain and Mind Research Institute. There, she co-founded the Tri-Institutional Minority Society to provide support to under-represented minorities in academia.

Ms. Nauvel lives in Jersey City, New Jersey, with her husband, Alex, and her faithful dog, Shadow.

Aufkälrung ist der Ausgang des Menschen aus seiner selbstverschuldeten Unmündigkeit.

Immanuel Kant.

ACKNOWLEDGEMENTS

I wouldn't be here without my parents and my brother. Thank you for always supporting me in my endeavors, and always encouraging me to learn.

Niko Schiff, thank you for passing on your passion and excitement. Your guidance gave me the independence and confidence to explore my own ideas, for which I will always be grateful.

Jonathan Victor, thank you for being an invaluable mentor. You were always so generous with your time, and your insightful feedback and questions have heavily influenced the way I think about and approach a problem.

Thank you to my committee members, David Christini and Barbara Finlay, for your advice throughout this process. I truly appreciate all the time you have spent not only helping me with my thesis, but also giving me advice on navigating a career in academia.

Thank you to Keith Purpura, my unofficial mentor, for always taking the time to listen to my ideas and having practical solutions.

I would not have made it through long days testing in the hospital without my friend and mentor Mary Conte. Your attention to detail in making posters, or collecting data, taught me how to be a better scientist, and your good humour (and snacks) got me through graduate school.

To all my colleagues in the Schifflab, Jennifer Hersh, Peter Forgacs, Esteban Fridman, Jon Drover, Sudhin Shah, Jon Baker, thank you for all your support and advice over the years. A special thank you to Andrew Goldfine for his guidance from day one, and Wanda Hyde for always having a word of encouragement. Thank you to my fellow graduate students Dan Thengone, Brian Fidali, Tamar Melman, and Jackie

Gottshall. There are no other people in this world I would rather be enclosed in a small windowless room with.

I'd also like to thank the nursing staff at Rockefeller Research Hospital for their understanding and help during every inpatient admission. A special thank you to everyone in the Tri-Institutional program in Computational Biology and Medicine, especially Margie Hinonangan-Mendoza, for their help and friendship.

To my husband Alex, for supporting me every step of the way, from writing my undergraduate thesis in college, to late nights running experiments as a research tech, to painstakingly formatting and editing with me and getting me through these last few weeks, I couldn't have done this without you.

To everyone at TIMS, especially Marcus Lambert, for helping me discover a community I never even knew existed and striving to increase diversity in STEM.

Finally, thank you to these funding agencies for making this research possible: The James S. McDonnell Foundation, The Tri-institutional Training Program in Computational Biology and Medicine, The Jerold B. Katz Foundation; The Stanley Medical Research Institute (HSM), The Woodrow Foundation (HSM), Emory Healthcare (HSM)

.

TABLE OF CONTENTS

LIST OF FIGURES

LIST OF TABLES

LIST OF ABBREVIATIONS

EEG – Electroencephalography

fMRI – functional Magnetic Resonance Imaging

DTI – Diffusion Tensor Imaging

PET – Positron Emission Tomography

DOC – Disorders of Consciousness

MCS Minimally Conscious State

VS – Vegetative State

scDBS - Subcallosal Deep Brain Stimulation

SCC – Subcallosal cingulate

TRD – Treatment Resistant Depression

PS – Patient Subjects

HC – Healthy Control Subjects

DS – Deep Brain Stimulation Subjects

Chapter One: Introduction

Why study functional dynamics?

Deciphering how the human brain functions remains the most challenging question of the 21st century. The brain is a complex network, composed of billions of neurons able to communicate and synthesize information at incredible speeds with exceptional efficiency. In 2009, the NIH launched the Human Connectome Project an initial foray tasked with characterizing neural networks in the hope of mapping the neural pathways which underlie human consciousness. However, this cartographic approach towards the structural relationships between brain areas is necessarily incomplete—instead, it is imperative to also comprehend the dynamics of the brain in order to understand how the architecture supports neurophysiological function. Global brain dynamics offers comprehension of the behavior of not just one, but billions of neurons working simultaneously, and understanding the cooperative interactions of these large-scale assemblies of neurons provides the clearest insight into the mechanisms of human cognition.

Neuroimaging techniques and tools are essential to exploring these functional connections and are responsible for transforming the study of human cognition. Neuroimaging has only recently allowed researchers to explore the frontiers of neuroscience research, from human cognition and behavior, to disorders of the

nervous system. None of this would be possible without the exponential jump in computational power--a trillion fold in the past 60 years--leading to the development and implementation of new algorithms and quantitative measures able to process the large amounts of complex multivariate data collected from functional imaging techniques. Together, these developments have combined to create an explosion of neuroimaging methods (Bandettini 2009), each with their strengths and weaknesses. Although many methods exist to calculate functional networks (Bullmore & Sporns, 2009) using a variety of both imaging techniques and coupling measures, it is important to find measures which are reliable over time. This thesis demonstrates the importance of the use of human electroencephalography in understanding complex neurological disorders. In particular, we concentrate on the study of the disruption of healthy functional networks, both in treatment resistant depression and disorders of consciousness.

The human electroencephalogram

Non-invasive measurements of human brain function

To better study functional connectivity, it is imperative to find a measure capable of providing information on how neural assemblies in the brain communicate, and how neuronal activity is integrated across the cortex. Neuroimaging tools are widely used to study the relationships between brain and behavior. The functional magnetic resonance imaging (fMRI BOLD) is an indirect measure of neural activity, based on the relationship between cerebral blood flow and neuron energy consumption (Salvador et al., 2005). Additionally, positron emission tomography (PET) provides an indirect measure of brain activity by measuring metabolic activity produced by neural activity. Such techniques allow for in-vivo studies of the human brain, enhancing our

knowledge and understanding of brain activity with high spatial and temporal resolution.

The electroencephalography (EEG) and magnoencephalography (MEG) are the only non-invasive recording techniques able to directly measure the summation of large populations of neurons firing in the cortex, reflecting underlying cortical networks and circuitry. The MEG has a similar high temporal resolution as the EEG, and somewhat higher spatial resolution, but suffers from a lack of portability and ease of use in a clinical setting. Unlike the BOLD signal, which is 2-3 times slower, the EEG has a high temporal resolution making it a great tool for studying neurocognitive processes in real time, as it is known that cognitive processes occur in the span of hundreds of milliseconds. (Cohen, 2011, Toga and Gazzaniga, 1996). Moreover, the EEG (Stam & Van Dijk, 2002) has superior flexibility, more so than the MEG, fMRI, and PET. EEG equipment is portable and cheap, making it easily accessible to patients in clinical settings. Therefore, the EEG has become a primary tool for neurologists and is currently used in the diagnosis of diseases such as epilepsy (Kaplan & Lesser, 1990, Gotman et al., 1981), measuring mental states (sleep or awake) (Niedermeyer & da Silva, 2005, Steriade et al., 1990), level of anesthesia (Rampil, 1998) and in the diagnosis of coma (Schomer & da Silva, 2010).

The EEG has many advantages over other imaging techniques. The patient is not required to remain absolutely still, a requirement that may be impossible depending on the patient's condition. Patients with pacemakers or defibrillators can have an EEG, but are barred from fMRIs. EEG equipment is widely available due to its low cost and easy access, and is routinely found in hospitals across the world, whereas fMRI remains largely restricted to large hospitals and research institutions. Finally, the EEG has a better time resolution than brain imaging techniques (Nunez, 2006), thus enabling measurement of rapid fluctuations in brain activity. The high

temporal resolution of the EEG is a great advantage – we know that the timing of electrical activity can carry information (Jensen 2007). It can capture differences in patterns of activity during different cognitive activities or at rest. The EEG in healthy adults has also been shown to remain stable over time (Näpflin, 2008). We aim with this thesis to design methods particularly suited to studying large-scale, global brain functional recovery over time.

Time-series measurements of high temporal resolution provide a way of studying important properties of the network. Spectral analysis methods are ideally suited to the analysis of EEG signals (Mitra & Bokil). More recent techniques that apply spectral analysis methods to topology of the functional connections between nodes, allowing the summarization of complex interactions is a new frontier that this thesis explores. My research here demonstrates the importance of human electroencephalography in understanding complex neurological disorders. I study the recovery of functional networks, in treatment resistant depression and disorders of consciousness

What is the source of the EEG?

The mechanisms underlying the EEG are well understood, as it is a direct assay of the summation of inhibitory and excitatory postsynaptic potentials. Signals arise from the synchronized firing of tens of thousands of pyramidal cells in the cortex, characterized by their unique orthogonal orientation with respect to the cortical surface. The laminar organization of the synapses and cell bodies, and the interlaminar extension and parallel stacking of many of the cell's dendrites guide the flow of currents in the cortex. Postsynaptic currents generated at cell bodies in deeper layers of the cortex (e.g. layers V), are returned by current sources in the more superficial layers (cell bodies and dendrites layers II and III, and the apical dendrites of layer V

pyramidal cells). In turn, synaptic currents generated in the superficial layers are returned by current sources in deeper layers. These current sinks and sources generated by synaptic activity in turn generate the electrical fields we measure at the scalp surface by the EEG.

The summation of these vertical currents in the cortex generate electrical dipoles, creating electrical fields dependent on both the distance from the origin, and the angular orientation of the sources (Nunez and Srinivasan 2006). The propagation and amplification of these signals to the scalp can be modeled through the study of multipole radiation. (Srinivasan 2007) Multipoles describe electromagnetic or gravitational radiation from distant sources, which due to their particular shape, are able to propagate and are sufficiently amplified to be recorded via scalp electrodes. It has been estimated that between 10 000 and 50 000 neurons dominate the EEG signal (Murakami and Okada 2006, Wang et al 2005, Cohen 2011).

Brain activity can be measured on different scales (Cohen, 2011), such as the microscopic scale, measuring individual action potentials. These dynamics are most likely not picked up by the EEG, since the quadripolar shape of the action potential does not travel to the scalp. Instead, the EEG measures activity at a mesoscopic scale, which may be resolved with high density EEG recordings or by electrodes placed on the surface of the dura or cortex (electrocorticography). However, most of the activity measured by the EEG is at a macroscopic scale, which can be observed by eye.

EEG Oscillations

In 1929 Hans Berger noted the occurrence of regular waveforms in the first observations of an EEG. This observation of patterns was the first step to the visual interpretation of the clinical EEG still in use today. However, modern techniques allow for digital recording of the EEG and use quantitative methods to mathematically

analyze the content of the signal through frequency domain analyses (see Chapter II). These oscillations in the EEG therefore reflect the fluctuations in synaptic electrical activity of large populations of neurons, synchronously active, and large enough to travel through brain tissue, fluid, skull and skin.

In short, the EEG provides a wealth of information - it can measure processes taking places over short periods of time (milliseconds), or changes in states measured over hours, or years apart. EEG oscillations can be summarized quantitatively by three pieces of information: frequency, power, and phase. Frequency is represented by the number of cycles per second (units of hertz, Hz), and describes the speed of the oscillations. Power reflects the degree of synchronization between contributing neurons. It is known that local changes in spectral amplitude correspond to more than $1cm^2$ of cortical surface (synchronized postsynaptic currents of millions of neurons), (Nunez, 1995), whereas phase describes the alignment of one signal to another, measured by spectral coherence. Additionally, it is important to note that power and phase are independent of each other, conveying different information. This allows for the EEG to be studied in multiple dimensions (time, electrode location, frequency and phase), providing a meaningful way of summarizing complex multivariate human neurophysiology data.

Spectral Analysis

Each EEG signal is generated by the average contribution of multiple brain current sources over a large region of the cortex. Two traditional spectral measures are often used to measure EEG synchrony. However, synchronous firing produces synchronized oscillations, which can be measured by the EEG spectrum. In spectral analysis, different brain rhythms can be grouped by frequency ranges (or bands), which were defined by a combination of studies of the neurobiological mechanisms of

brain oscillations (Buzsaki 2006, Anastassiou and Koch, 2012, Kopell et al, 2010, Steriade 2005, Kopell, 2010]. Lower range frequency bands such as delta (1-4Hz) and theta (4-8Hz) are thought to generally reflect the coordination of large scale networks ((von Stein and Sarnthein, 2000). The alpha band (8-12Hz) is thought to correlate negatively with cortical activation, suggesting that alpha reflects active and selective inhibition (Jensen, Bonnefond, and VanRullen 2012; Klimesch, Sauseng, and Hanslmayr 2007). Beta (12-30Hz) band activity over motor areas has been linked with motor responses (Lattari et al. 2010; Neuper, Wortz, and Pfurtscheller 2006), whereas high gamma oscillations (30Hz+) are thought to reflect spatially local processing.

The graph theoretic approach - functional networks in the brain

The brain is theorized to function according to two primary organizational principles: functional segregation and functional integration (Tononi and Sporns, 2003). Functional segregation reflects the idea that neurons assemble together to form more specialized functional groups, whereas functional integration describes how these neural assemblies communicate producing higher cognitive function. It is necessary to understand how these neural assemblies are connected, and whether or not these patterns change in disease. The spectral measures outlined above are often used as bivariate measures of connectivity, allowing us to study pair-wise interactions between two regions based on a specific hypothesis. However, we also know that it is the simultaneous occurrence of local and long range synchronization of oscillatory neural activity that facilitates the exchange of information throughout the brain. As a result, it is necessary to examine multivariate interactions - between multiple regions at the same time - to comprehend study human cognition. (Bassett and Bullmore, 2006, 2016)

While structural network measures have been found to help understand brain development (Gong et al, 2009) or brain genetic variability (Bartley et al, 1997), functional networks are a particularly promising tool to explore recovery as changes in functional measures have been shown to correlate with changes in disease, such as Alzheimer's disease (Supekar et al., 2008, Stam et al., 2007, He et al., 2008) or schizophrenia, often described as a dysconnectivity syndrome (Liu et al., 2008, Rubinov et al., 2007, Bassett et al., 2008). This suggests that characterizing functional networks may also provide insight into the therapeutic effects of pharmacological or psychological therapies for neuropsychiatric disease. For example, dopaminergic drugs have been shown to modulate network measures, both in animal and human fMRI and MEG studies (Honey et al., 2003, Schwarz et al., 2007, Stoffers et al., 2008). In the study by Honey et al., functional connectivity networks are used to better understand the pathways modulated by dopaminergic drugs. Functional connectivity of caudate nucleus was modulated specifically by dopaminergic drugs, whereas non-dopaminergic drugs modulated a different pathway, between caudate and both thalamus and ventral midbrain. Functional networks have also been used to better understand the impact of behavioral therapies in aphasia, (Marcotte et. al., 2013). Marcotte and colleagues showed that increased graphical connectivity in the posterior areas of a default-mode network was concurrent with language improvement. They also hypothesized that pre-therapy connectivity may help predict therapy outcome.

A graphical network therefore provides an abstract representation of the system's elements and their interactions (Bullmore & Sporns, 2009). One can study three types of graphical networks:

1) Anatomical connectivity networks concentrate on the physical links between neural assemblies, and most often rely on DTI measurements;

2) Functional connectivity networks rely on the statistical dependencies between neural assemblies; and

3) Effective connectivity network, which concentrate on causal interactions between neural assemblies).

These graph theoretic methods provide a simple way of summarizing multi-dimensional data using neurobiological meaningful and easy to compute measures (Sporns and Zwi, 2004).

Rationale for approach

As reviewed above, capturing the dynamics of global brain networks as they change is particularly challenging. Any measure used needs to be robust to noise, have a biophysical source, and be meaningful at our studies' timescale. Graph theoretic approaches combined with more traditional spectral techniques suggest themselves as potentially powerful tools to summarize the EEG signal and measure global functional connectivity changes in complex brain networks. The problems of disorders of consciousness and the use of deep brain stimulation (DBS) in treatment resistant depression have particular relevance and interest because they address a very difficult problem in neurology – the diagnosis and characterization of brain states independent of behavior.

In the context of disorders of consciousness, brain function may change for many reasons. In disease, one might see decline in function, or we might see recovery, either over time or because of an intervention. These changes can take place over the course of a few hours on drugs, for example, months, with DBS, or years, with spontaneous recovery over time. It is therefore important to think of measurements that are behaviorally validated, and can reflect changes on a various time scales. In

this thesis, we use three optimally designed datasets to examine the value of our measures.

1) First, we use traditional spectral measures to study a cohort of patients with deep-brain stimulators to treat severe depression. This instrumental case allowed us to look at the impact of stimulation on brain function, and find a marker of treatment-resistant depression which would allow for the selection of potential DBS patient responders.

2) Second, we use graph theoretic spectral measures to study the mechanisms underlying recovery of communication in patients following severe structural brain injuries.

3) Finally, we look at alternative ways of analyzing the EEG to study changes in brain states.

In summary, the EEG is a unique tool that offers the opportunity to use novel quantitative measures to better understand and measure changes in brain states. In Chapter 2, I introduce the methods used for data collection and analysis. In Chapter 3, I test the hypothesis that alpha asymmetry normalizes in treatment-resistant depression patients who improve with scDBS, and may be used as an indicator of the potential efficacy of deep brain stimulation. In Chapter 4, I then test the hypothesis that changes in functional networks reflect underlying cortical reorganization in patients recovering from disorders of consciousness. I also demonstrate the test-retest reliability of our measures in a group of healthy volunteers, studied twice in a six month period. Finally, in Chapter 5, I summarize my thesis findings, and discuss their importance and contributions to the scientific community. I also address the limitations of this current work, and outline potential directions for future research.

Chapter Two: Methods

Electrophysiological Data

Electrophysiological Data Recording

All of the data used presented here (except for Chapter 3 – See Chapter3 Methods) were collected from participants at rest using either a double banana montage or an augmented double banana montage (19+18 channels), placed according the 10-20 international system (Jasper 1958), using a standard clinical recording system (Xltek, of Natus Medical). Signals were sampled at 200- 250Hz, and all data were stored and analyzed under the Rockefeller Research Hospital (RUH) and Weill Cornell Medical College protocols.

Resting State EEG

The resting state EEG is collected while subjects are awake, with their eyes open. It is thought to be a measure of baseline brain activity during rest - when a person is awake, but not consciously performing any physical or mental task. By collecting resting state EEG data, we are able to study neural activity related to the internal monitoring of brain states, memory recall, and mind wandering. Therefore, we collect resting state EEG data to study both the short and long-term effects of

stimulation on global brain activity, and the spontaneous global brain changes that may accompany recovery from severe traumatic brain injuries.

For healthy volunteers, awake resting state data were collected at RUH by asking volunteers to keep their eyes open for 5 to 20 minutes at a time, sampled over the course of 5 hours. Drowsiness was monitored by watching the subjects during the task and talking to them before and after. For all patients analyzed in chapter 4, awake resting data was sampled over multi-day inpatient visits at either NYP or RUH. Arousal was measured through individualized behavioral testing based on the Coma Recovery Scale-Revised (CRS-R) (Kalmar and Giacino 2005), and monitored using continuous video recordings. (See Table 1.)

Table 2.1 Summary of Healthy Control Subjects

ID	Time Between Timepoints	Timepoints	Number of 3s epochs	Time sampled
HC 1	23 weeks	T1	137	14:46-14:52
M;51				16:31-16:42
				18:08-18:15
				19:16-19:21
		T2	188	13:51-13:59
				14:46-14:51
				16:14-16:19
				16:41-16:46
				17:16-17:23
				17:45-17:53
HC 2	23 weeks	T1	107	13:05-13:26
F;26				15:25-15:31
		T2	116	12:51-13:13
				14:32-14:43
				15:44-15:59
				18:46-18:58
HC 3	25 weeks	T1	122	13:20-13:40
M;26				15:03-15:09
				16:59-17:10
				18:32-18:41
		T2	143	13:41-13:57
				14:39-14:49
				16:12-16:17
				17:25-17:35
HC 4	28 weeks	T1	107	13:08-13:28
F;41				15:49-15:54
				16:57-17:07
				18:36-18:46
		T2	127	13:05-13:20
				13:46-13:56
				15:47-15:52
				16:27-16:32
				17:18-17:28
HC 5	28 weeks	T1	111	14:45-14:57
F;36				16:17-16:32
				17:48-18:02
				15:01-15:09
		T2	69	16:13-16:20
				17:21-17:24
				17:26-17:29
				17:33-17:35
HC 6	25 weeks	T1	122	14:03-14:24
M;23				15:17-15:27
				17:04-17:14
				17:53-18:03
		T2	114	14:02-14:17
				15:05-15:10
				16:03-16:13
				17:12-17:17
				18:31-18:36

EEG Pre-processing

Pre-processing steps are known to help minimize the effect on artifacts, and maximize the signal to noise ratio. There are many artifacts in the EEG which can affect quantitative EEG studies. Biophysical sources are a dominant source of noise in the EEG, which can heavily affect any analysis results. Eye movements, such as eye blinks and saccades, create strong changes in electric potentials. Similarly, muscle contractions can also be seen in the EEG as EMG noise, which may change depending on the cause. A number of methods currently exist to minimize noise, such as Independent Component Analysis (Makeig et al 1996) and robust spectral analysis (Melman et al, 2015). However, while these methods are efficient they are known to also eliminate meaningful biological data along with the noise in the EEG. Thus, visual inspection of the data still plays an important role in EEG analysis. While slower, visual inspection remains the gold standard.

For all analyses in this thesis, we manually selected artifact free epochs. For all studies, we collected a minimum of 90s of data, since it has been shown that EEG features computed from a minimum of 60s epochs were more reliable (Salinsky et al, 1990). Slow variations (e.g., movements of a patient for EEG data) were removed using the Loess method (MATLAB function, locdetrend.m). We did not analyze data above 50Hz.

Assumptions

The EEG is a complex signal which contains both non-stationary (stochastic) and stationary (deterministic) components. While it is impossible to know whether the dynamics represent real underlying stochastic processes, or sampling fluctuations, we can measure the average spectral power over a particular time period. One main

assumption of Fourier transforms is that the data are stationary. Stationarity assumes that the time series remains stable in its mean, covariance, and other descriptive measures over time. By using a Fourier transform, we are therefore ignoring any short term dynamics which are not being characterized by long term averaging. While we know that the brain's nonstationarity reflects neurophysiological processes (Kaplan et al, 2005), we can assume that there is stationarity within brief periods of time (Florian and Pfurtscheller, 1995). Since spectral methods assume stationarity and require larger amounts of data, the approach used here is to try to not average signals from different cognitive states. In order to characterize non-stationary dynamics, a better approach would be the use of spectrograms (Hudson et al).

Volume Conduction

EEG Spectral analysis suffers from the inverse problem – we do not know the location of the EEG sources. Finding a high coupling measure such as a strong coherence between two EEG channels is usually assumed to show a high level of cooperation or neural synchronization between two areas of the brain. However, due to volume conduction effects, it can be argued that the signals are synchronous simply because they both stem from the same generator (Cohen 2014). These effects make it difficult to make any direct conclusions on exact source localizations, and may confound inferences about connectivity To take into account spatial filtering, we applied a surface Hjorth Laplacian montage (Winter et. al, 2007) to minimize volume conduction.

Time Series Analysis

The sampled EEG signal is a time series, which can be analyzed using either power based or phase based methods. The most common method for analyzing the

EEG is to calculate its power spectrum. The power spectrum decomposes the EEG signal into a set of oscillatory signals each at a unique frequency. The spectrum is the amplitudes (or power levels) of the oscillations at each individual frequency. The power of each oscillatory component is thought to be related to the synchrony of its underlying sources (Nunez and Srinivasan, 2006). The higher the power, the stronger the synchrony. A reduction in power is believed to be caused by desynchronization of the sources of the EEG signal (Pfurtscheller 2008). Increases in synchronization and desynchronization can occur independently at different frequencies, and the power spectrum can be used to track such changes in the activity in neural populations. Coherence in the EEG is a different spectral measure which quantitatively measures the levels of synchronization between two neural populations at each frequency in their spectra. For the EEG it is a large scale measure which identifies synchronous neuronal assemblies. High coherence reflects synchronized neuronal oscillations (suggesting functional integration between neural populations) while low coherence suggests independently active populations (suggesting functional segregation). Coherence is primarily a measure of phase correlation, and is believed to reflect functional cortical connectivity on a centimeter scale, either directly via corticocortical fiber systems or indirectly through networks that include other cortical or subcortical structures. (See Figure 2.1). Importantly, coherence cannot tell us about the causal links between two populations or whether two sites are synchronized by direct coupling or by both being driven by another population.

Power and coherence have been linked to changes in attention, cognitive, perceptual, motor, linguistic, and other functional processes, (Klimesch 1999, 2012), reflecting the importance of oscillations in cognitive function. This makes spectral measures an exciting tool of study, reinforcing the hypothesis that spectral power and coherence are important measures of EEG and reflect neurobiological information. For

each subject, the power and coherence spectra for all artifact-free epochs were averaged. The EEG power spectral densities and coherence were computed using the method of multitaper spectral estimation (Thompson, 1982; Percival and Walden, 1993), as implemented by the MATLAB Chronux toolbox (Mitra and Bokil, 2007, http://www.chronux.org). The multitaper spectral analysis method reduces bias and variance when estimating spectral measures. Coherence values were averaged according to band of interest ([0-4Hz], [4-8Hz],[8-12Hz],[12-20Hz],[20-50Hz]).

Figure 2.1. Electroencephalographic (EEG) patterns and their corresponding patterns (Adapted from Schiff et al, 2014

The power spectrum describes the frequency content of a single channel of EEG. The example of panel A1 shows prominent oscillations at approximately 10 Hz (alpha range), both in the raw tracing (left) and the power spectrum (right). The example of panel A2 shows oscillations at approximately 25 Hz (beta range), superimposed on smaller and slower fluctuations; correspondingly, the power spectrum has two main peaks, a large one at approximately 25 Hz and a smaller one at 7 Hz. A1: normal subject, channel Oz (Laplacian derivation); A2: minimally conscious patient subject, bipolar channel Fz-Cz. Note that the power spectrum is calculated from many samples of EEG, totaling 489s for A1 and 348s for A2, but only one typical second of the raw trace is shown. Error bars (barely visible in Panels A and B) indicate 95% confidence intervals.

B. The coherence identifies the relationship between activity in pairs of EEG channels. Panel B1: EEG spectra from two locations (POz, upper trace, and P4, lower trace, Laplacian derivations) have similar dynamics (left) and the coherence (right) shows that the dominant theta-range peak (arrows) is highly synchronous on these channels. Panel B2: EEG spectra from two locations (F8-FC6, upper trace, and F4-FC2, lower trace) also have similar dynamics (left) but the coherence (right) shows that the activity in the 20 Hz range is synchronous, while that in the 12 Hz range is not (arrows).

A. Electroencephalographic (EEG) patterns and corresponding spectra

1. Alpha oscillations

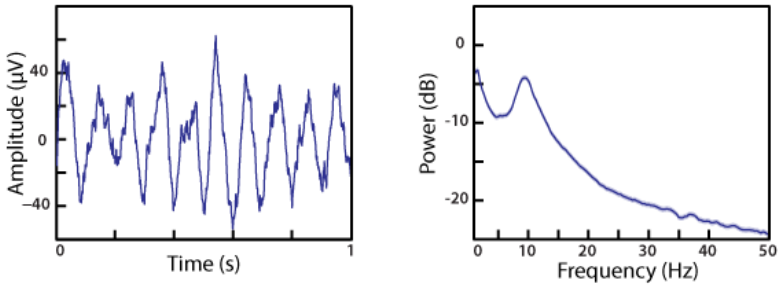

2. Beta oscillations

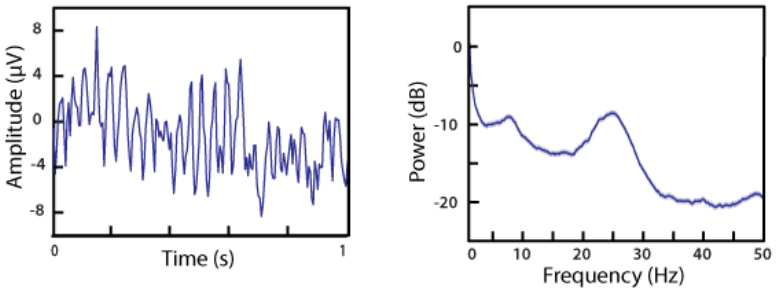

B. Coherence quantifies synchronization across channels

1. Coherent at 8Hz

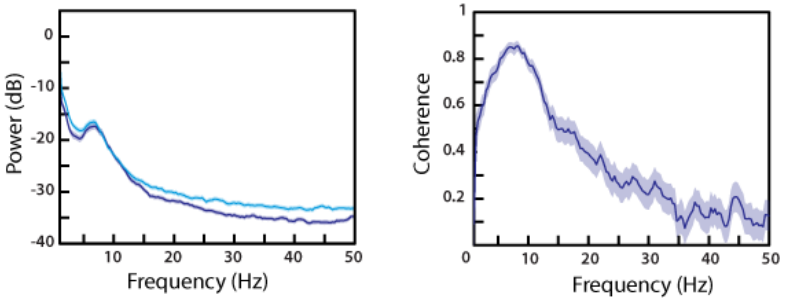

2. Coherent at 20Hz and incoherent at 12Hz

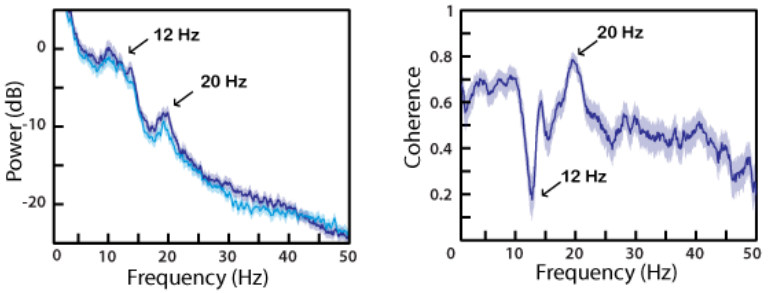

Longitudinal measures of the EEG

When choosing a clinical measure capable of tracking recovery, it is important to choose a measure with high test-retest reliability and intra-individual stability. The EEG is the only such measure for neurological disorders. Indeed, prior studies have shown that EEG spectral features are highly stable, both in short and long term recordings (Gasser et al, 1985, Salinsky et al, 1991, Näpflin et al, 2007, Oken and Chiappa 1988). Such stability is especially important when studying neurological disorders such as brain injury, where states of arousal may fluctuate over the course of minutes, and recovery can be measured over months or years. The stability of the spectral power and coherence in healthy volunteers is illustrated in Figure 2.2, 2.3 and 2.7.

Figure 2.2 Example of spectra stability within the same assessment in a healthy volunteer

Examples of power spectrum collected from HC 1, using 5 tapers and a frequency resolution of 2Hz. All segments were collected during eyes open awake rest times, sampled 6 times over the course of 4 hours, each assessment ranging from 5 to 10 mins. We obtained between 10 to 55 3 second artifact free epochs from each baseline, for a total of 188 3s epochs. Error bars indicate 95% jackknife confidence intervals.

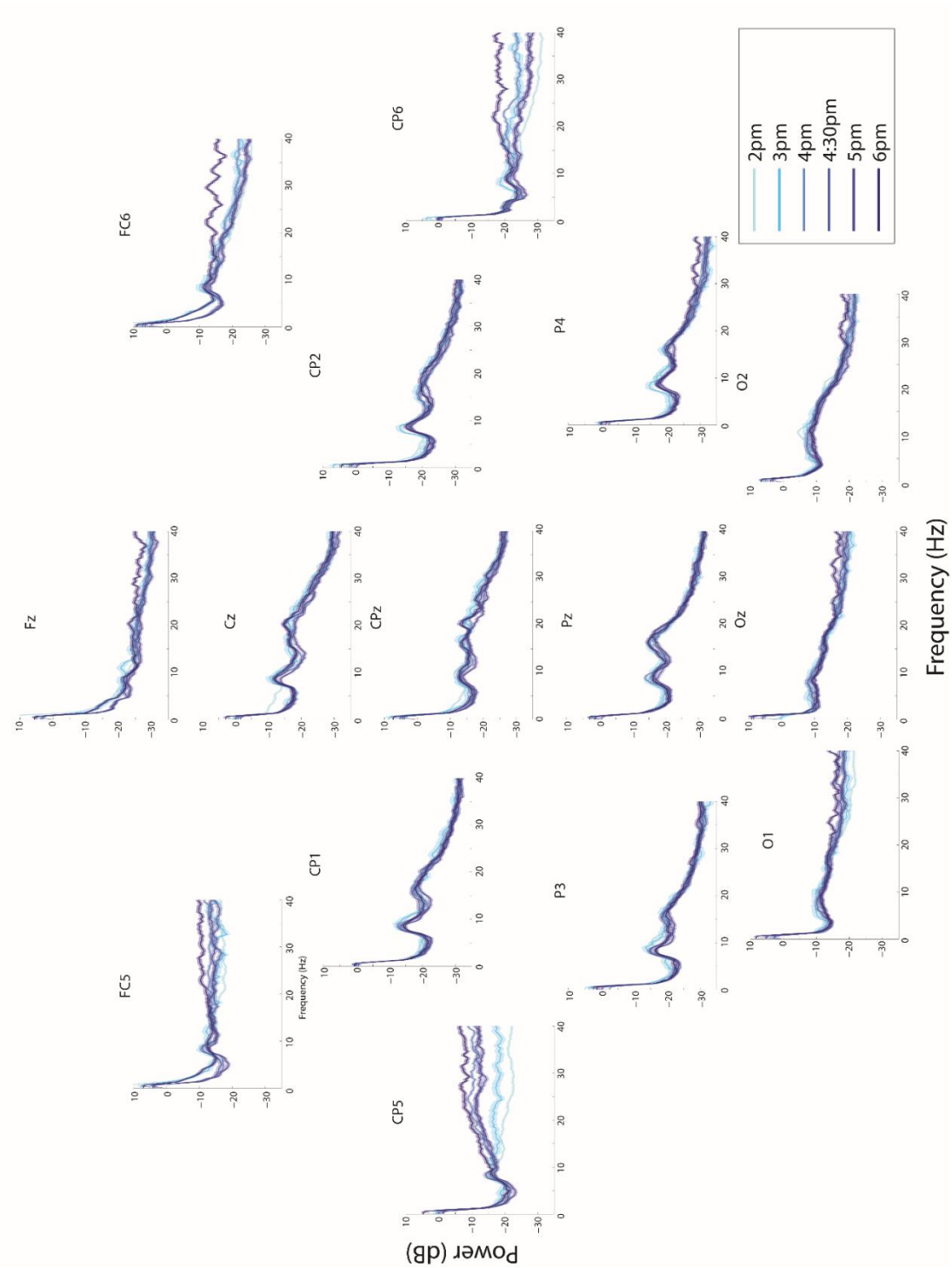
Fz
Cz
CPz
Pz
Oz
FC5
CP1
P3
O1
CP5
FC6
CP2
P4
O2
CP6
2pm
3pm
4pm
4:30pm
5pm
6pm
Power (dB)
Frequency (Hz)

Figure 2.3 Example of spectra stability over 6 months in a healthy volunteer

Examples of power spectrum collected from HC 1 during during eyes open awake rest times, using 5 tapers and a frequency resolution of 2Hz. EEG was sampled at two timepoints 6 months apart, totaling 411s for T1 and 564s for T2. Error bars (barely visible because of the large amount of data) indicate 95% jackknife confidence intervals.

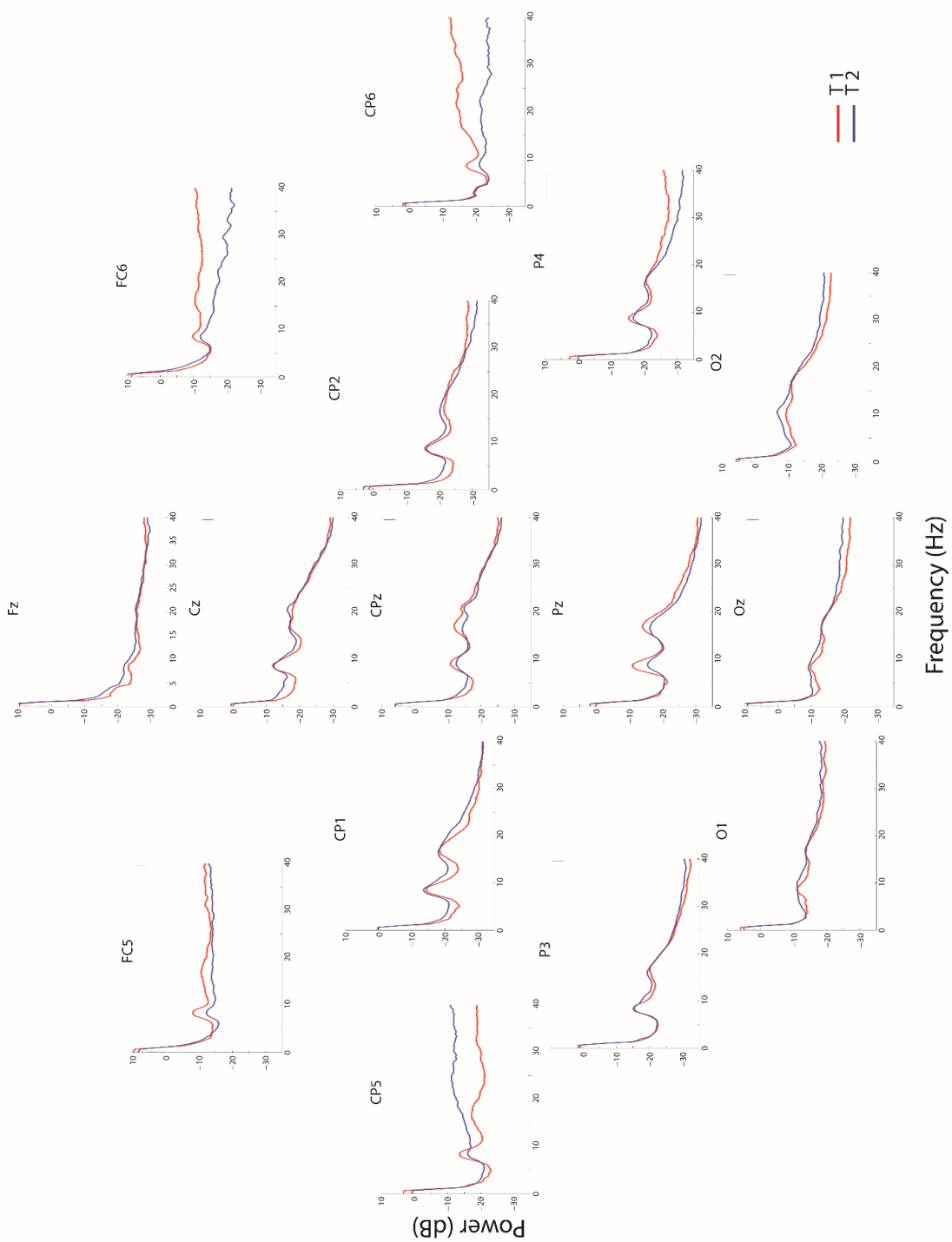
Fz
FC6
Cz
CP2
CPz
P4
Pz
CP6
Oz
O2
FC5
CP1
P3
O1
CP5
Power (dB)
Frequency (Hz)
T1
T2

We note that while the shape of the spectra is relatively stable over different timepoints (Figure 2.3), there is often a difference in baseline power. Most EEG studies involve testing paradigms in within one recording session. However, when testing subjects over time, many artifacts may affect the EEG, such as changes in baseline noise, artifact level, or electrode placement. These might affect the EEG in a variety of ways, which we can take into account by applying normalization procedures. Many normalization procedures exist for spectral power, the most common being simply subtracting the mean power from the values, or taking the mean power over a particular frequency band. For our purposes however, this is not as useful. In cases where both power and frequency are being modulated, simply averaging over a set frequency band may risk "averaging out" important features. We therefore choose to use a simple normalization procedure based on Gottselig et al 2012. (Illustrated in Figure 2.4 and 2.5).

Figure 2.4 Illustration of normalization procedure for spectral power

A) We plot the power spectrum of channel FC5 in a healthy volunteer (HC4) over 2 timepoints.

B) Each spectra is normalized using log-log values of spectra between frequencies of interest (grey bars). The black line represents the power law function generated using 5–6 and 13–13 Hz as the range used for fitting

C) At each data point, the resultant of the power law function is subtracted from the power spectrum within the range of the band of interest (here 6-13Hz).

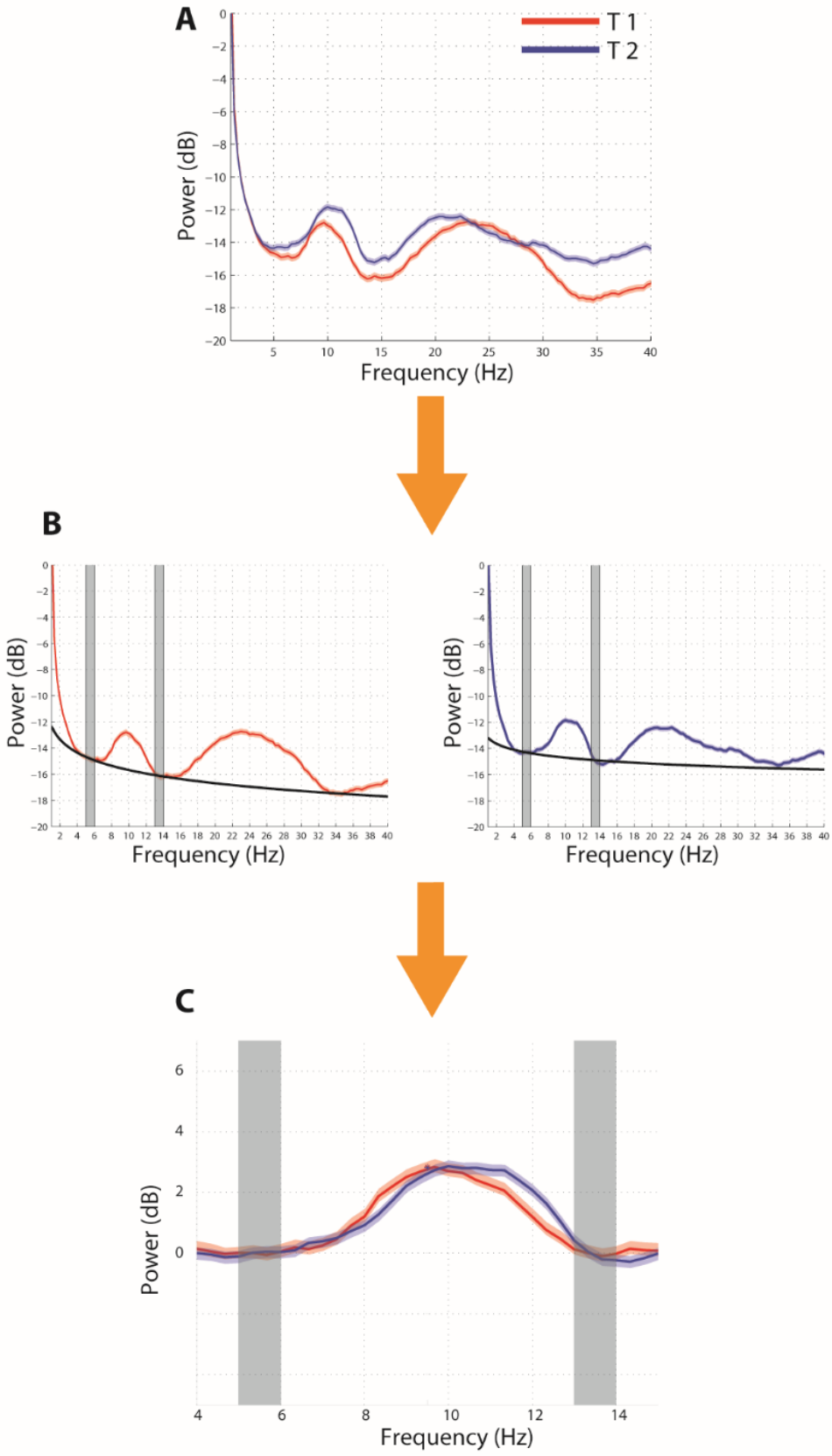
A
T 1
T 2
Power (dB)
Frequency (Hz)
B
Power (dB)
Frequency (Hz)
Power (dB)
Frequency (Hz)
C
Power (dB)
Frequency (Hz)

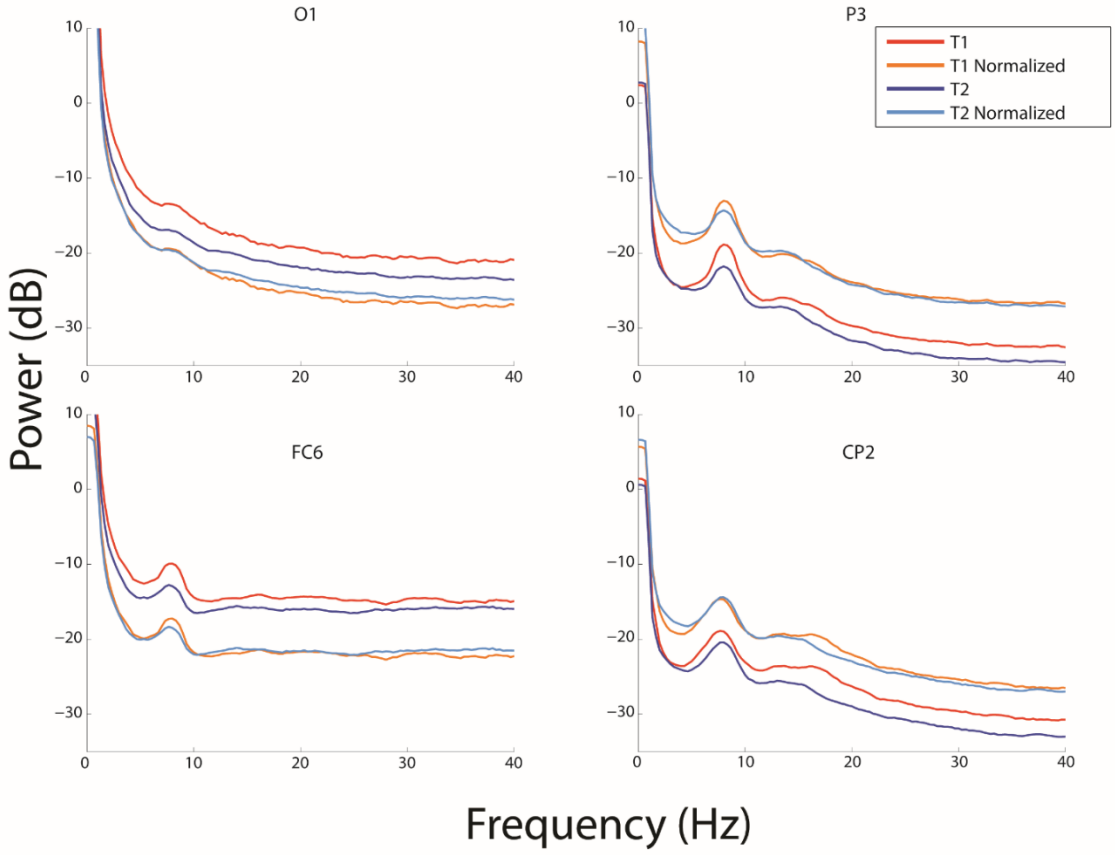

Figure 2.5 Example of spectral normalization in 4 EEG channels

We show the power spectrum of four channels (O1, P3, FC6 and CP2) over two timepoints (red and blue) 6 months apart in HC1 We use the Gottselig et al 2012 procedure for normalization of the alpha band, and plot the resulting power spectrum. (orange and light blue).

This allows us to normalize the spectral power, taking into account differences based on different recording environments, while keeping important feature information As well as the spectral power, the spectral peak power and frequency are also important information that can be lost when measurements are made during different visits on different days. In example from Fig. Look up citation about spectra

peak frequency. We use a simple quadratic extrapolation to extract the peak frequency and power. (Figure 2.6).

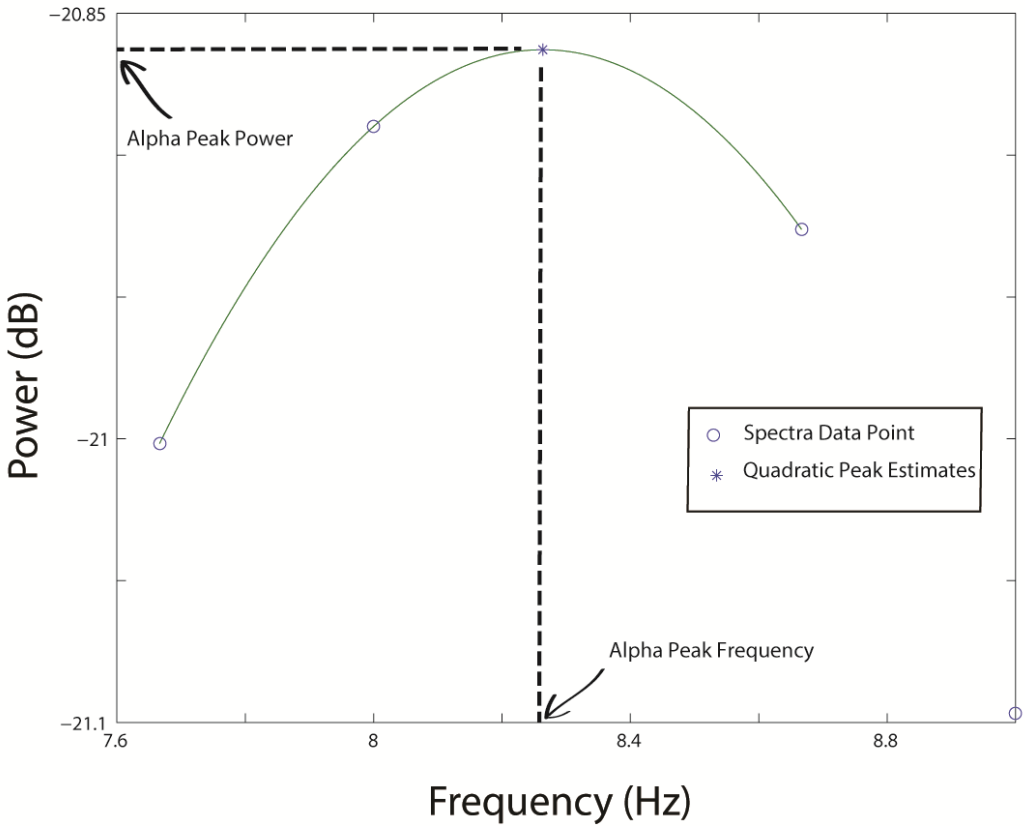

Figure 2.6 Quadratic fit of the alpha peak of a power spectrum

Using a manual cursor script in Matlab, we marked the center frequency of the peak of interest. We fit the closest 3 points (open circle) in the power spectrum to the peak, and fit a simple quadratic to those points (green line). We then used the peak of the quadratic to estimate the peak power and frequency.

Figure 2.7 Example of coherence measured in 2 timepoints 6 months apart in HC1

Spectral coherence (Laplacian derivations) over trials between pairs of channels (illustrated by green line on wireframe plot). Stars along the X-axis represents significance via the two group test significance, $p \leq 0.05$.

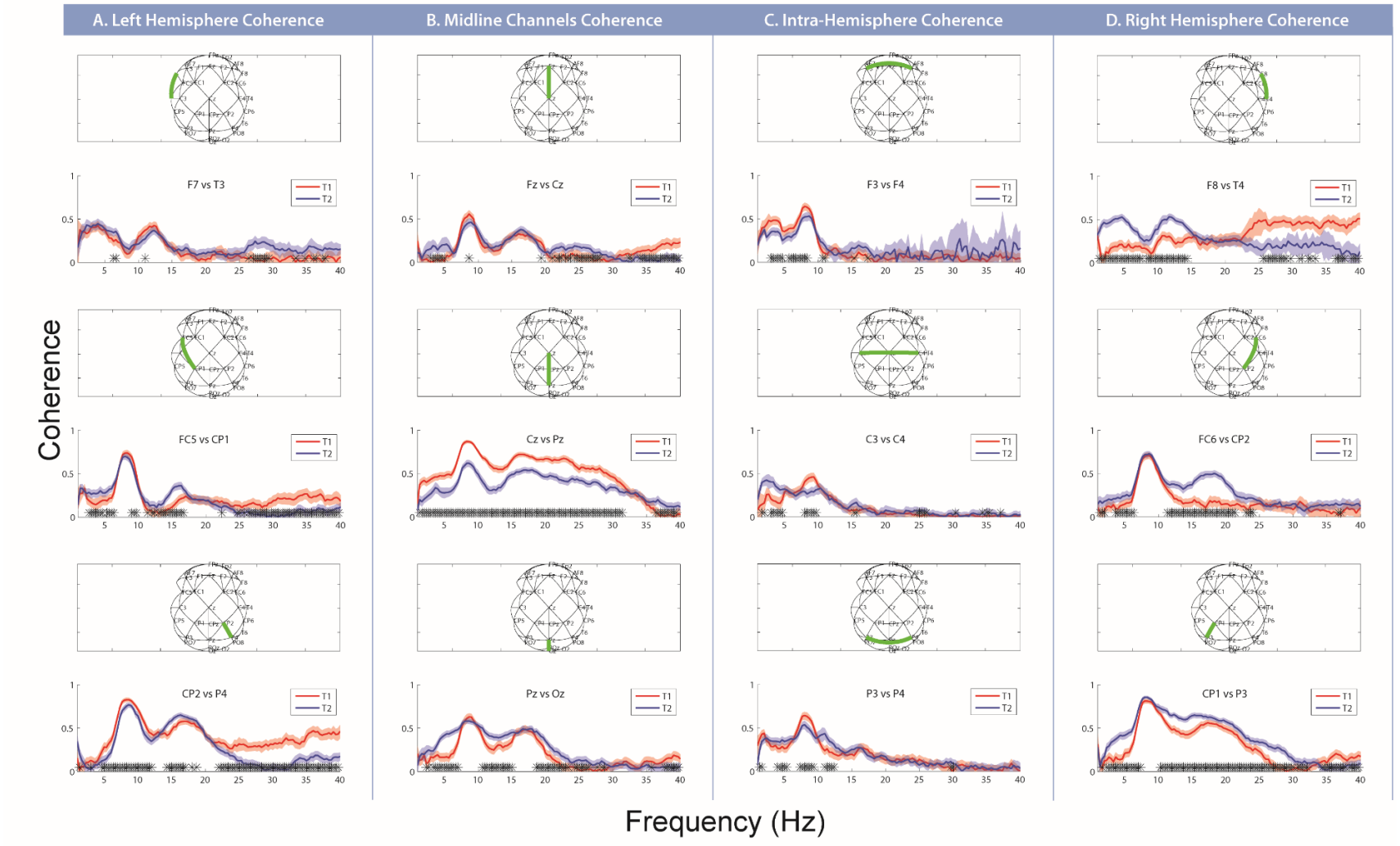
A. Left Hemisphere Coherence
B. Midline Channels Coherence
C. Intra-Hemisphere Coherence
D. Right Hemisphere Coherence
Coherence
Frequency (Hz)
F7 vs T3
Fz vs Cz
F3 vs F4
F8 vs T4
FC5 vs CP1
Cz vs Pz
C3 vs C4
FC6 vs CP2
CP2 vs P4
Pz vs Oz
P3 vs P4
CP1 vs P3
T1
T2

Graph Theoretical Approach

A natural approach to explore multivariate functional networks is through the use of graph theory – the mathematical study of networks - in which a graph is defined as a set of nodes (such as electrodes in EEG, anatomical regions of interest in MRI) linked by either a functional or anatomical connection (Friston, 1994). Nodes in neuroscience tend to represent specific regions of interest of the brain, including internal structures in DTI or fMRI studies, or only scalp regions, as in EEG studies. Links represent the type of connectivity between two nodes or regions which may be binary in nature (present or not), weighted (containing information about the strength of the connections), or directional (one node affects or causes the other). The hardest problem is to differentiate meaningful connections from weak and non-significant links representing spurious connections.

Choice of coupling measures

Various coupling measures may be used to construct functional networks using time series data acquired from brain imaging. The core of most of these methods involves computing a measure of connectivity to generate either a directed, also known as effective connectivity. These are comprised of methods measuring the influence of one neural system over another, either at the synaptic level or a population level. Methods used to measure effective connectivity rely on either model-based approaches, such as dynamic causal modeling (DCM), (Friston et al., 2003), and granger causality, (GC), (Brovelli et al., 2004), information-theoretic approaches, such as transfer entropy (TE) or symbolic analysis techniques (King et al, 2013). Model based approaches are often criticized for generating large amounts of spurious

connections (Lee et al, 2013), whereas information theoretic approaches are not dependent on any a priori assumptions.

Many different measures have been useful in distinguishing between very different states of consciousness, such as vegetative or minimally conscious states (King et al, 2013 Lee et al, 2013 Chennu et al, 2017), one might argue that the information extracted from all of these measures is already present in the spectral power or coherence. (Schiff et al, 2013). There are a large number of ways to quantify coupling between two signals, and selecting the correct coupling measure is a difficult choice. This choice depends on the paradigm, and how the hypothesis to be tested relates to the goals of the study. Depending on the measure used to quantify it, functional connectivity may reflect linear or nonlinear interactions, or interactions observed at various time scales. Indeed, functional connectivity does not describe a causal link between function and organization of the brain but only describes the pair-wise associations of neural populations through an indirect measure of neural activity; i.e. the BOLD signal. The challenge is to define rigorous estimates which reveal the underlying complex network associated with the observed pairwise connectivity patterns that are more directly linked to the underlying neural activity.

It remains unclear which measures are the most appropriate for the study of the recovery from severe brain injury. Each existing measure provides a different focus, and may require the data to satisfy different assumptions, therefore requiring different analysis methods. However, recent studies suggest that functional networks, even though they are derived from very different imaging techniques, may show similar properties. Furthermore, functional connectivity measures the statistical covariance between signals recorded in different brain regions, regardless of inferred direction, or model based assumptions.

We propose that undirected functional connectivity based on spectral measures, particularly coherence, are a natural choice to measure and understand long term changes in neurological states. Spectral measures have been extensively studied, and provide unique insights on the underlying neurobiological mechanisms. While measures such as the weighted phase lag index (Stam et al, 2007) are known to reduce the effects of volume conduction, the biological significance of such a novel measure has yet to be studied. As the field of functional connectivity is growing very quickly, it is important to assess any measure for its stability and biological significance. We compare our coherence measures here to wPLI measures (computed as implemented by the Fieldtrip toolbox (www.fieldtrip.org), and averaged according to the same bands of interest) (See Fig. 2.8). However, for this thesis, we ultimately decide to use coherence as our coupling measure, which is better studied and understood and which lends itself more readily to biological interpretation and hypothesis testing.

Figure 2.8 Visual comparison of different coupling measures

Visual comparison of average theta band (4-8Hz) connectivity between 2 timepoints of 2 healthy controls (HC2, HC5). Values represent either spectral coherence (first row) or weighted phase lag index (second row).

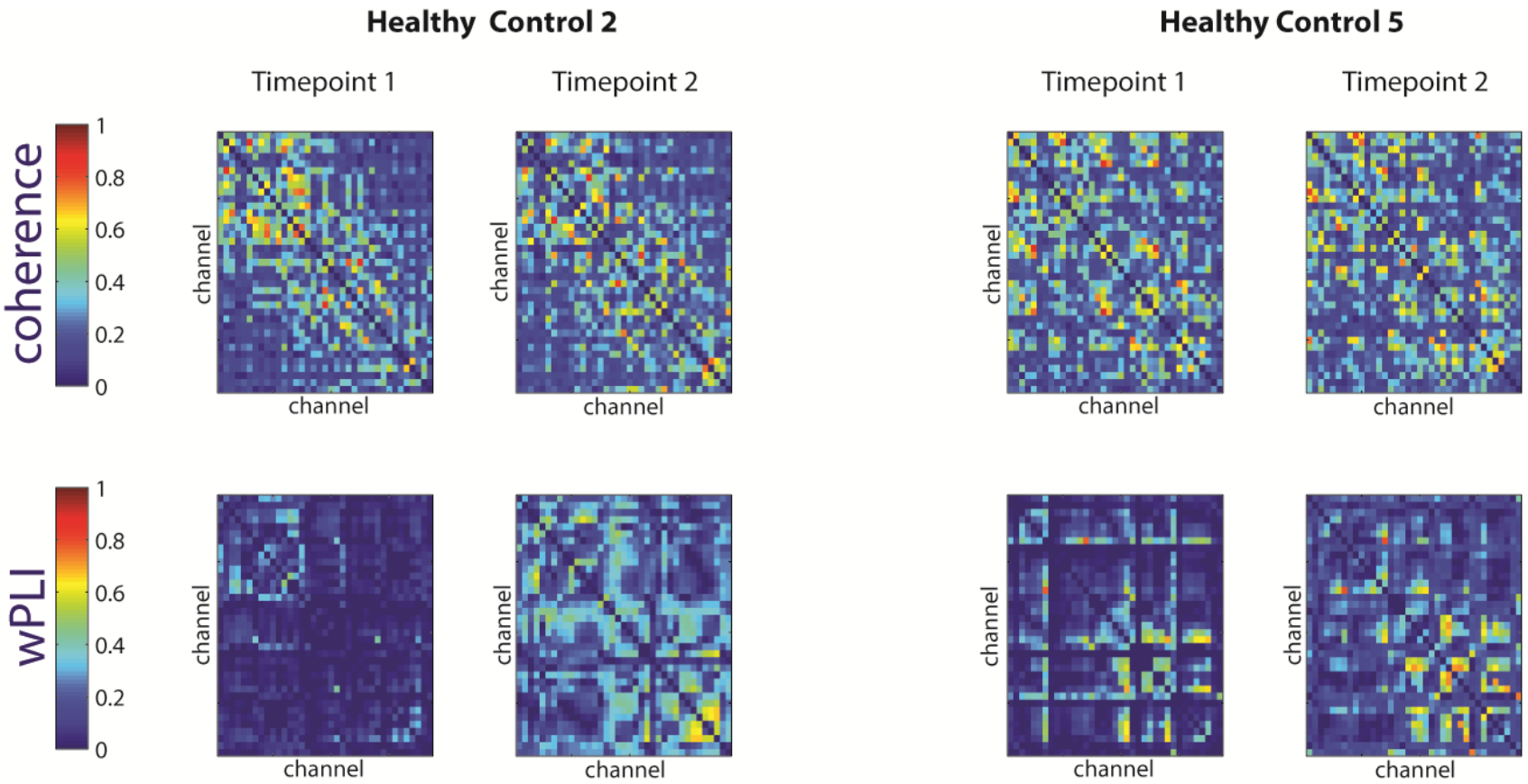
Healthy Control 2
Timepoint 1
Timepoint 2
coherence
wPLI
1
0.8
0.6
0.4
0.2
0
channel
channel
Healthy Control 5
Timepoint 1
Timepoint 2
channel
channel

Fortunately, there exist a few options to minimize volume conduction in spectral coherence measures, such as the hjorth laplacian montage (Winter et al, 2007, Robinson 2003). Srinivasan and co-workers (2007) and Robinson (2003) showed that for EEG coherences between moderately separated electrodes, surface laplacian EEG methods consistently minimize the volume conduction effect by emphasizing smaller scale sources. If all connectivity were due to only volume conduction effects, we would expect to see only strong connectivity at neighboring electrodes, and decreasing connectivity strength over increasing distances, resulting in a simple lattice network. Finally, since we are looking at changes over multiple time points, we are only interested in differences in connectivity, which would be equally affected by volume conduction effects (von Stein, et al 1999, Weiss & Mueller, 2003).

Network Construction

Weighted Matrices

Once all of the functional coupling values are estimated between all pairs of electrodes by spectral coherence, n being the number of electrodes. The total number of weighted edges would be equal to $\frac{n(n-1)}{2}$ in an undirected graph. Networks can be generated by weighted measures, or by thresholding the weights and generating binary networks. There are advantages and disadvantages to both methods. When using all weights, the results may be affected by many non-neural phenomena. For example, noise characteristics, might affect all the coherence measures. It has also been shown that the use of the weighted version of a topological metric is generally not a valid (Ginestet 2011) approach to this problem. An accepted approach is therefore to only concentrate on the most significant edges in the network, as determined by a threshold, for constructing the undirected binary graph.

Selecting Thresholds

There exist many ways of filtering a weighted matrix. The simplest is to set an arbitrary threshold, setting all weights w_{ij} below the threshold T as 0, and all those above as 1. However, this can lead to many issues. For one, different baseline levels of connectivity might lead to very dense or very sparse networks due to the selected baseline alone. It is therefore important to compare graphs with the same number of edges (Achard and Bullmore, 2007, Rutter et al, 2013). One method commonly used is to set the value of the density at each threshold, $K(t)$.

Since there is no singular correct way of selecting the threshold T, we decided to explore a range of values. It is easy to imagine that a threshold which is too low would simply include all, if not most of the edges of the graph, creating close to a complete network. Similarly, a threshold too high would be so sparse it would no longer be informative. One study (Achard & Bullmore, 2007) showed that at such extreme thresholds, networks cannot be differentiated from a random or lattice network.

A common approach (deVico Fallani et al, 2009, Rutter et al 2013) is to concentrate on a useful sequence of thresholds, based on a range of admissible densities with respect to random or lattice networks. We can then compare the properties of all the graphs in the range, by either testing the difference between the topological properties at each threshold, (Bassett, 2012), or by integrating the metric over a collection of available thresholds (cite).

We quantify the network measures in our healthy volunteers, and display the values for the thresholded coherence graphs. (See Figure 2.9 and 2.10). Because differences in density can have significantly effects of graph metrics, we plot all of our results as a function of graph density (Stam et al 2007). It is important to note that

when the mean degree K_{net} is less than the log of the number of regions, small-world properties are not estimable. (cite Achard et al, 2006).

For small worldness, we therefore selected our lowest value of $K(t)$ to fulfill two criteria, based on Rutter et al, 2013:

-largest connected component has to contain at least 99% of the nodes

- $K_{net} < \log(n)$

We calculated graph theoretic metrics for 100 thresholds, between 0.01 and 1 in 0.01 intervals.

Figure 2.9 Example of theta coherence networks over time

Graph theoretic measures sampled over 2 timepoints.6 months apart in HC1.

A) These four plots represent the density of the networks over the range of coherence thresholds between 0 and 1.

We plot the density of the networks in all EEG channels, the density between only the channels in the left hemisphere, the density between the channels in only the right hemisphere, and the density only between intra-hemispheric EEG channels.

B) These two plots represent the efficiency and average clustering over the range of total densities (0 – 1).
C) These two plots represent the small world metric computed over a range of total densities (0-1). We use 2 methods to compute the small world metric (see Chapter 2 methods).

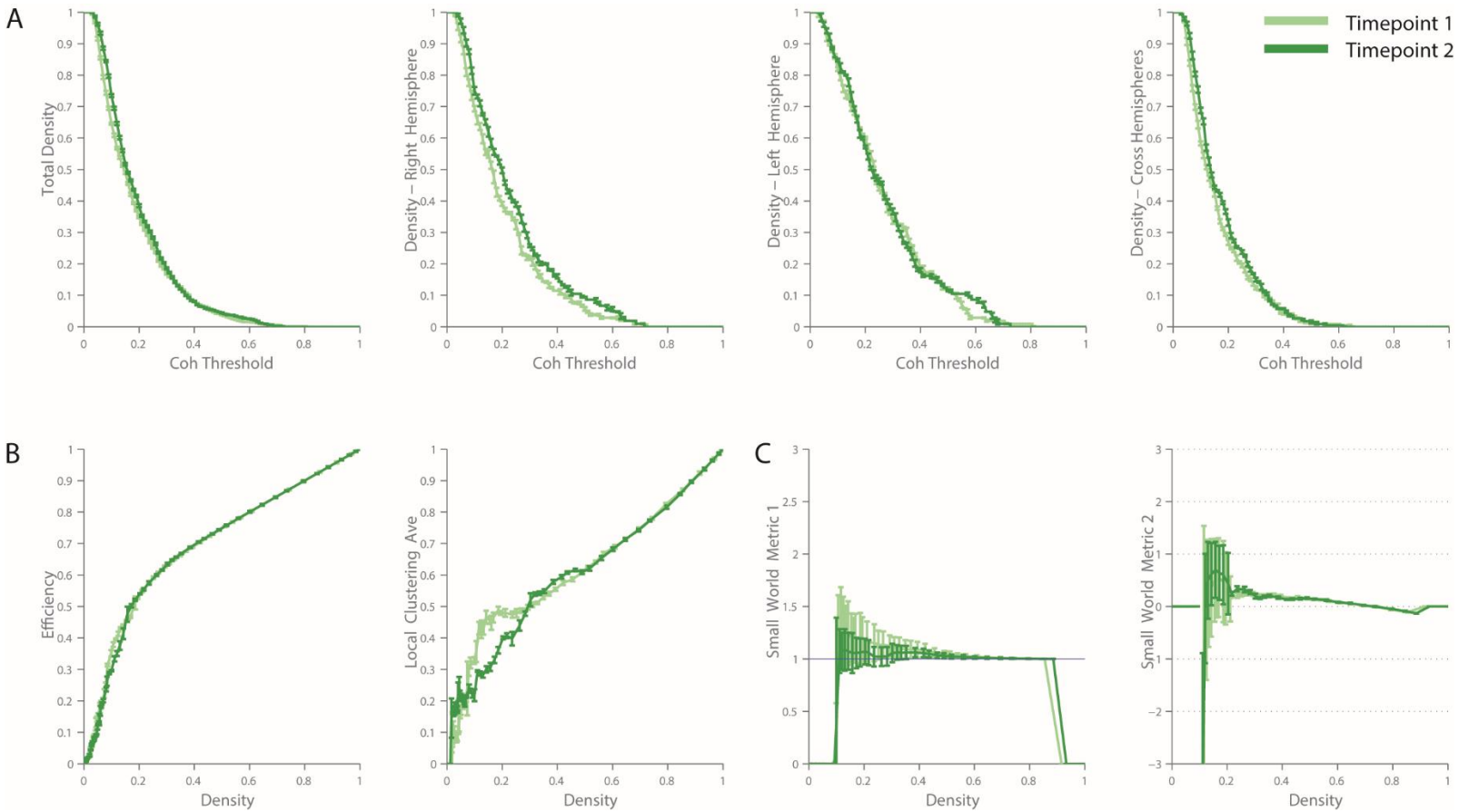
A
Total Density
Density – Right Hemisphere
Density – Left Hemisphere
Density – Cross Hemispheres
Coh Threshold
Timepoint 1
Timepoint 2
B
Efficiency
Local Clustering Ave
Density
C
Small World Metric 1
Small World Metric 2

Figure 2.10 Example of graph theoretic mesures in Theta weighted phase lag index networks for a healthy volunteer

Graph theoretic measures sampled over 2 timepoints.6 months apart in HC1.

A) These four plots represent the density of the networks over the range of wPLI thresholds between 0 and 1.
   We plot the density of the networks in all EEG channels, the density between only the channels in the left hemisphere, the density between the channels in only the right hemisphere, and the density only between intra-hemispheric EEG channels.
B) These two plots represent the efficiency and average clustering over the range of total network densities (0 – 1).
C) These two plots represent the small world metric computed over a range of total network densities (0-1). We use 2 methods to compute the small world metric (see Chapter 2 methods).

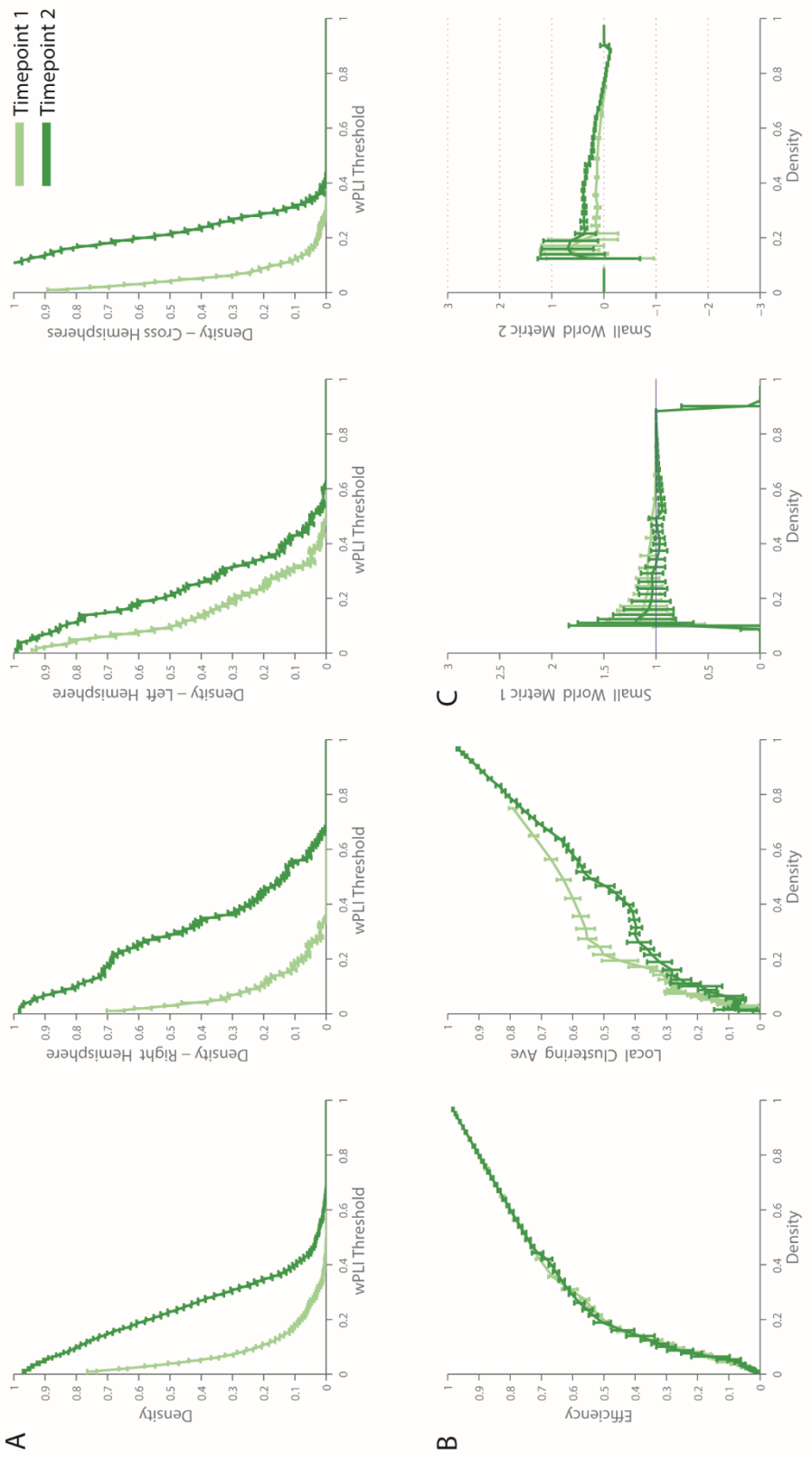
A
B
C
Timepoint 1
Timepoint 2
Density
wPLI Threshold
Density – Right Hemisphere
Density – Left Hemisphere
Density – Cross Hemispheres
Efficiency
Local Clustering Ave
Small World Metric 1
Small World Metric 2
Density

Graph theoretic metrics

Listed below are a number of useful graph theoretic metrics which we have employed here and find useful for studying resting state networks from the EEG collected from subjects that are awake, with their eyes open.

Network Density. K Simply measures the strength of the coupling between all of the node pairs. For our study, it is equivalent to the mean of coherence power or wPLI in the band of interest.

Degree of a Node

The degree is a measures of centrality, which compares how brain regions interact. It is the sum of all of the edges connected to a node. The absolute degree of all of the nodes in a network is defined as follows:

$$K_i = \sum_{j \in N} a_{ij}$$

where N is the set of all nodes in the network, and n is the number of nodes, a_{ij} is the connection link between nodes i and j

Global efficiency and Path Length.

Path length is an indirect measure of a networks ability to rapidly integrate information. It is the measure of the distance (number of connections) it takes to go from one node to another. Paths (a_{uv}) are the sequence of nodes to edges to get from one point u to another point, v in the graph, and the path length finds the shortest such path between every point in the graph.

$$d_{ij} = \sum_{a_{uv} \in g_{i \to j}} a_{uv}$$

where $g_{i \to j}$ is the shortest path (geodesic distance) between i and j. Note that $d_{ij} = \infty$ for all disconnected pairs i, j.

Characteristic Path Length (Watts and Strogatz, 1998) is the extension of the simple path length, summarizing the whole network behavior.

$$\mathrm{L} = \frac{1}{n} \sum_{i \in N} L_i$$

where L_i is the average distance between node i and all other nodes.

Efficiency is a way of measuring the networks resilience to change. For instance, patients with neurodegenerative disorders have been shown to loose edges or nodes (Alstott et al, 2009), and global efficiency, by measuring the average inverse shortest path length, is used to look at how much more or less efficient the network has become.

Global Clustering coefficient.

Clustering coefficient is a measure of local connectivity. In EEG networks, clustering coefficient is the proportion of electrodes a and b which are also connected to electrode c. It can also be thought of as the sum of all closed triplets, (or $3\ x\ number\ triangles$) over the total number of triplets (both open and closed). This gets to the idea of clustering – triangles tend to be between strongly connected to their neighboring nodes.

$$t_i = \frac{1}{2} \sum_{j,h \in N} a_{ij} a_{ih}\, a_{jh}$$

where t_i represents the number of triangles around a node i, connected to nodes j and h.

Small World. σ Small world networks are networks with a combination of relatively high clustering coefficients, but low path lengths. (Watts and Strogatz. 1998). One of the first applications of small world measures was to EEG data. Sigma is defined as follows:

$$\sigma = \frac{\frac{C}{C_{rand}}}{\frac{L}{L_{rand}}}$$

Where C and $C_r$are the clustering coefficient and the randomized clustering coefficient, and L and L_r are the path length and randomized path length of the respective tested network and a random network. Small-world networks often have $S \gg 1$.

We calculate an alternative small world index (Telesfold et al, 2011), which normalizes the measure using lattices (graphs in which all of the edges are connected) instead of random graphs, allowing for less fluctuations. Furthermore, this new metric is restricted to -1 to 1, as opposed to increasing with network size.

$$\omega = \frac{L_{rand}}{L} - \frac{C}{C_{latt}}$$

Values close to zero are considered small world: near zero, $L \approx L_{rand}$ and $C \approx C_{latt}$. Positive values therefore represent graphs with more random characteristics, and negative values indicate a graph with more regular “lattice” like characteristics.

Test-Retest Reliability

The application of graph theoretic methods is a relatively new field in neuroscience research, starting with the characterization of structural brain networks (Sporns et al, 2004). We've seen an exponential growth of applications of graph theoretic methods used to better understand a host of neurological disorders. Given the wide range of recording approaches and analysis methods, the identification of networks depends on the methodology used for estimating network edges as well as the graph metrics. Even with the same type of data, there are dozens of methods to approach the analysis. It is therefore essential to establish strong reproducibility in any measure one hopes to apply to longitudinal datasets.

We know that strong reproducibility of graph metrics has been reported for MEG (Deuker et al, 2009), DTI (Vaessen et al, 2010, Dennis et al, 2012), fMRI (Telesford et al, 2010), and EEG (Hardmeier et al, 2014) networks. This gives us strong confidence that the measures we choose will also have high test-retest reliability.

However, parametric statistical analyses are often not appropriate for many graph theoretic metrics, since they might not be normally distributed (ref Cohen). A non-parametric way of assessing test-retest reliability is to use intraclass correlation coefficient statistics (ICC). ICC measures the agreement between two assessments of the same measure. ICC is calculated according to the following formula:

$$ICC = \frac{MS_B - MS_W}{MS_B + (n-1)MS_W}$$

Where MS_B represents the mean square between subjects and MS_W represents the mean square within subjects. Finally, n stands for the number of assessments for each subject (here $n = 2$). According to Montgomery et al, 2002, we can interpret an ICC value of above 0.8 as almost perfect agreement, and an ICC above 0.6 considered as strong evidence for agreement. (Telesford et al., 2010; Montgomery et al., 2002). We calculated ICC coefficients between 6 healthy volunteers, seen at 2 timepoints. We looked at the test-retest reliability of both coherence and wPLI networks across all bands of interest. (See Fig. 2.11 and 2.12)

Figure 2.11 Intraclass Correlation Coefficient (ICC) for Coherence Network Measures

For each plot above, the ICC metric of reliability is plotted for every coherence the horizontal line at 0.6 and 0.8 mark the ICC thresholds. ICC values above 0.6 denote very reliable measures, and ICC values above 0.8 denote highly reliable measures.

A) ICC's distribution over the range of coherence values from 0 -1 for total density, density of left hemisphere, cross hemisphere, and right hemisphere. The network density was consistently the most reliable network measure, with an ICC-value above 0.8 over most threshold ranges (0.1–0.8) across frequencies.
B) ICC's distribution over the range of coherence values from 0-1 for network average clustering measures. Mean clustering coefficient had a slightly lower yet still robust ICC values spanning 0.30–0.7.
C) ICC's distribution over the range of coherence values from 0-1 for network Efficiency. Mean clustering coefficient had a slightly lower yet still robust ICC values spanning 0.30–0.7.
D) Small-worldness (SW) had a high reliability index between thresholds of 0.2-0.3, but above and below that range was highly variable. The results depend heavily on the sparsity of the graphs. Error bars represent jackknife 95% confidence intervals

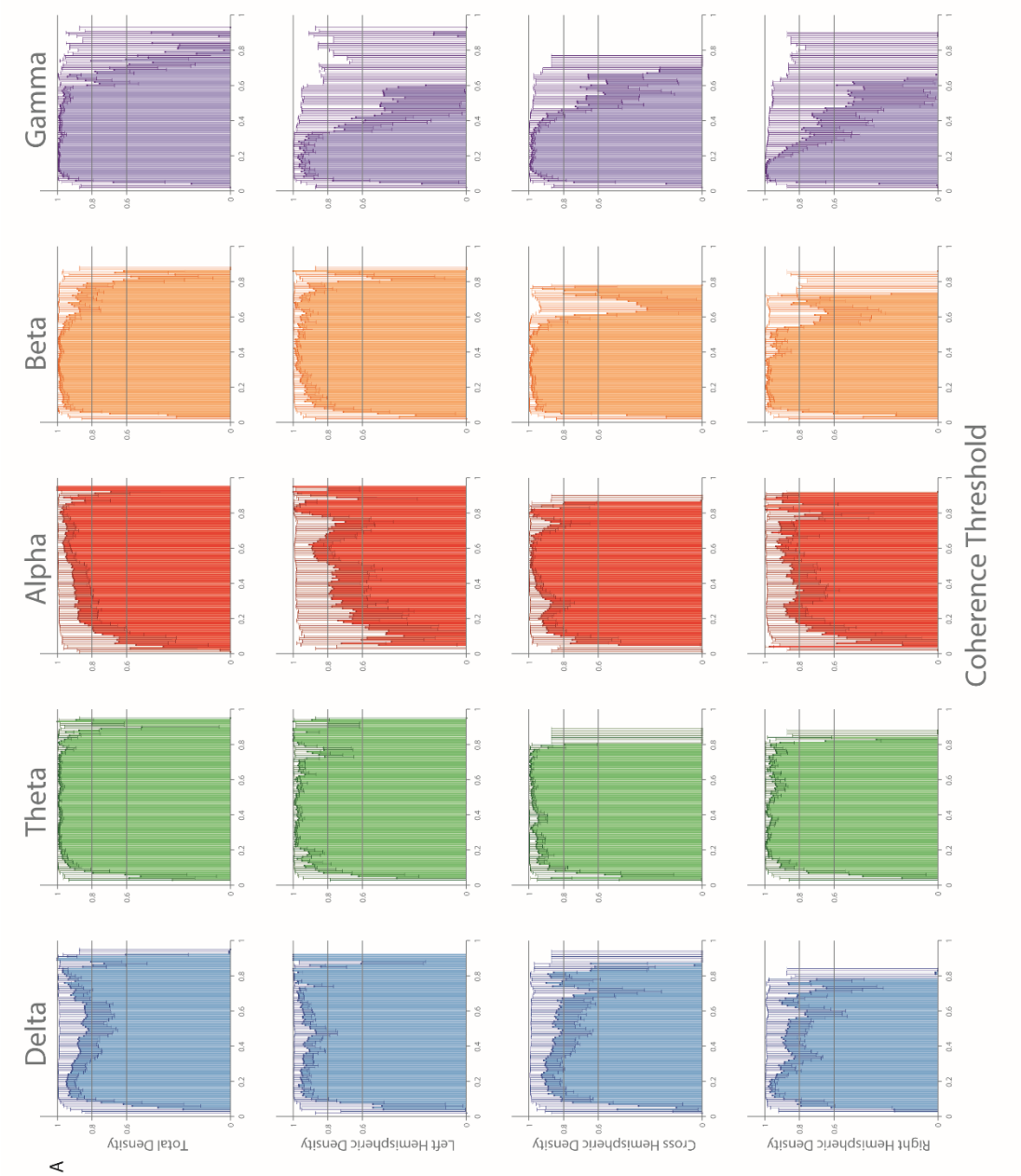
A
Delta
Theta
Alpha
Beta
Gamma
Total Density
Left Hemispheric Density
Cross Hemispheric Density
Right Hemispheric Density
Coherence Threshold

Figure 2.11 Continued.

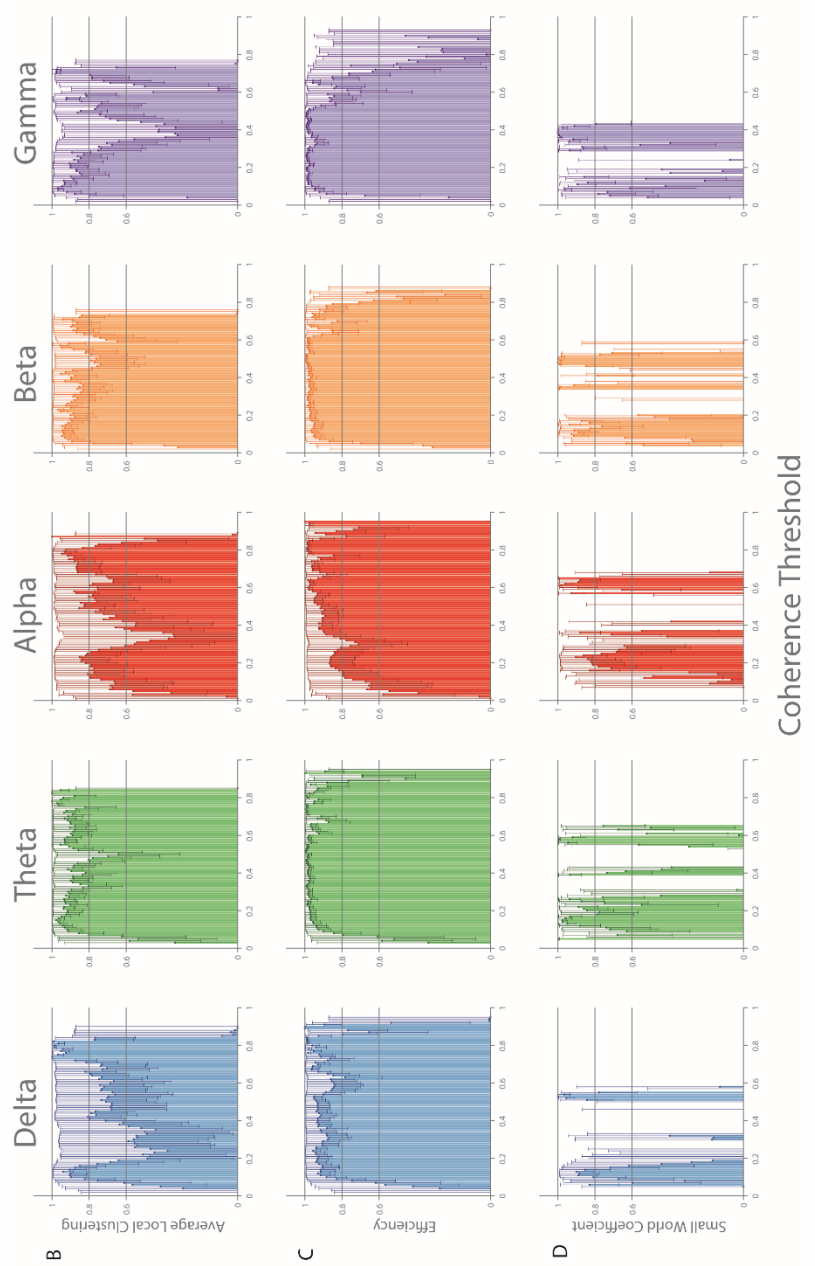

Figure 2.12 Intraclass Correlation Coefficient (ICC) for weighted Phase Lag Index (wPLI Network Measures)

For each plot above, the ICC metric of reliability is plotted for every wPLI estimate. The horizontal line at 0.6 and 0.8 mark the ICC thresholds. ICC values above 0.6 denote very reliable measures, and ICC values above 0.8 denote highly reliable measures.

A) ICC's distribution over the range of coherence values from 0 -1 for total density, density of left hemisphere, cross hemisphere, and right hemisphere. The network density was consistently the most reliable network measure, with an ICC-value above 0.8 over most threshold ranges (0.1–0.8) across frequencies.
B) ICC's distribution over the range of coherence values from 0-1 for network average clustering measures. Mean clustering coefficient had a slightly lower yet still robust ICC values spanning 0.30–0.7.
C) ICC's distribution over the range of coherence values from 0-1 for network Efficiency. Mean clustering coefficient had a slightly lower yet still robust ICC values spanning 0.30–0.7.
D) Small-worldness (SW) had a high reliability index between thresholds of 0.2-0.3, but above and below that range was highly variable. The results depend heavily on the sparsity of the graphs. Error bars represent jackknife 95% confidence intervals

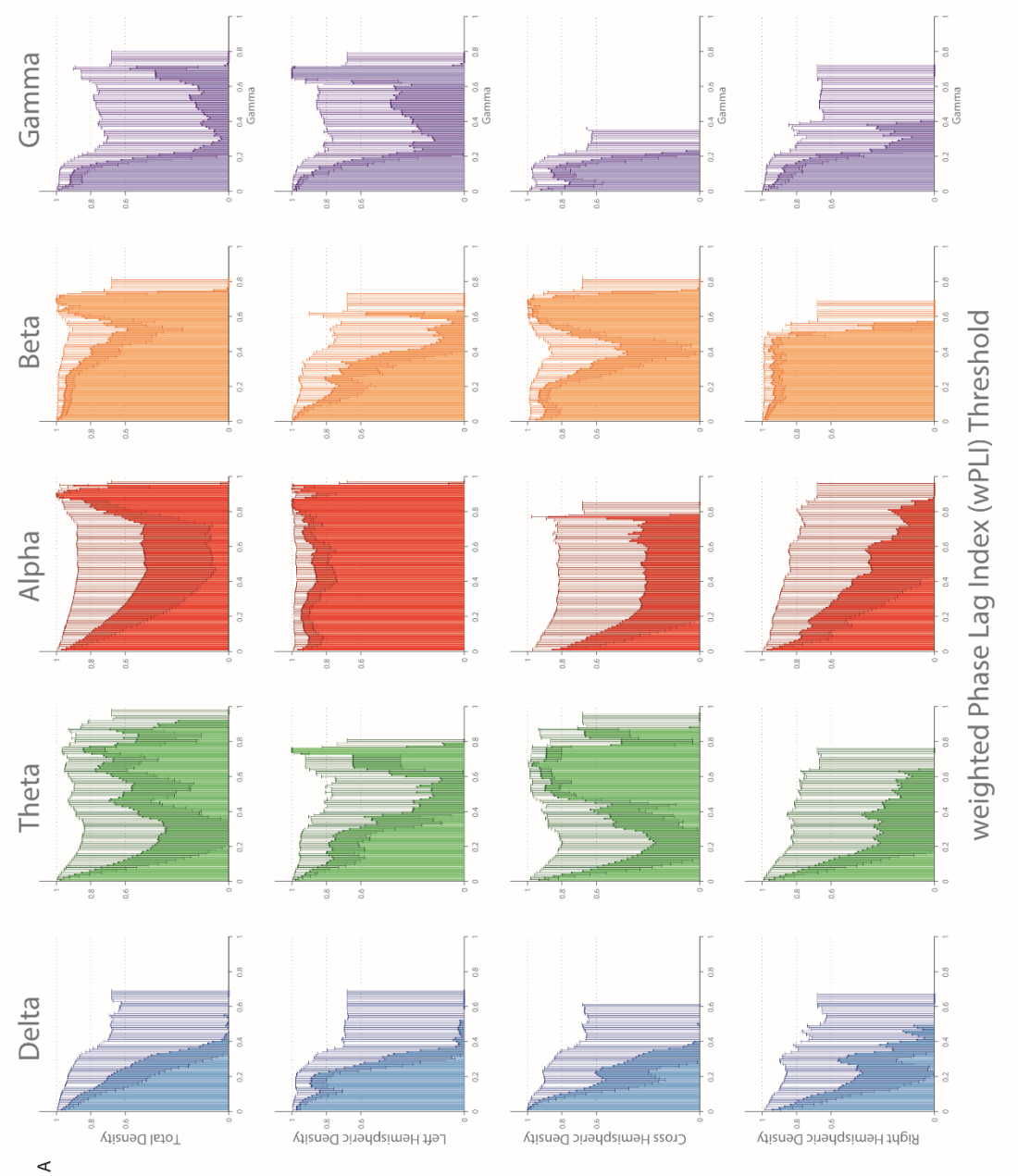
A
Delta
Theta
Alpha
Beta
Gamma
Total Density
Left Hemispheric Density
Cross Hemispheric Density
Right Hemispheric Density
weighted Phase Lag Index (wPLI) Threshold

Figure 2.12 Continued.

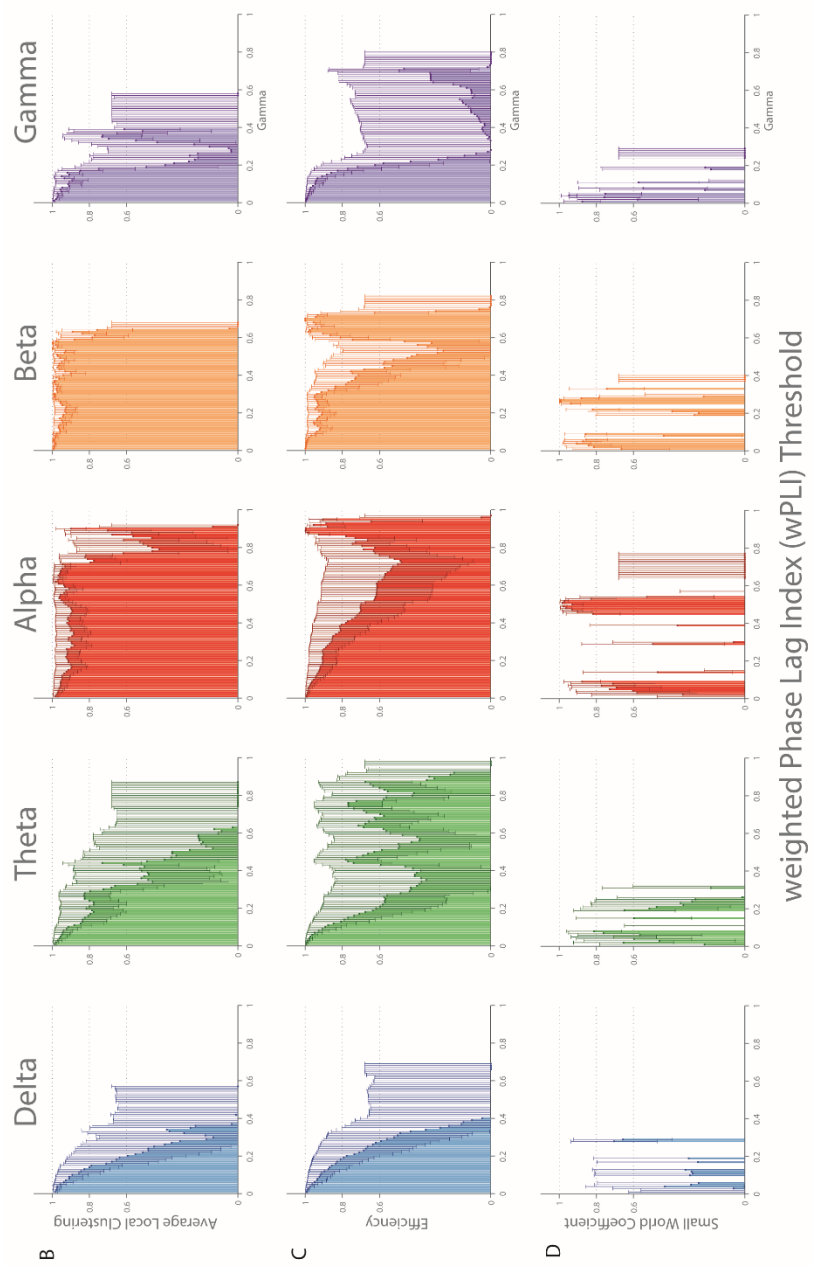

Statistical Procedures

Null Networks – Random & Density Matched

The most common model for creating random networks was put forward by Erdös and Rényi (1959). In this model, there is a probability p that an edge between 2 nodes exists. The location of the nodes has no effect on whether or not these nodes are connected, creating a truly randomized network. Such networks are characterized by low average shortest path lengths, since the networks are randomly connected. (Van Straaten and Stam, 2012).

Furthermore, generating a null network that preserves the nodal degree distribution is essential to compare many measures. It is very unlikely that a very sparse network will have a high path length, and we cannot compare its path length to a very dense network without first normalizing for the probability of having high path lengths inherent to the density of the network.

Null Networks – Jackknife

In order to generate confidence limits we used a standard drop-1 jackknife approach. The jackknife is a statistical resampling procedure, which was proposed by Quenouille in 1949 It is less computer intensive than the bootstrap. For all of our measures, we computed coherence leaving out 1 epoch at a time, and generated a jackknife 95% confidence interval.

Chapter Three: Longitudinal study of the effects of subcallosal cingulate deep brain stimulation for treatment-resistant depression on the power spectrum of the resting electroencephalogram

Introduction

Major depressive disorder is a psychiatric disorder which affects approximately 14.8 million adults in the US (Kessler et al, 2005). While most cases of depression are treatable with either medication or psychotherapy or both, up to 20% of the patients do not respond to conventional interventions such anti-depressants or ECT. Such patients remain severely depressed despite multiple rounds of treatment, and as of now have no treatment options available. It is believed that these patients suffer from a system level disorder, affecting more than a single neurotransmitter or brain region, but a complex network of systems and pathways linking cortical, subcortical, and limbic sites, as well as the neurotransmitters and molecular mediators potentially involved (Maletic 2007). Based on the preliminary observation that the Brodmann area 25 (BA25) is metabolically overactive in treatment-resistant

depression, Mayberg et al studied whether the application of chronic deep brain stimulation to modulate BA25 could reduce this elevated activity and produce clinical benefit. They found that deep brain stimulation of the subcallosal cingulate gyrus CG25 which consists of BA25 as well as parts of BA24 and BA32 gray matter, reversed the pathological metabolic activity in these areas. (Mayberg 1997, 2009).

One of our goals here was to define a biomarker in the EEG activity that could be used to predict which patients are most likely to respond to scDBS. Due to the invasive nature of scDBS therapy it is important to reduce the number of patients that will be exposed, unnecessarily to the risks inherent in brain surgery and electrode implantation. Resting-state EEG showed that frontal theta spectral measures predicted response to scDBS (Broadway et al. 2012) and was therefore considered a promising biomarker for predicting responders to this therapy. In this study, we concentrate on the use of the alpha band frequency in the EEG to try and identify electrophysiological differences between populations that improve with stimulation. Our hypothesis relies on previous electrophysiological studies of depression. It is well known that alpha network activity is often disrupted in patients with depression (Gotlib, 1998). Increased α-network activity is considered a hallmark of the depressive state, as demonstrated in EEG studies (Fingelkurts et al. 2007). Indeed, alpha frontal networks play an important part in emotional processing in depressed patients (Aftanas et al. 2001). In particular, the EEG alpha power asymmetry between left and right hemispheres in the frontocentral region is thought to be the most promising biomarker for depression (Davidson 1998, Allen et al, 2004, Gordon et al, 2010).

We therefore predict that treatment with scDBS will modulate the alpha band in patients with severe depression. We use alpha power to characterize spectral changes in the EEG, and study the effect of long term scDBS on the resting state EEG.

Finally, we ask whether changes in the resting state EEG will help us understand underlying electrophysiological effect of scDBS.

Methods

In order to quantify spectral power over time, we concentrate on four key differences: changes in overall power, the alpha peak's power (normalized) and frequency, and the alpha band's average power. (See Chapter 2). First, we quantified changes in healthy subject spectral power, tested at two time points 24-28 weeks apart to assess the test-retest reliability of the EEG power spectrum. We then looked at the changes in alpha band spectra in patients after 24 weeks of scDBS stimulation.

Cohort and DBS Parameters

Eight patient subjects (PS) diagnosed with either major depressive disorder or bipolar II disorder were enrolled in the SCC DBS study (Broadway et al, 2012). All had failed at least four treatments, including antidepressants and electroconvulsive therapy. For all demographics, see Broadway et al (Table 12). 2 patient subjects were eliminated due to EEG artifact contamination. 6 healthy volunteers were recruited as controls (for detailed demographics see Chapter 2, Table 2.1), and tested between 23-28 weeks apart.

The PS were bilaterally implanted with deep brain stimulation electrodes (Libra system, St. Jude Medical Neuromodulation) in the subcallosal cingulate white matter (SCC) (See Figure 3.1), the most ventral portion of the cingulate gyrus, thought to be an important hub of regulation in depressive disorders (Mayberg, 1997, 2009). Patients received single blind sham stimulation for 4 weeks followed by active stimulation for 24 weeks (DBS parameters: 130Hz continuous stimulation, 90-μs pulse width, 4-8 mA) For additional information on anatomical target and surgery, see

Holtzheimer et al 2012, Mayberg et al 2005, Hamani et al 2009 and Broadway et al 2012.

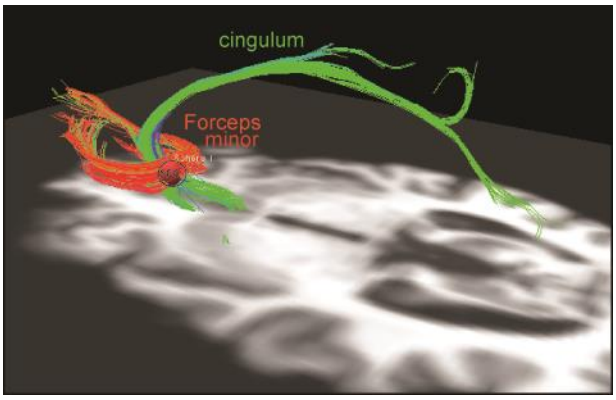

Figure 3.1 Model of Surgical target of DBS

(Image courtesy of H. Mayberg). Image of prospective tractography based surgical targeting, illustrating connectivity of the sub callosal cingulate white matter. The red circle indicates the target and surrounding grey matter that is stimulated.

EEG Analysis

All data were recorded using a BioSemi Active-Two amplifier system (Amsterdam, The Netherlands), digitized at 1024 Hz using a 32 EEG augmented montage (19 + 13). The EEG was collected at 2 time points, at baseline (T0) before implantation of the electrodes, and after 24 weeks of active stimulation (T24). Patients were monitored for drowsiness throughout resting-state EEG recording (eyes open), and the EEG recorded with DBS turned OFF. We collected between 15 to 136, 3s artifact-free epochs for spectral analysis from each timepoint. Spectral power was calculated using the Chronux matlab toolbox, (see Chapter 2) on a laplacian montage. Alpha band power and alpha peak frequency and power were computed across the scalp. Edge electrodes were excluded due to artifact contamination (AF7, AF8, T5, T6, T7, T8)

Alpha asymmetry was computed by subtracting alpha power at the left scalp sites (e.g., left fronto-central sites F3, FC3) from the homologous right sites (F4, FC4), and dividing this difference by their sum. Positive values reflect greater right versus left frontal alpha power. The asymmetry ranges from 0 to 1 (max).

Results

Behavioral Results

Chronic scDBS had a significant impact on the behavioral status of the patients in the study. A positive response to stimulation was seen in 5/8 patients after 24 weeks (8/8 after 2 years). (See Table 3.1) A positive response was defined as a >50% change in Hamilton Depression Rating Scale (HDRS), which measures.

Table 3.1 Behavioral response of patients

The behavioral response of patients to scDBS is assessed using the Hamilton Depression Rating Scale (HDRS). A positive response (green) is defined as a ≥50% decrease in HDRS score after 24 weeks of scDBS stimulation, as opposed to a negative response (red).

	ID#5		ID#10		ID#24	
HDRS Score	T0	6M	T0	6M	T0	6M
	23	17	20	18	25	16

	ID#16		ID#17		ID#18 *		ID#19		ID#20	
HDRS Score	T0	6M	T0	6M	T0	6M	T0	6M	T0	6M
	21	10	21	9	20	10	25	3	25	3

EEG Results

The alpha peak changes significantly in all patients who receive scDBS. We illustrate the spectral power for 2 patients, one who showed a strong behavioral

decrease in HDRS (Figure 3.2), and one who did not. (Figure 3.3). Other frequency bands also show changes, but there are no consistent patterns that emerge across the cohort. We look at changes in the alpha band power, and alpha spectral peak power and frequency. The normalized alpha band power is relatively stable over time in healthy controls and patients who show a positive response to scDBS treatment (referred to as "responders" (See figure 3.4). The only significant difference in alpha power is in patients with no response to scDBS treatment, in the anterior frontal electrodes.

Figure 3.2 Example power spectrum of –responder

Blue represents spectral power of a responder at the first timepoint pre implantation of DBS electrods (201s of data), and magenta the second timepoint (372s of data), after 24 weeks of active stimulation. Arrows point to the marked changes in power at approximately 10Hz (alpha range).

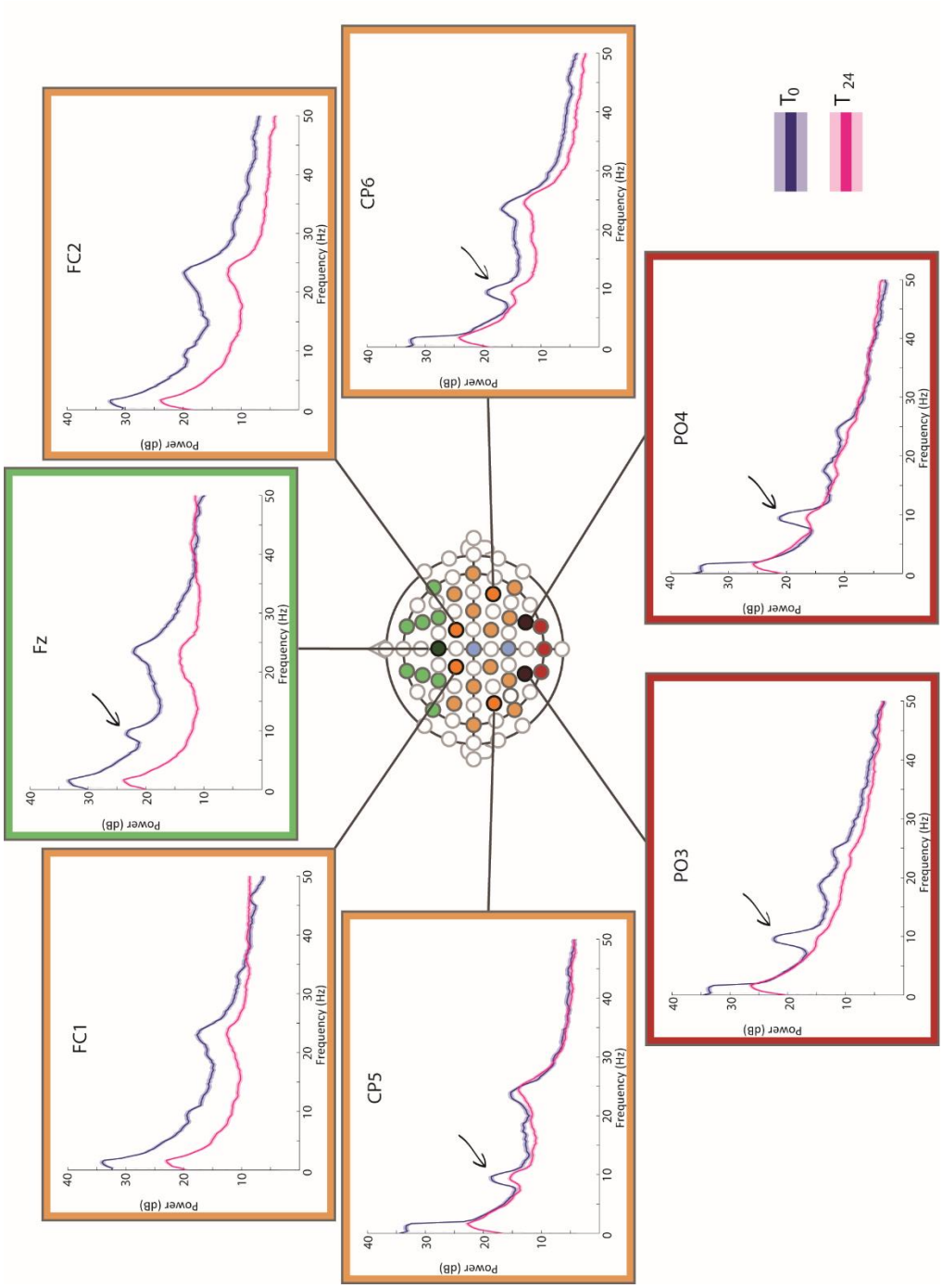
FC2
Fz
CP6
FC1
CP5
PO4
PO3
Power (dB)
Frequency (Hz)
T0
T 24

Figure 3.3 Example power spectrum of non-responder

Blue represents spectral power of a non-responder at the first timepoint pre implantation of DBS electrodes (144s of data), and magenta the second timepoint (87s of data), after 24 weeks of active stimulation. Arrows point to the marked changes in power at approximately 10Hz (alpha range).

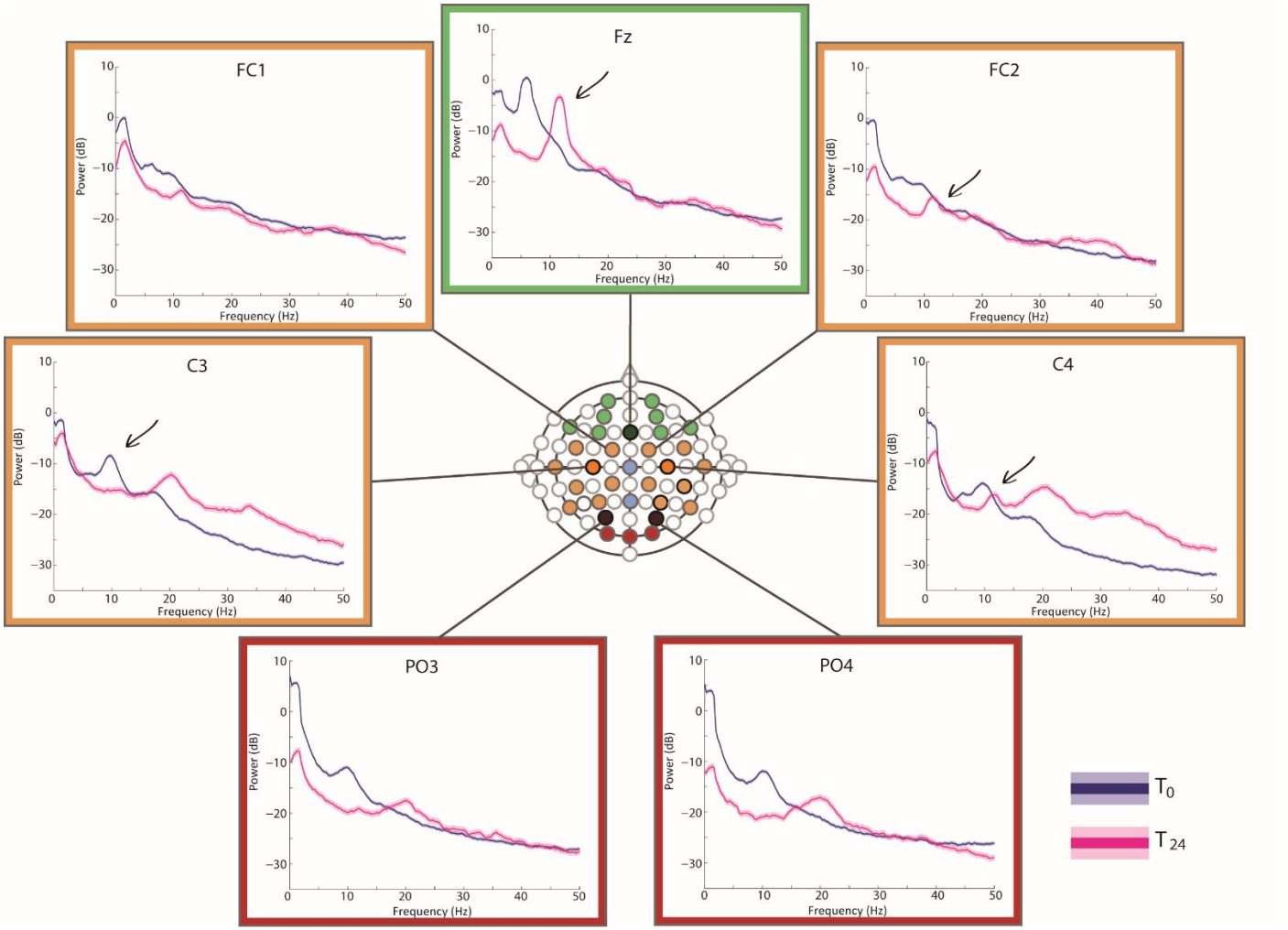
FC1
Fz
FC2
C3
C4
PO3
PO4
Power (dB)
Frequency (Hz)
T0
T24

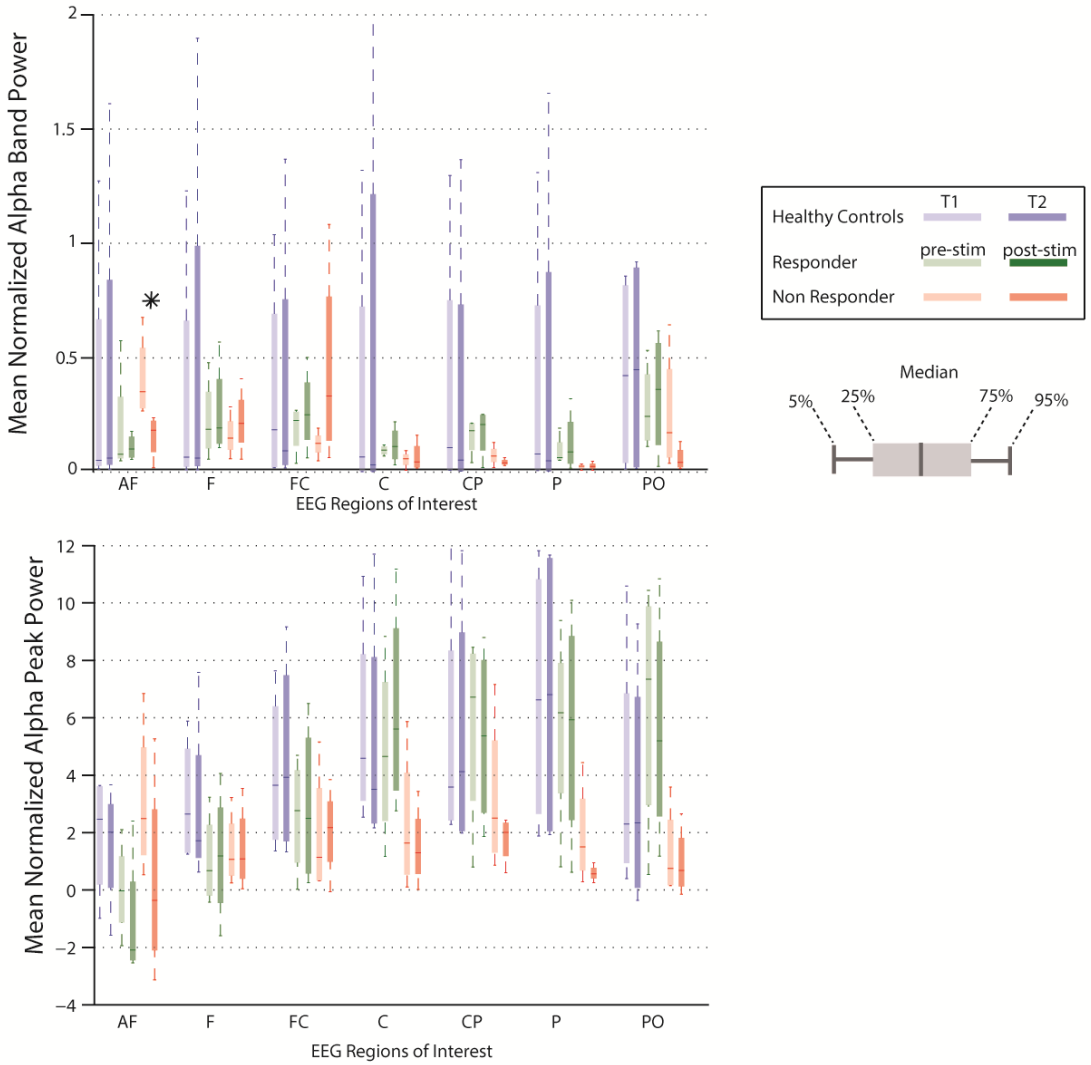

Figure 3.4 Means of normalized alpha band spectral power

Boxplot showing the distribution of the mean alpha band power (A) and mean alpha peak power(B) across EEG regions of interest for all HC and patients X axis represents the EEG regions of interest, (AF-anteriofrontal electrodes used: Fp2 - Fp1, F-Frontal: F8, F7, F4, F3,FC- Frontocentral: FC2, FC1 , FC6, FC5, C-Central: C4, C3, CP-Centroparietal: CP2, CP1, CP6, CP5, P-Parietal: P4, P3, PO-Parietooccipital: PO4, PO3, O2, O1). * represents significance (KS test, $p \leq 0.05$).

There are no significant differences in normalized alpha peak power between healthy controls over time, or patients before and after stimulation. (See figure 3.4). However, there is a significant trend showing decreased alpha peak power between

non-responders when compared to healthy volunteers in central and parietal brain regions.

The alpha peak frequency is also relatively stable in healthy volunteers tested over time. (See Figure. 3.4). However, patients who did not respond to scDBS showed an increase in alpha peak frequency, which shifts from approximately 9.5Hz to close to 11Hz on average.

The mean asymmetry index values are close to zero across all brain regions, in the healthy controls. This indicates there is no asymmetry in healthy adult brains in the alpha frequency range. There is a clear change in alpha band asymmetry between patients compared to healthy volunteers (See Figure 3.5). In patient subjects with scDBS, we see marked changes in different regions of the brain. Both responders and non responders show a normalization (increase or decrease, but closer to 0) of the asymmetry. Of note, we see a decrease mean asymmetry after stimulation in both responders and non-responders in frontal, frontal central, central, and parietal occipital regions. However, anterior frontal channels show no significant changes in responders, but a large decrease in non-responders.

In summary, we see that the mean alpha band is stable over 6 months in healthy volunteers. It is also stable in patients with a positive response to scDBS. However, non-responders show either an increase or decrease in alpha band power after stimulation. (see Figure 3.6). Similarly, the alpha peak power is stable in healthy volunteers. However, responders show a decrease in alpha peak power in anterior-frontal regions after stimulation. Non responders also show a decrease in alpha power, in AF channels.

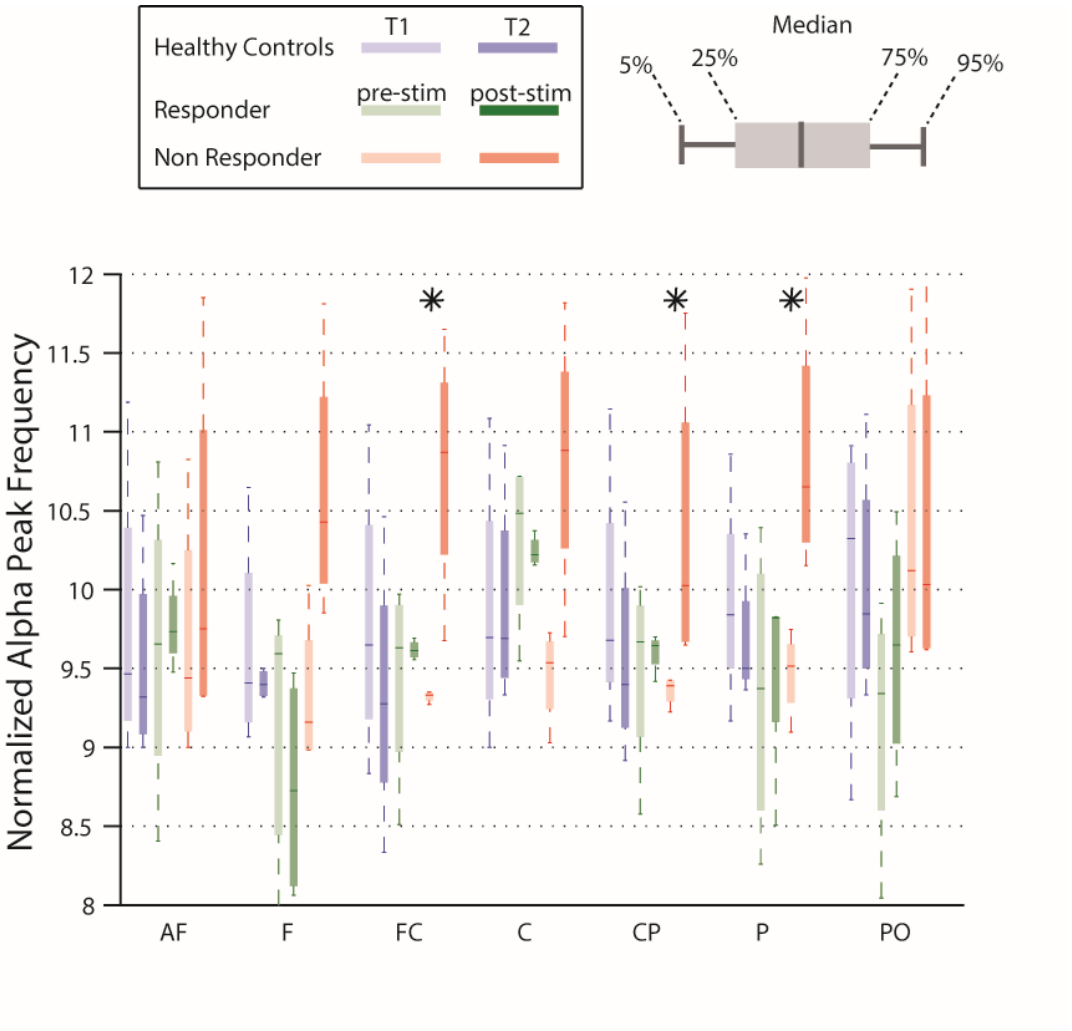

Figure 3.5 Means of normalized alpha band spectral frequency

Boxplot showing the distribution of mean alpha peak frequency across EEG regions of interest for all HC and patients X axis represents the EEG regions of interest, (AF-anteriofrontal electrodes used: Fp2 - Fp1, F-Frontal: F8, F7, F4, F3,FC- Frontocentral: FC2, FC1 , FC6, FC5, C-Central: C4, C3, CP-Centroparietal: CP2, CP1, CP6, CP5, P-Parietal: P4, P3, PO-Parietooccipital: PO4, PO3, O2, O1). * represents significance (KS test, $p \leq 0.05$).

Figure 3.6 Alpha Peak Asymmetry.
Boxplot showing the distribution of alpha band asymmetry in healthy volunteers (left) and patient subjects (right). The green asterisk shows the large decrease in asymmetry in the anterior frontal region between in the non-responders, which is not present in the responders. (AF-anteriofrontal electrodes used: Fp2 - Fp1, F-Frontal: F8, F7, F4, F3,FC- Frontocentral: FC2, FC1 , FC6, FC5, C-Central: C4, C3, CP-Centroparietal: CP2, CP1, CP6, CP5, P-Parietal: P4, P3, PO-Parietooccipital: PO4, PO3, O2, O1).

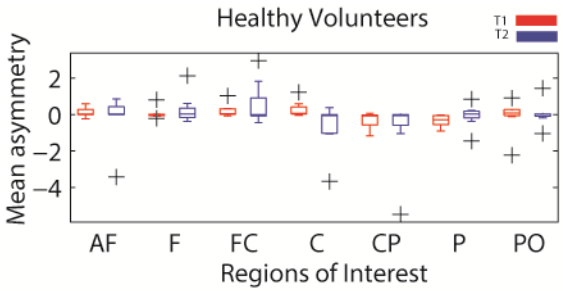
Healthy Volunteers
T1
T2
Mean asymmetry
2
0
−2
−4
AF
F
FC
C
CP
P
PO
Regions of Interest

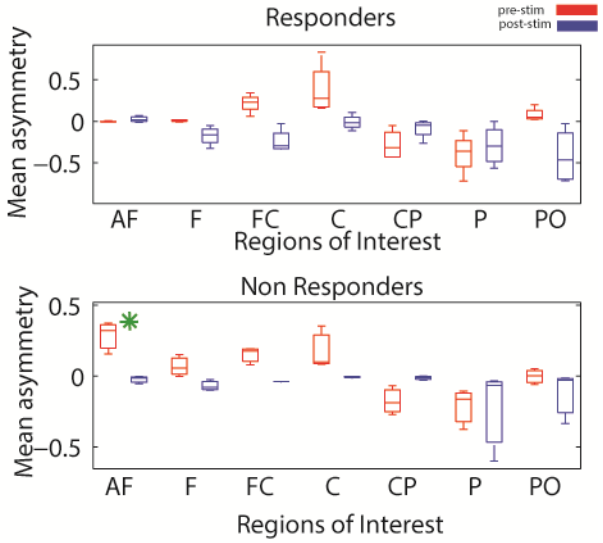
Responders
pre-stim
post-stim
Mean asymmetry
0.5
0
−0.5
AF
F
FC
C
CP
P
PO
Regions of Interest
Non Responders
Mean asymmetry
0.5
0
−0.5
AF
F
FC
C
CP
P
PO
Regions of Interest

Discussion

The alpha band is the most stable feature of the EEG. It has been shown that peak alpha frequency and the mean frequency in the alpha band were highly reliable both over short time periods 12-16 weeks (Salinsky et al, 1991), and long time periods (Napflin et al, 2007). While the average power in the alpha band can be useful, it fails to take into account changes in frequency peaks, and may also minimize changes in peak frequency power, which are known to vary significantly. Therefore, in order to keep track of frequency peak changes, we use a method developed in Gottselig et al to quantify peak measures. We quantified the peak changes in healthy volunteers over time, to characterize changes due to normal fluctuations in cognitive state and other artifacts. We see that alpha peak changes significantly in most subjects across multiple channels, more so in non-responders. While the alpha band power and alpha peak power show similar small changes, the alpha peak frequency is the most variable in patients who do not respond to stimulation, and alpha peak asymmetry in anterior frontal regions differs in responders and non-responders.

These findings demonstrate that scDBS can fundamentally alter the spectral power distribution of the resting EEG demonstrating a physiological correlate of long-lasting network changes induced by the therapy. When we do note changes in spectral peak frequency, they are not limited to one channel but many (10-50% of channels). This shows that the stimulation of the SCC has a global effect on brain function. The decrease in mean asymmetry noted in both responders and non-responder patients is indicative of the normalization of brain activity – post stimulation, the asymmetry values in most regions trend to 0 (no asymmetry), matching healthy volunteer values. It is important to note that the non-responders, while non-responders at 24 weeks, were considered responders at a 2 year follow up. This may indicate the importance of

the anterior forebrain in depression networks. In responders, the mean asymmetry in anterior-frontal channels is already close to 0. However, non-responders have abnormally high left asymmetry. This specific change in dynamics, observed in some patients by 24 weeks is indicative of a recovery to normal alpha network activity.

Finally, the changes in alpha peak frequency indicate that shifts towards higher frequencies might be indicative of abnormal dynamics inviting further consideration of the role of abnormal network activity in patients who are not responding to scDBS. For patients who are non-responders it is particularly important to consider the site of tissue activation. Findings by Choi and Riva-Posse (2014) indicate that scDBS impacts fibers linking the two frontal lobes via the forceps minor relative to uncinate fasiculus fibers connecting SC25 to the ipsilateral medial frontal cortex. A difference in tissue activation may help explain the differences in alpha peak frequency observed in the non-responders. The EEG alpha band might therefore prove to be an efficient way to monitor the correct activation of the medial frontal cortex, and also a way to identify potential future responders to scDBS.

Chapter Conclusion

In summary, we find that there are many ways to compare spectral power, and that these measures are appropriate to study differences in human neurophysiology over time. In this chapter, we focused on the characterization of the alpha band and its properties as PS respond to scDBS therapy for treatment resistant depression. As seen here, innovations in normalization techniques can provide more details than simply averaging the power in one spectral band of interest, and correct for any changes due to new recording artifacts such as changes in levels of baseline noise or different electrode placement.

However, the spectral changes noted may be linked to changes in internal state. To quantify measures linked to more direct structural and functional changes, we consider graph theoretic approaches to spectral coherence. In the next chapter, we apply these measures to patients with recovery from severe traumatic brain injuries.

Chapter Four: Common brain network reorganization underlies recovery of communication

Abstract

Late recovery of communication after severe brain injuries can occur at arbitrarily long time intervals and often go unnoticed, framing an ethical and scientific challenge which affects both medical decision making and care-giver life preserving decisions (Fins, 2015). Reestablishing the use of language or a proxy communication system represents an ethical "bright-line" distinction amongst minimally conscious patients crucial to harnessing further rehabilitation. Thus, understanding the underlying mechanisms of recovery is important to improve methods for recognizing recovery. Single-subject studies have tracked the recovery of communication in brain injured patients and suggest a key role for brain structural reconfiguration in both expressive language networks and cross-hemispheric connectivity (Voss et al., 2006, Thengone et al., 2016). Here we verify and extend these results to patients in following severe brain injuries. To prospectively capture recovery of communication, we longitudinally measured wakeful resting electroencephalographic (EEG) activity

over time. Similar measurements were obtained in an age-matched control group of healthy volunteers. We employ graph theoretic methods to characterize global and local changes in EEG derived brain networks. We use spectral coherence as a measure of network connectivity and, based on earlier studies, test an a priori hypothesis that dominant language hemisphere and cross-hemisphere coherence network will increase in the EEG of patients recovering communication over time (Thengone et al. 2016).

We summarize our results here. Ten patients with severe brain injuries (eight in minimally conscious state, two studied after emergence from minimally conscious state) and six age-matched healthy volunteers were studied longitudinally (from a total of 36 independent in-patient admissions, each with 1-3 days of continuous video-EEG recording). We computed spectral coherence between all electrode pairs, global coherence network measures (total, left, right, and cross-hemisphere density, degree centrality small-world coefficient and efficiency) and local coherence network measures (clustering) for all subjects using coherence estimates obtained with multi-taper spectral analysis within different frequency bands. In healthy volunteers, network estimates based on theta frequencies (4-8Hz) demonstrated optimal stability, and no statistically significant changes arose over longitudinal measurements. In patient subjects, a subgroup of 7 out of 10 patients studied showed late recovery of communication. All seven patients demonstrated changes in theta network graph theoretic measures. Coherence network density increased in the dominant language hemisphere of all seven subjects, and in the non-dominant and in cross-hemisphere networks of a subset of five subjects. These findings support our a priori hypothesis

that increases in functional and structural connectivity of the dominant language hemisphere and across the cerebral hemispheres are linked to recovery of communication. This pattern of recovery is similar to the reorganizational processes observed in aphasic patients who recover language after a stroke (Rijntes, 2006), and changes observed in healthy subjects while learning new languages (Schlegel, 2012). This suggests that after a severe brain injury, the brain follows an inherent process of recovery regardless of etiology, which we believe is driven by inner speech.

Introduction

Measurements of changes in brain function that evolve over time after severe structural injuries present a significant challenge. While neuroimaging techniques allow whole brain visualization, structural injuries and patient movement significantly limit the ability to consistently obtain longitudinal measurements using these techniques. The EEG is a direct measure of electrophysiological activity reflecting underlying cortical networks and circuitry (Nunez, 2006) that can be easily obtained over long periods of time. Oscillations in the EEG reflect fluctuations in the synaptic electrical synchrony between neuronal assemblies (Buzsáki and Wang, 2012) and the linear correlation of oscillations across brain regions can be quantified by coherence, a measure of the phase consistency between two electrodes. This measure is well validated in the literature (Nunez 1997, Weiss and Mueller 2003). Coherence measures can also be used to explore brain networks using the methods of graph theory (Stam et al 2012, Lee et al 2013, Kramer et al 2010, Matlis et al, 2015). Combining graph theoretic approaches with more traditional spectral techniques provides powerful tools to summarize the EEG signal and measure global functional connectivity changes in complex brain networks (Bassett and Sporns, 2017). Recent studies have demonstrated that EEG graph networks are statistically robust when estimated from resting states in healthy volunteers and demonstrate changes in neurological disease (Hardmeier et al, 2014, Telesford et al, 2013). Other studies have shown the efficacy of EEG brain network measures to predict metabolism and diagnosis of disorders of consciousness (Sitt et al, 2014, Chennu et al, 2014, 2017) suggesting their use to characterize longitudinal changes that may arise following severe brain injuries. Here, we use network EEG measures to track the recovery of communication and language longitudinally.

We prospectively and longitudinally collected EEG data from a cohort of severely brain-injured patient subjects (n=10) and a group of age-matched healthy volunteers (n=6). Each patient subject had 48-72 hour recordings made at each time point of evaluation and concurrent standardized quantitative behavioral assessments (See Methods). For all subjects we obtained at least 90 seconds of artifact free EEG from resting periods identified as eyes-open awake from each time point through visual observation from contiguous video recordings and review of the raw time evolving EEG signal (See Methods). For each set of EEG recordings we computed functional networks from the weighted spectral coherence within separate frequency bands (Kramer et al. 2008, see Fig. 4.1 and Methods); network measures were summarized utilizing density, degree centrality, clustering, path length, and small worldness (see Methods).

Figure 4.1 Schematic of graph theoretic methods and summary of findings in patient 1.

A) Clean resting awake EEG data in channels F7 and F8.
B) Patient 1 shows a significant decrease in delta coherence, and a significant increase over the theta band.
C) Weighted theta networks for Patient 1 over 5 timepoints. Frontal cross hemispheric coherence power increases over the 5 visits, as well as intrahemispheric pairs within the left hemisphere.
D) A low threshold (0.2 coherence) generates a graph with a high density (many connections between pairs of electrodes). A high threshold (0.6 coherence) generates a graph with low density. The blue box shows the range of interest (0.1-0.6). All error bars represent 95% jackknife confidence intervals.

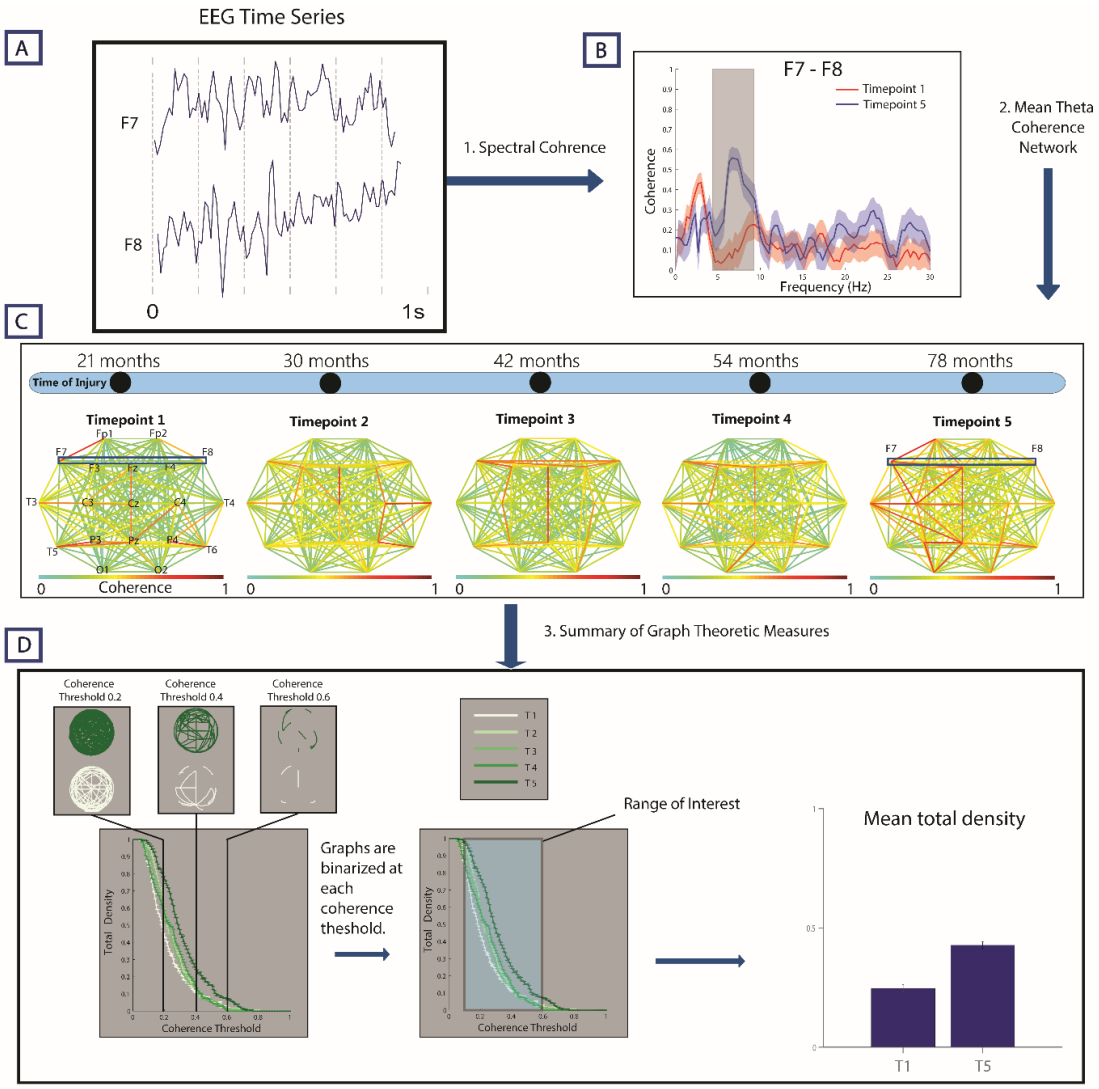
EEG Time Series
A
F7
F8
0
1s
1. Spectral Cohrence
B
F7 - F8
Timepoint 1
Timepoint 5
Coherence
Frequency (Hz)
2. Mean Theta Coherence Network
C
21 months
30 months
42 months
54 months
78 months
Time of Injury
Timepoint 1
Timepoint 2
Timepoint 3
Timepoint 4
Timepoint 5
Coherence
3. Summary of Graph Theoretic Measures
D
Coherence Threshold 0.2
Coherence Threshold 0.4
Coherence Threshold 0.6
Total Density
Coherence Threshold
Graphs are binarized at each coherence theshold.
T1
T2
T3
T4
T5
Range of Interest
Mean total density

Dynamical studies of the brain at rest are particularly valuable in the study of neurological disorders such as traumatic brain injury where the effects of the injury are pervasive across the whole brain. Mechanisms of recovery in these cases take place across the brain (Fridman et al, 2014), suggesting that global measures might indicate recovery across multiple levels, making functional networks a natural measure to explore.

Here we used network density measures to assess the relative EEG coherence connectivity strength within left, right, and between hemispheres. The density was assessed at a range of coherence thresholds (between 0 and 1 with 0.01 steps) in order to explore the full range of possible thresholds, and exclude any possibility of binarization bias (see Methods). To establish test-retest reliability of these measures, we first assessed their behavior in the longitudinal records of the healthy volunteers. Across frequency bands examined, all our measures remained stable in specific threshold ranges. Reliability was assessed across two measurements taken 6 months apart in healthy volunteers using the intraclass correlation coefficient statistics (ICC), a non-parametric way of assessing test-retest reliability (Telesford et al., 2010; Montgomery et al., 2002). In the theta band, the ICC values were consistently above 0.8 between coherence thresholds of.1 to .8 for density and efficiency, denoting near perfect agreement. ICC values for clustering were consistently above 0.6, which shows very good agreement. Finally, ICC values for small world coefficient were only reliable for a small range of thresholds, corresponding to networks with denser connections for most graph theoretic measures. (See Chapter 2, Figure 2.10 and Figure 4.2)

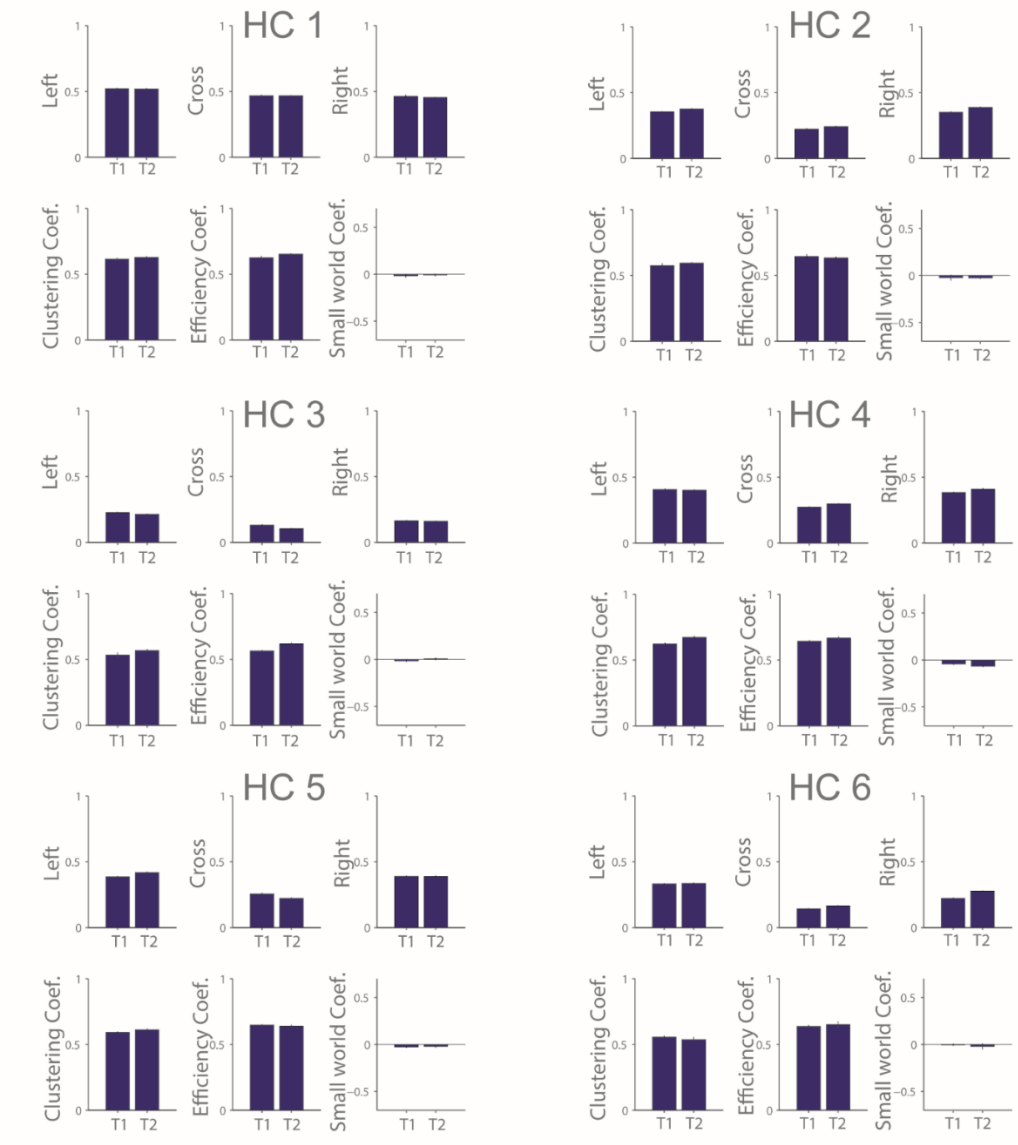

Figure 4.2 Test-Retest reliability of theta coherence networks in healthy volunteers.

Left, right and cross hemispheric density for theta coherence networks are averaged between coherence thresholds of 0.1 to 0.6. Clustering and efficiency are calculated and averaged for all thresholded networks containing between 10% and 90% of total density. Small world coefficient is calculated for all thresholded networks when estimable (see Methods). Error bars are 95% jackknife confidence intervals.

Having demonstrated the stability and consistency of the density measures and hub structures in our healthy volunteers we then applied the same analysis to longitudinal records obtained from ten severely brain-injured patient subjects. In the patient cohort, longitudinal measurements ranged from intervals of 7 to 121 months (average interval 30 months, median 17m) (See Fig. 4.3).

Figure 4.3 Summary of graph theoretic measures in theta coherence networks
Significance is only shown when the difference between visits is larger ($p<0.05$) than the mean difference between visits in healthy volunteers. Error bars are 95% jackknife confidence intervals. Significance is denoted by *** and represents $p<0.001$ (t-test).

A) Summary of graph theoretic measures in patients who recover an overt mean of communication over time.

B) Summary of graph theoretic measures in patients who do not show any recovery of communication

A
PS 1
PS 10
PS 2
PS 3
PS 6
Left Hemisphere
Cross Hemisphere
Right Hemisphere
Clustering Coeff.
Efficiency Coeff.
Small world Metric
T1
T2
T3
T5

Figure 4.3 Continued

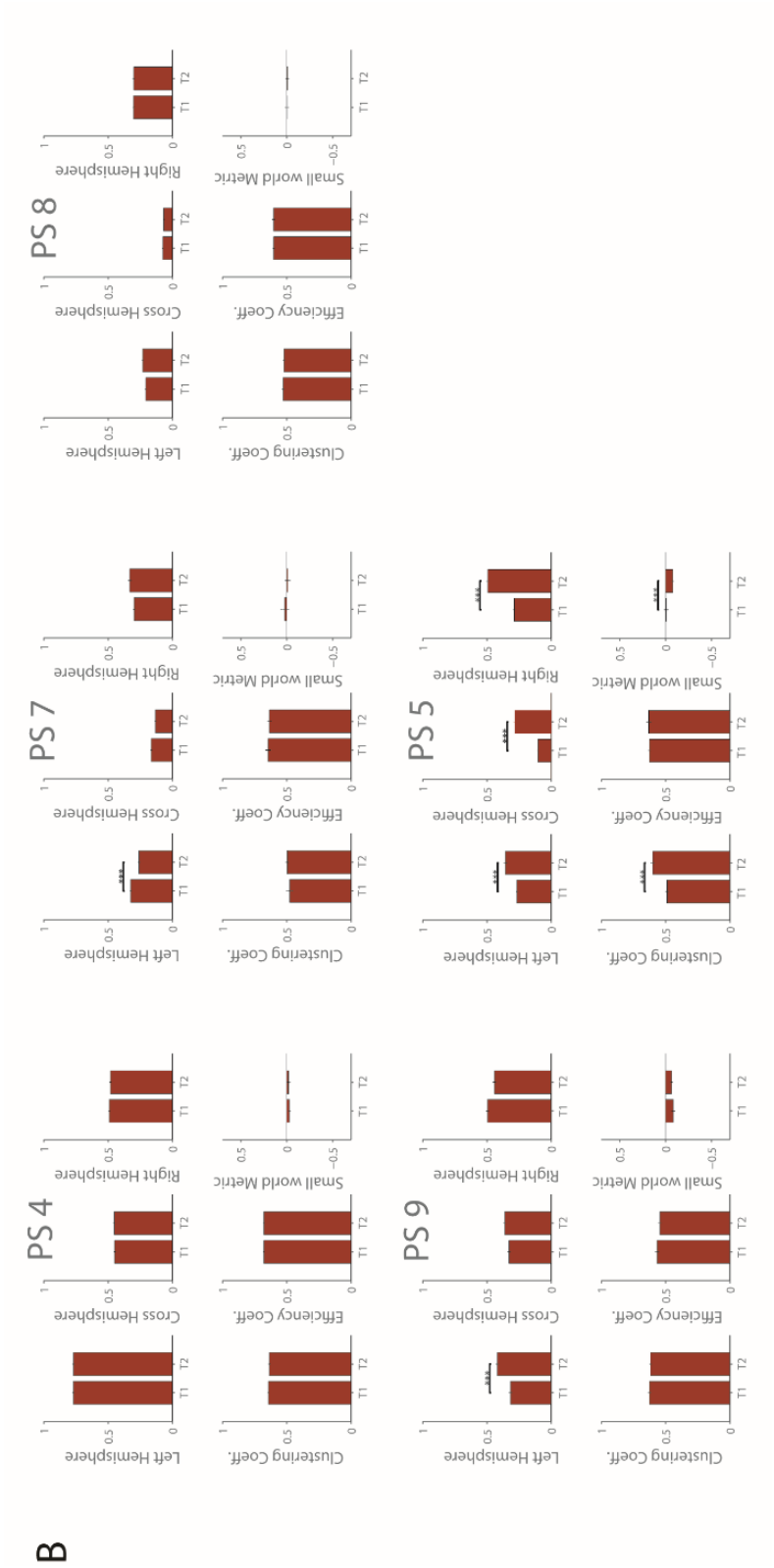

Five patients within the cohort demonstrated late recovery of communication. The transition from non-communicative to gestural or spoken language communication was captured in our measurements in two of the five subjects who demonstrated recovery (one subject had reestablished communication shortly before our studies after a 19 year period). The remaining three patient subjects showed no behavioral changes between each measurement. Other bands of interest did not show similarly robust findings across either healthy volunteers or patients (See Chapter 2. Fig. 2.11 for HC test-retest reliability.).

Of those five patients without changes, four are MCS; out of these four MCS patients, two show changes in density which were similar to a patient who recovers communication. Moreover, these two subjects show remarkably similar node degree structures to the healthy group (see Figure 4.4). We observe a common pattern of network changes in all five patients with measured recovery of communication. We find that all five subjects with a behavioral measured transition to the recovery of a communication system show a common pattern of significant network changes over time. All patients show an increase in the left language dominant hemispheric density networks ($p<0.001$). (Fig. 4.3A). Furthermore, the degree centrality showed consistent increases between the first and last visit, with both showing absolute hub strength increasing across all regions (Fig. 4.4) for patient 10. Of the patients who show recovery of language via either spoken or gestural communication, four have significant Inter-hemispheric right increases in network density. (Fig. 4.3A) (values <0.001), and 3 have significant increases in network local clustering (Fig. 4.3A) (values <0.001). Of the five patients who showed no behavioral improvements, we see significant network changes in two patients (Fig. 4.3B). These two patients show increases in network density and degree centrality.

Figure 4.4 Theta coherence network centrality over time

A) Bar graphs represent the absolute node degree of the EEG channels (see colors in headplot).The black lines in the bar graphs show the average healthy control response. We only plot one patient with recovery (patient 10) because this is the only patient with recovery recorded with 37 channels. The rest of the patients only have 19 EEG channels, making it impossible to compare to the rest of the cohort, because the node degree is not normalized.
B) Absolute node degree of 6 healthy controls at two timepoints (approx.6 months apart, 1st timepoint on left, second timepoint on right)
C) Absolute node degree of 5 patient subjects who show no behavioral recovery of communication.
D) Absolute node degree of one patient with recovery of language over time.

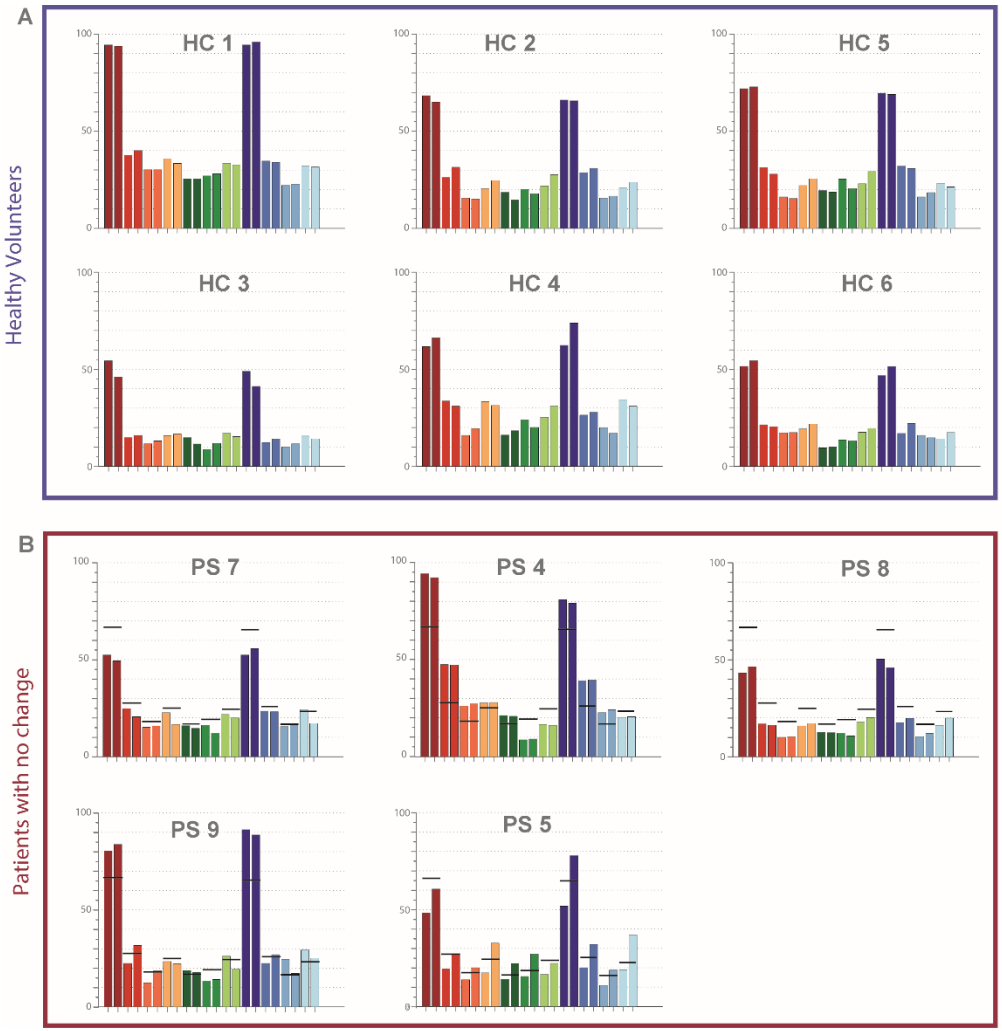
A
Healthy Volunteers
HC 1
HC 2
HC 5
HC 3
HC 4
HC 6
B
Patients with no change
PS 7
PS 4
PS 8
PS 9
PS 5
Legend
ParOccRight
TmpRight
CenParRight
FrtRight
ParOccMid
CenParMid
FrtMid
ParOccLeft
TmpLeft
CenParLeft
FrtLeft
C
PS 10

Our results here uncover a common pattern of global reorganization in patients who recover communication: coherence graph theoretic networks in the theta frequency range consistently show increases in their density within the left hemisphere of all five patients who recover communication. Additionally, the right and cross hemispheric theta graph network coherences demonstrated increases in 4 out of the 5 patients with recovery, while all of these measures remained stable over time in healthy volunteers (Figure 4.1 and 4.2). The reliability of our healthy volunteer findings is comparable to recent studies (Chu et al., 2012) that demonstrate a stable or core template of EEG graphs emerging over time and across brain states (sleep or awake) in healthy subjects. Similarly, other studies using related EEG graph theoretic measures show good reliability in healthy volunteers followed over one and two year time periods (Hardmeier et. al. 2014). Consistent with these prior studies we find that our measures are most reliable in healthy subjects within the theta and alpha bands. No prior study, however, has examined the reliability of coherence EEG graph theoretic measures in longitudinal 24-hour EEG recordings using pasted electrodes and continuously recorded video to validate state measures.

Of the four patients who demonstrated recovery of communication across our measurements, initial evaluations in each occurred at least 12 months after injury (range 12 months to 21.5 months). The recovery of a measurable communication channel (CRS-R Comm 1) arose at least 7.5 months after initial evaluation (range 7.5 months to 10 years) in each case. The fifth patient with recovery of communication had remained without an evident communication channel for 19 years after injury when spontaneous recovery of spoken language first developed; our measurements here track a period beginning 8 months after first recovery of communication and span an additional 18 months during which further improvements in cognitive and motor functions were measured (Voss et al. 2006). Thus, these common network changes

that correlate with the functional recovery of communication in this group of patient subjects can arise very late in the convalescence period following a severe brain injury. Moreover, in our group of five subjects with late recovery of communication, changes occurred across a wide age range (18-58 years old at the time of initial injury; 20-61 years old at the time of recovery of communication) and following a broad mix of underlying etiologies (traumatic brain injury (2), stroke (1), intracranial hemorrhage (1), hypoxic-ischemic encephalopathy (1)). Our observations of such a long latency recovery process are consistent with small cohort studies of the natural history of disorders of consciousness in patients followed longitudinally (Luaute et al. 2010, Katz et al. 2009, and Yelden 2017). These observations demonstrate the existence of general mechanisms underlying recovery of communication in the injured brain that allow for similar large-scale network reorganizations in young adults following traumatic injuries and middle-aged adults with global hypoxic neuronal injuries.

Discussion

Prior studies have shown the utility of EEG in the study of disorders of consciousness, particularly in the theta range (Schiff et al, 2014). Sitt et al (2014) identified quantitative EEG features that reliably characterized patients as either in coma, vegetative state or minimally conscious state; specifically, the absolute power within theta and alpha bands efficiently indexed states of consciousness. Chennu et al. expanded on these results, demonstrating that certain quantitative metrics of functional EEG networks correlated strongly with brain metabolism and successfully indexed patients as minimally conscious prior to any behavioral diagnoses. (2012, 2017). Thus, our findings of progressive changes in theta coherence networks are consistent with a stratification of these measures in cross-sectional cohort studies. Changes in

states of consciousness induced by propofol anesthesia also show a disruption of the theta coherent networks, including a decrease in degree centrality of the hubs after loss of consciousness (Lee et al, 2013). These results can be compared with the recovery profile of patient 10 which shows an increase in degree centrality (Figure4.3).

Our findings comport with previous reports of longitudinal structural changes in patients recovering from traumatic brain injuries utilizing diffusion tensor imaging (DTI) (Sidaros et al. 2008). Prior prospective longitudinal studies of recovery of communication in minimally conscious patients, however, have been restricted to only single case studies (Voss et al., Thengone et al). Thengone et al. previously reported on longitudinal changes in DTI and functional magnetic resonance imaging measures in patient 1, tracking their recovery of inconsistent communication through an eye tracker slowly over 4 years (see Fig. 1). In this subject BOLD activation patterns measured using fMRI at timepoint 1, 3 and 4 (Figure 1), showed growing clusters of activity in Broca's area during the presentation of language stimuli and increasing positive inter-hemispheric correlations (Thengone et al. 2016). DTI measured across timepoints 1 and 4 showed marked increases in fractional anisotropy (FA) of fibers arising from the expressive speech region (Broca's area) connecting inter- and intra-hemisphere areas important for expressive speech. Thengone et al. propose that the DTI measured changes reflect a mechanism of recovery in this patient of ongoing structural changes occurring across a period of ~3 years. Here we find correlative changes in the EEG coherence graph consistent with structural and functional change reported by Thengone et al. emanating from the left hemisphere and extend the results to a fifth time (Figure 2) that shows a further significant increase in left hemisphere graph density supporting the inference that such an ongoing process of structural reorganization continued. In patient 2 studied here, as earlier reported by Voss et al. (2006), correlated changes in FA measured by DTI correlated with cerebral metabolic

changes and ongoing behavioral improvements including articulatory speech; in this subject reemergence of language pre-dated the studies. Of note, the most prominent change in hub degree observed for this patient matches the regions of medial posterior parietal increases seen in FA (Voss et al. 2006, Supplementary Figure).

Collectively, our EEG coherence network increases observed across the cohort of patients recovering communication correlate with the prior DTI measurements in patient 1 (316) and 2 (346) and support a role for structural changes in the white matter underlying our findings. Myelin production may occur in the adult brain and may be modulated by neuronal activity (Tomassy et al, 2016). Ongoing changes in healthy brain structure and function are common. For instance, increases in EEG coherence are particularly likely during the first year of life, when there is widespread myelination of axons and synaptogenesis (Huttenlocher et al, 1990); however, changes in structure may also occur later in life and correlate with increased neural synchrony in theta, beta and gamma bands observed in late adolescence (Uhlhaas et al, 2009). Increased theta band connectivity has been specifically linked to stronger white matter connectivity (Cohen, 2011), and isolated increases in theta and beta coherence increases in node degree have been correlated with function recovery and clinical improvement after stroke. (Nicolo et al, 2015).

Our findings can be directly compared with DTI studies of new language acquisition and recovery from aphasia. In healthy adult subjects, acquiring a new language results in increased white matter tracts traditionally associated with left hemisphere language areas and their right hemisphere analogs via the frontal lobe genu of the corpus callosum (Schlegel et al, 2012). DTI findings in recovery of language in aphasia show increases in FA in language dominant left hemisphere, right hemisphere or bilateral connectivity, strongly correlating the patterns of EEG theta coherence graph networks measured here during recovery of communication (Schlaug,

2009, Bohland & Guenther,2006; Brown, et al, 2004; Özdemir et al., 2006). Of interest, we also find that all patients subjects who show an increase in right hemispheric networks (n=5) also show an increase in cross hemispheric networks, indicating that these two mechanisms might be mechanistically linked.

Importantly, in two patients (5 (373) and 9 (435)) measured here we observed similar changes in left hemisphere and cross-hemisphere EEG theta coherence network density and reorganization of hub degree to match the dominant pattern in our healthy volunteer cohort in the absence of behavioral improvement. While both patients had assessment scores in the MCS range, evaluation of command following utilizing fMRI or EEG methods showed that both could carry out high-level mental imagery. These findings are consistent with the patients demonstrating cognitive motor dissociation, CMD, in which imaging or electrodiagnostic evidence of higher-integrative brain function is present in behaviorally unresponsive or minimally responsive patients (Schiff 2015). CMD patients show evidence of highly preserved cerebral integrity (Forgacs et al. 2014, Stender et al. 2014, Schiff 2017). Correlating our EEG graph network changes, both patients showed significant increases in global FDG-PET signal measured across the two time points (Supplementary Figure); these observations suggest the possibility that in CMD patients a similar mechanism of language recovery may be present without evidence of language function.

Emergence of expressive language has recently been noted to correlate with inner speech in young humans. Recent studies have shown that inner speech may also play an important part in the development of language in infants, (Perrone-Bertolotti et al, 2014, Mani & Plunkett, 2010, Ngon & Peperkamp, 2016), showing that toddlers are capable of producing covert words and using these words to prime responses to spoken matching tasks. Inner speech is estimated to occur for as much as 25-30% of the wakeful day in healthy adults and provides an intrinsically generated, frontal

language-related network activation pattern of activation (Heavey and Hurlburt, 2008). Thus, recovery of inner speech may precede overt recovery of communication in patients with limited or no motoric output. The possibility that inner speech can be restored prior to outer speech is supported by observations in patient 1 (316) and 4 (363), who both produces instances of spoken single words 5 years and 8 years after injury. Each case occurred after years of intermittent communication (Patient 1) and fluent augmented technology (Patient 4). Thus, one of the strongest potential drivers of recovery of communication after injury may be the innate generative nature of speech.

Our data provide novel evidence of a consistent modular functional re-organization of the brain over time following many types of severe-injury to support recovery of communication. These changes are likely ongoing in many prior to behavioral evidence and likely follow an intrinsic drive of the brain to restore functional communication, analogous to the developmental processes underlying language acquisition. Tracking the EEG functional networks described here may provide an efficient and statistically robust method to identify early recovery in patients. Such approaches are critical to identifying potential patients with the potential for cognitive motor dissociation disorders (Schiff 2015) or in need of rehabilitation. When combined with the findings from Kashi, Richardson, Luaute et al, 2010, and Yelden, we have clear evidence that the severely injured brain is trying to heal, albeit slowly. This recovery in brain injured adults appears to be a process that can emerge over extraordinarily long time scales, systematically showing slow alterations of brain structure and connectivity (as seen in Thengone et al).This finding strongly encourages greater efforts to track recovery across this patient population. Here we provide a cheap and efficient tool to screen large populations. While we have found that the process of recovery of communication is one that can be engaged over

long time intervals, a supervised effort to initiate and track recovery of language networks may aid a large number of currently ignored brain-injured patients.

Methods

The EEG was recorded using either a double banana montage or an augmented double banana montage (19+18 channels), placed according the 10-20 international system (Jasper 1958), using a standard clinical recording system (Xltek, of Natus Medical). Signals were sampled at 200- 250Hz, and all data were stored and analyzed under RUH and WCMC protocols.

EEG was collected during baseline resting state, during which patient subjects were awake. They were monitored for changes in arousal level, and resting data of 5-10 minutes was collected every hour over a 6-hour study session. Healthy subjects (6 volunteers, 3 F, 3 M, Mean Age 33.8) were admitted to the Rockefeller University with no history of neurological disease. They spanned a range of ages (23-51) matching our patient population and were tested twice, between 22-26 weeks apart. Patients (4 F, 6 M, Mean Age 28.7, range 22-59, at first timepoint) were admitted to either the Rockefeller University or the NY Presbyterian hospital (See Table 4.1). Data of 2s or 3s segments were visually selected from the record, eliminating muscle and eye movement artifacts, and selecting segments where the patients were awake. A minimum of 90s of clean data was used in all of our calculations.

We applied a surface laplacian montage to minimize volume conduction artifacts. The laplacian estimates are calculated by averaging the signals from the nearest-neighbor (e.g. Hjorth). This approach has been shown to eliminate all reference and most volume condition effect at distances a little longer than inter-electrode spacing (Nunez, 2006; Nunez and Pilgreen, 1991). The channel CPz was

used as the reference electrode. Data were analyzed with Matlab R2014b software (Math Works, Natick, MA) and using scripts based on the EEGLAB 11.0.5.4b toolbox (Swartz Center for Computational Neurosciences, La Jolla, CA; http://www.sccn.ucsd.edu/eeglab). All data were filtered at a 0.1Hz filter to minimize slow drifts.

Table 4.1 Summary of Patient Demographics

Subject	Timepoint	Age at injury (y)	Time since injury	Sex	Race	Etiology	Cortex lat.	Thalamic lat.	Best CRS-R	*CRS-R Communication Subscale*
316	1	22	**21.5m**	F	W (NH)	CVA (basilar)	none	b/l	**9**	0
	2		30.5m						**9**	0
	3		42m						**13**	1
	4		54m						**14**	1
	5		78.5m						**12**	1
354	1	58	12.5m	F	W (NH)	CVA (fat emboli)	b/l	b/l	**14**	0
	2		20m						**19**	1
	3		32m						**22**	2
356	1	20	20y	M	W (NH)	TBI	R	none	**23**	2
	2		21y						**23**	2
388	1	20	15m	M	W(H)	TBI + ICH	L	none	**9**	1
	2		11y						**23**	2
435	1	18	17m	F	B	TBI			**10**	0
	2		34m						**23**	2

Patients with Behavioral Recovery of Language

Subject	Timepoint	Age at injury (y)	Time since injury	Sex	Race	Etiology	Cortex lat.	Thalamic lat.	Best CRS-R	*CRS-R Communication Subscale*
363	1	23	25m	M	W (NH)	TBI	b/l	none	**14**	n/a
	2		6y 4m						**23**	2
392	1	17	9y 4m	M	W (NH)	TBI	L	b/l	**9**	0
	2		10y 5m						**11**	0
414	1	21	5y 5m	M	W (NH)	TBI	L	L	**17**	1
	2		6y 4m						**14**	0
419	1	12	10y6m	F	W(NH)	TBI			**12**	0
	2		13y8m						**13**	0
373	1	16	8y	M	W(NH)	TBI			**9**	0
	2		9y2m						**7**	0

Patients with No Behavioral Recovery

Methods – detailed procedure (Fig.4.1)

- We selected 30+ 3s segments of awake baseline, using video to verify arousal state.

•We calculated average coherency was calculated for all bands of interest, using a multi-taper approach (Chronux Matlab toolbox, Bokil et al). 5 tapers were used, for a frequency resolution of 2Hz, and coherency values were averaged in every band of interest (delta,[0-4] theta [4-8], alpha [8-12], beta [12-20], gamma [20-50]).Coherence values in each band were averaged in each band of interest, creating a weighted matrix of values.

•Functional networks were calculated from the weighted coherence measures by thresholding the graphs at varying coherence thresholds between 0 and 1, 0.01 steps apart. For each binary network, graph theoretical measures were calculated, with 96% jackknife estimate error bars.

•In healthy volunteers, we assessed reliability of the networks using the intra-class coefficient (Deuker et al, 2009, Braun et al, 2012, Telesford et al, 2010). We used the ICC to decide on the threshold ranges to use in our summary measures.

•We estimated the density, (left, right and cross hemispheric), efficiency, clustering coefficient, degree centrality and small worldness of all the networks at coherence thresholds from 0.01 to 1, in 0.01 increments.

•For the density measures, we averaged all measures between coherence threholds of 0.1 and 0.6. For clustering, we used any range which contained between 10% and 90% of graph network edges. Finally, for small worldness, we used only ranges which contained networks with connected graphs and with densities > 0.2 (see methods) to avoid errors caused when the networks are too sparse.

•Language recovery is measured by a combination of motor behavior (response to commands) or positive command following functional imaging paradigms as

developed by expert neurologists (Goldfine et al, 2011, Bardin et al, 2012, Forgacs et al, 2014).

•Network centrality was assessed by calculating the node strength at every EEG electrode. We then added the values of the node strength for electrodes in the same brain location (See Figure 4.4)

Chapter Five: Towards novel quantitative approaches to monitoring neurological disorders

This research provides novel methods for accurately diagnosing brain disorders through proper application and interpretation of the EEG. EEG, MRI and PET are important research tools for the diagnosis and prognosis of brain disorders and all have well-validated and routine use in hospitals. However, functional measurements of the brain using fMRI or clinical PET have failed to translate into the realm (Matthews, 2006 Bullmore, 2012). EEG, however, holds significant promise to bridge research applications with clinical measurements. With the addition of spectral analyses as common displays in the clinical setting, quantitative displays of the EEG are rapidly increasing in popularity, allowing physicians to better assess changes (Scheuer, 2002). Indeed, by using principled time-frequency spectral analysis methods, the dynamics of the EEG can be visualized easily, and allow for the characterization of timescales from a few seconds to full days of monitoring. Spectral measures may also provide unique insight into the mechanisms of neurological diseases. They provide a global summary of neurological activity, allowing for longitudinal observations of individual patients over long periods of time.

Study Limitations

Study 1: Long term sub-callosal deep brain stimulation.

In the first study, we track the electrophysiological effects of scDBS using spectral analysis methods. This is the first study which uses multitaper methods to calculate spectra from TRD patients undergoing scDBS. These methods have been found to produce more accurate estimates (Brown 2017). We found that alpha band asymmetry between left and right hemisphere, common in patients with severe depression, normalizes after deep brain stimulation. Such measures may be useful in assessing the efficacy of deep brain stimulation in patients ongoing the treatment before deciding to conduct further invasive surgery through re-implantation, or even in selecting patients with better odds for recovery. This study corroborates previous studies, such as Quraan et al, 2014, which showed that hemispheric power asymmetry was statistically different between responders and non-responders. However, the Quraan et al. study only used one channel for their measurements, which can be very limiting. Also, they did not collect baseline data from their patients and were therefore unable to confirm that the changes were only due to deep brain stimulation effects.

In order to better understand the mechanisms underlying the changes in spectral power, we hope to correlate our findings with other neuroimaging techniques in future studies. In particular, we will be using diffusion tensor imaging and computerized tomography to estimate the activation volume and particular white matter tracts activate in each specific patients studied (Riva-Posse et al, 2014). This would allow us to better understand the pathways stimulated by scDBS and their effect on treatment-resistant depression. Indeed, it has already been shown that nonresponders do not consistently show the same activation as responders. Correlation

of the activation of specific white matter tracts and EEG would give us insight into the biological changes occurring in patient responders who show optimal recovery. This is an important step, since scDBS is not always successful, and might require re-implantation or can even produce negative symptoms. Furthermore, any findings would provide insight into the biological understanding of the effects of deep brain stimulation on mechanisms underlying alpha oscillations in the brain, which are not yet fully understood (Leuchter et. al, 2015).

Study 2: Long term recovery of consciousness in minimally conscious state

In the second study, we investigated the brain mechanisms underlying recovery of communication in severely brain-injured patients who spontaneously recovered communication. We identified a common EEG signature of local and global brain network reorganization with an increase in theta coherence networks (regions across the brain that oscillate at similar frequencies), which arises coincident with recovery of spoken or gestural communication. These findings support a proposed mechanism of selective functional and structural reorganization of language networks associated with recovery of communication. Our findings may provide great value to the medical community – for the first time, physicians may be capable of following the covert recovery of capacity for communication after severe brain injury, allowing patients to reunite with the outside world. Graph theoretic approaches to study changes in coherence networks of patients with traumatic brain injury can also provide a powerful framework to study topological interactions between large numbers of nodes and understand the structure of such networks. They have been extensively used to study both structural and functional brain states (Bullmore & Sporns, Bassett et al), showing that changes in the topology of brain networks are markers of disease. However, the

added value of these topological inferences depends on the intrinsic meaning of the derived graph measures and whether the tools of graph theory present information above and beyond the traditional calculation of differences in inter-regional coherence. With respect to this question, our results are indeterminate. The main findings rest on differences in graph density which simply reflect the average coherence in the theta band. Graph theoretic density in this context is therefore an alternative way to reduce complex coherence connectivity data to a small number of parameters, but does not provide us with any further insight into the topology of the network. However, average coherence is still a meaningful measure which may be informative. Our study suggests that the increase in left hemispheric coherence networks might be linked to biological changes in myelination in the brain and indicative of strong functional and structural changes occurring over time in the injured brain.

In several individual instances, other graph theory measures showed significant changes in our patient subjects not present in longitudinally studied healthy controls. However, these changes were not consistent across patients with recovery of communication and those without. Coherence EEG measures are a very global measure, and as such might not be allow for more complex topological network results. However, future studies might find correlated network measures in other levels of scale. Graph theoretic measures can be translated into many levels of biological complexity in the brain, from cell to cell local networks to large scale network structural connections. Establishing the meaning of these graph changes seen would therefore require more examples to establish a robustness of findings and potential correlation with other measurements such as fMRI or DTI.

An important additional limitation of this work is the choice of the connectivity threshold and its effects on graph theoretic measures is still an ongoing question in the field (Bordier 2017). One solution is to fix the density of the graph

(Bassett et al, 2008, Lynall et al, 2010) and analyze only a stable threshold. Another solution utilizes bootstrap procedures to identify only the significant edges in the network (Kramer et al). Sparsification procedures have been applied to remove weaker links, which are often affected by noise (van den Heuvel and Fornito, 2014). Finally, ranges of densities can be explored to analyze only stable parameters. All of these methods have their limitations, but can be used depending on the hypothesis being explored. When we attempted to use a fixed the density threshold to study other graph theoretic measures such as clustering, path length, and small world, we do not see any consistent changes in patients who recover communication (see Chapter 4, Fig 3). While such measures have been observed in the context of brain injury (Chennu et al), they have only been used to differentiate between very different groups of patients, such as vegetative versus minimally conscious state. The fact that our patients are similar in state might explain the lack of differentiation in network topology.

We hope to continue to explore graph theoretic measures in traumatic brain injury. While we did not see any topological changes in coherence networks, other measures of connectivity might provide more insight. For example, weighted phase lag index measures ignore possible connections due to common sources in the EEG, and might therefore be a better candidate to study topological network changes. Percolation analysis (Bordier 2017) might provide a way to better select the optimal threshold to better study structural topology.

Other advances and future directions

There are some disadvantages to sole reliance on the average EEG spectra and coherence. These measures inherently rely on the stability of a brain state, which is known to fluctuate in disorders of consciousness (Schiff 2014). In both of our studies, we carefully select data from visually observed similar states. However, in some

patients, visual observation of state changes might not be informative due to the nature of the brain injury. In such cases, short term fluctuations in state might be averaged, and different approaches, such as the use of spectrograms and coherograms may be more appropriate in these scenarios (Prerau et al). We hope to therefore study fluctuations in state using spectrograms (Brown 2017).

One important application is using spectrograms to study the recovery of consciousness on zolpidem. Zolpidem produces paradoxical recovery of speech, cognitive and motor functions in select minimally conscious subjects. In 2013, Williams et al. demonstrated that 3 patients with different etiologies shared a common a spectral signature. This signature included an abnormal low frequency peak around ~7Hz, which disappeared ON zolpidem. They suggested that this might be a marker for deafferentation in brain injured patients. They also proposed that the increase in Beta oscillations suggest a similarity to paradoxical excitation in propofol, with both showing a release in thalamocortical outflow. Recovery here occurs over the timecourse of a few hours, therefore the state of consciousness of the patient is changing quickly. It would therefore be very informative to also characterize non-stationary dynamics during the observed state transitions.

Studies where large fluctuations in state can occur over short periods of time would greatly benefit from such approaches. In particular, we will be applying such methods to our drug studies and to sleep studies. Because spectrograms are not time averaged, they are more easily contaminated by noise, and can benefit from a robust spectral approach (Melman et al, 2015) to reduce artifact contamination. We can also use clustering and Markov chain modelling (Hudson et al, 2014) to study the transitions between states of consciousness during either sleep or recovery of consciousness on zolpidem. In our preliminary findings, we use adapted methods from Hudson et al, 2014. We analyze one bipolar channel (Fz-Cz) from two patients who

show recovery of consciousness after a dose of zolpidem. We then normalize the data by total power, and subtract the mean and generate robust spectrograms (Melman et al, 2015) and the average 30s of data for each time window. We reconstruct the data using the top 3 principal components, and use a cluster analysis (kmeans) on the reconstructed data. The states identified by the cluster analysis change in a way that corresponds to drug administration and behavior. (See Figures 5.1 and 5.2 for preliminary findings).

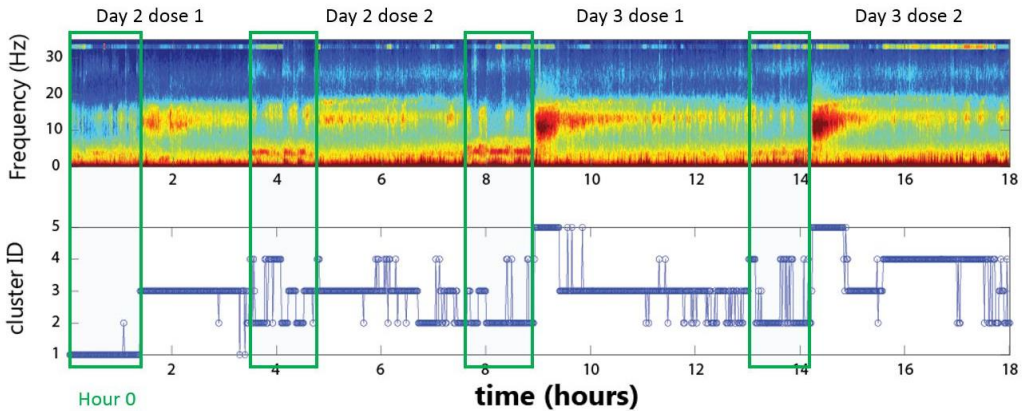

Figure 5.1 Time-resolved spectrograms of the EEG in a patient recovering consciousness on Zolpidem reveal discrete state transitions

Analysis of spectral power over the time course of Zolpidem doses. Each dose was of 10mg of Zolpidem, administered at different times of day (either morning, dose 1, or afternoon, dose 2). Green box highlights the baseline EEG, collected an hour prior to the Zolpidem administration.

A) Clean resting awake multitaper robust EEG spectrogram of bipolar channel Fz-Cz. Each time window represents a robust multitaper estimate generated from 30s of uncleaned data. Changes in low frequency bands and broad beta frequency changes are present when Zolpidem is administered
The optimal number of clusters will have the highest silhouette value, which is a measure of how well the data points belong to their clusters. Here the mean silhouette on all kmeans clusters was 5, implying that there were 5 distinct electrophysiological states.

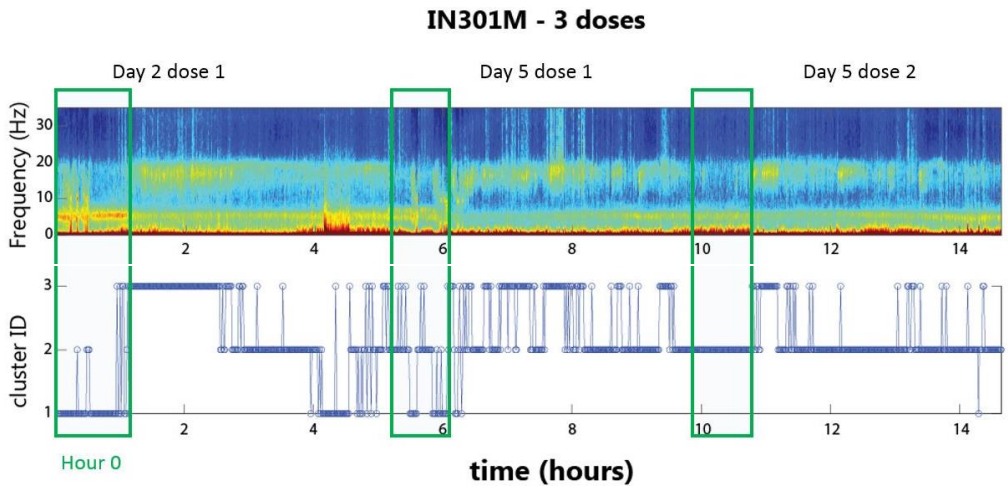

Figure 5.2 Time-resolved spectrograms of the EEG in a patient recovering consciousness on Zolpidem reveal discrete state transitions

Analysis of spectral power over the time course of Zolpidem doses. Each dose was of 10mg of Zolpidem, administered at different times of day (either morning, dose 1 or afternoon, dose 2). Green box highlights the baseline EEG, collected an hour prior to the Zolpidem administration.

A) Clean resting awake multitaper robust EEG spectrogram of bipolar channel Fz-Cz. Each time window represents a robust multitaper estimate generated from 30s of uncleaned data. Changes in low frequency bands and broad beta frequency changes are present when Zolpidem is administered
B) The optimal number of clusters will have the highest silhouette value, which is a measure of how well the data points belong to their clusters. Here the mean silhouette on all kmeans clusters was 3, implying that there were 3 distinct electrophysiological states.

Such an approach provides many exciting opportunities. For instance, our first finding indicates that the first baseline 'state' is only seen before the first dose of the study, and almost never reappears at any future dose. This is shown in both subjects studied. The first subject, who suffered a severe mixed traumatic and hypoxic-ischemic brain injury, demonstrated recovery of spoken language and accurate communication with first dose. The second subject suffered a traumatic injury due to a fall, and OFF zolpidem could stand, but showed no attempts at verbal communication. On zolpidem, this patient regains spoken language. Our preliminary results show that

the amount of time spent in the ‘awake state’ depends on the number of doses that day and in the previous day, implying that the effects of the drug are cumulative. This could provide potentially invaluable information on predicting the correct dosage for treating patients with zolpidem and a framework for the study of interaction of the change in state that outlast the pharmacologic effects of the drug.

These advances represent just the first wave of discoveries that the EEG may unlock. When combined, quantitative analyses of the EEG may provide a valuable tool for clinical diagnostics and have great potential to replace visual inspection. Given the advent of cheaper and more portable EEG devices, medical providers and patient families will soon be able to conduct personal monitoring at home and other non-clinical settings. Patients with disorders of consciousness could receive more regular analyses in their own homes, instead of their current state of neglect (Finns 2015) by a medical system which relies on infrequent, expensive, and inaccurate screenings in hospitals. The widespread proliferation of the EEG in combination with the novel methods described herein are essential for identifying and treating patients with brain disorders and will continue to save and improve lives.

BIBLIOGRAPHY

1. Achard, S. et al. (2006). A resilient, low-frequency, small-world human brain functional network with highly connected association cortical hubs. *Journal of Neuroscience*, *26*(1): 63-72.
2. Achard, S., & Bullmore, E. (2007). Efficiency and cost of economical brain functional networks. *PLoS computational biology*, *3*(2), e17.
3. Aftanas, L. I., Varlamov, A. A., Pavlov, S. V., Makhnev, V. P., & Reva, N. V. (2001). Affective picture processing: event-related synchronization within individually defined human theta band is modulated by valence dimension. *Neuroscience letters*, *303*(2), 115-118.
4. Allen, J.J.B., Urry, H.L., Hitt, S.K., & Coan, J.A. (2004). Stability of Resting Frontal EEG Asymmetry Across Different Clinical States of Depression. *Psychophysiology*, *41*(2), 269–280. doi: 10.1111/j.1469-8986.2003.00149.x.
5. Bandettini, P. A. (2009). What's new in neuroimaging methods*? Annals of the New York Academy of Sciences*, 1156(1), 260-293.
6. Bartley, A. J., Jones, D. W., & Weinberger, D. R. (1997). Genetic variability of human brain size and cortical gyral patterns. *Brain: a journal of neurology*, *120*(2), 257-269.
7. Bassett, D. S., & Bullmore, E. D. (2006). Small-world brain networks. *The neuroscientist*, *12*(6), 512-523.
8. Bassett, D. S., & Bullmore, E. T. (2016). Small-world brain networks revisited. *The Neuroscientist*, 1073858416667720.

9. Bassett, D.S., & Sporns, O. (2017). Network neuroscience. *Nature Neuroscience*, *20*(3), 353-364.
10. Braun, U., Plichta, M. M., Esslinger, C., Sauer, C., Haddad, L., Grimm, O., ... & Walter, H. (2012). Test–retest reliability of resting-state connectivity network characteristics using fMRI and graph theoretical measures. *Neuroimage*, *59*(2), 1404-1412.
11. Broadway, J.M. et al. (2012). Frontal theta cordance predicts 6-month antidepressant response to subcallosal cingulate deep brain stimulation for treatment-resistant depression: a pilot study. *Neuropsychopharmacology*, *37*(7), 1764–72.
12. Brovelli, A., Ding, M., Ledberg, A., Chen, Y., Nakamura, R., & Bressler, S. L. (2004). Beta oscillations in a large-scale sensorimotor cortical network: directional influences revealed by Granger causality. *Proceedings of the National Academy of Sciences of the United States of America*, *101*(26), 9849-9854.
13. Bullmore, E. (2012). The future of functional MRI in clinical medicine. *Neuroimage* 62, 1267–1271.
14. Bullmore, E., & Sporns, O. (2009). Complex brain networks: graph theoretical analysis of structural and functional systems. *Nature reviews. Neuroscience*, 10(3), 186.
15. Buzsáki, G., & Wang, X.J. (2012). Mechanisms of gamma oscillations. *Annual Review of Neuroscience*, *35*, 203-225.

16. Carmichael, S.T., & Chesselet, M.F. (2002). Synchronous neuronal activity is a signal for axonal sprouting after cortical lesions in the adult. *Journal of Neuroscience*, *22*(14), 6062-6070.
17. Chennu, S. et al. (2014) Spectral signatures of reorganised brain networks in disorders of consciousness. *PLoS Computational Biology*, *10*(10), e1003887. doi: 10.1371/journal.pcbi.1003887
18. Chennu, S. et al. (2017). Brain networks predict metabolism, diagnosis and prognosis at the bedside in disorders of consciousness. *Brain*. doi: 10.1093/brain/awx163
19. Chu, C.J. et al. (2012). Emergence of stable functional networks in long-term human electroencephalography. *Journal of Neuroscience*, *32*(8), 2703-2713. doi: 10.1523/JNEUROSCI.5669-11.2012
20. Chu, C.J. et al. (2015). EEG functional connectivity is partially predicted by underlying white matter connectivity. *Neuroimage*, *108*, 23-33. doi: 10.1016/j.neuroimage.2014.12.033
21. Cohen, M. X. (2014). *Analyzing neural time series data: theory and practice*. MIT Press.
22. Cohen, M.X. (2011). Error-related medial frontal theta activity predicts cingulate-related structural connectivity. *Neuroimage*, *55*(3), 1373-1383. doi: 10.1016/j.neuroimage.2010.12.072
23. Cohen, M.X. (2011). It's about Time. *Frontiers in Human Neuroscience*, *5*(2). doi: 10.3389/fnhum.2011.00002

24. Davidson, R.J. (1998). Anterior electrophysiological asymmetries, emotion, and depression: Conceptual and methodological conundrums. *Psychophysiology*, *35*(5), 607–614. doi: 10.1017/S0048577298000134.
25. Davidson, R.J. (2004). What does the prefrontal cortex "do" in affect: perspectives on frontal EEG asymmetry research? *Biol. Psych.*, *67*(1-2), 219–233.
26. de Vico, F.F. et al. (2009). Evaluation of the brain network organization from EEG signals: a preliminary evidence in stroke patient. *Anat Rec.*, *292*(12), 2023-2031. doi: 10.1002/ar.20965
27. Dennis, E. L., Jahanshad, N., Toga, A. W., McMahon, K. L., De Zubicaray, G. I., Martin, N. G., ... & Thompson, P. M. (2012, October). Test-retest reliability of graph theory measures of structural brain connectivity. In *International Conference on Medical Image Computing and Computer-Assisted Intervention* (pp. 305-312). Springer, Berlin, Heidelberg.
28. Deuker, L., Bullmore, E. T., Smith, M., Christensen, S., Nathan, P. J., Rockstroh, B., & Bassett, D. S. (2009). Reproducibility of graph metrics of human brain functional networks. *Neuroimage*, *47*(4), 1460-1468.
29. Erdös, P., & Rényi, A. (1959). On the central limit theorem for samples from a finite population. *Publ. Math. Inst. Hungar. Acad. Sci*, *4*, 49-61.
30. Fins, J.J. (2015). *Rights Come to Mind: Brain Injury, Ethics, and the Struggle for Consciousness*. New York, NY: Cambridge University Press.

31. Florian, G., & Pfurtscheller, G. (1995). Dynamic spectral analysis of event-related EEG data. *Electroencephalography and clinical neurophysiology*, *95*(5), 393-396.
32. Florin, A., & da Silva, F. L. (2010). Celluluar substrates of brain rhythms. *Schomer, DL, da Silva Fernando L. Niedermeyer's electroencephalography: basic principles, clinical applications, and related fields 6th edn*, 33-63.
33. Fridman, E.A., & Schiff, N.D. (2014). Neuromodulation of the conscious state following severe brain injuries. *Current Opinion in Neurobiology*, *29*, 172-177. doi: 10.1016/j.conb.2014.09.008
34. Friston, K. J., Harrison, L., & Penny, W. (2003). Dynamic causal modelling. *Neuroimage*, *19*(4), 1273-1302.
35. Gasser, T., Bächer, P., & Steinberg, H. (1985). Test-retest reliability of spectral parameters of the EEG. *Electroencephalography and clinical neurophysiology*, *60*(4), 312-319.
36. Giacino, J.T. et al. (2012). Placebo-controlled trial of amantadine for severe traumatic brain injury. *New England Journal of Medicine*, *366*(9), 819-826. doi: 10.1056/NEJMoa1102609
37. Ginestet, C. E., Nichols, T. E., Bullmore, E. T., & Simmons, A. (2011). Brain network analysis: separating cost from topology using cost-integration. *PloS one*, *6*(7), e21570.
38. Goldfine, A.M., Victor, J.D., Conte, M.M., Bardin, J.C., & Schiff, N.D. (2011). Determination of awareness in patients with severe brain injury using

EEG power spectral analysis. *Clinical Neurophysiology*, *122*(11), 2157-2168. doi: 10.1016/j.clinph.2011.03.022

39. Gong, G., Rosa-Neto, P., Carbonell, F., Chen, Z. J., He, Y., & Evans, A. C. (2009). Age-and gender-related differences in the cortical anatomical network. *Journal of Neuroscience*, *29*(50), 15684-15693.
40. Gotman, J. (1981). Interhemispheric relations during bilateral spike-and-wave activity. Epilepsia, 22(4), 453-466.
41. Hamilton, R.H., Chrysikou, E.G., & Coslett, B. (2011). Mechanisms of aphasia recovery after stroke and the role of noninvasive brain stimulation. *Brain and Language*, *118*(1-2), 40-50. doi: 10.1016/j.bandl.2011.02.005
42. Hardmeier, M. et al. (2014). Reproducibility of functional connectivity and graph measures based on the phase lag index (PLI) and weighted phase lag index (wPLI) derived from high resolution EEG. *PloS One*, *9*(10), e108648. doi: 10.1371/journal.pone.0108648
43. Hjorth, B. (1975). An on-line transformation of EEG scalp potentials into orthogonal source derivations. *Electroenceph. Clin. Neurophysiol.*, *39*(5), 526-530.
44. Holtzheimer, P.E. et al. (2012). Subcallosal cingulate deep brain stimulation for treatment-resistant unipolar and bipolar depression. *Arch Gen Psychiatry*, *69*(2),150-158. doi:10.1001/archgenpsychiatry.2011.1456
45. Huttenlocher, P.R. (1990). Morphometric study of human cerebral cortex development. *Neuropsychologia*, *28*(6), 517-527.

46. Jasper, HH. (1958). The ten-twenty electrode system of the International Federation. Electroencephalogr. *Clin. Neurophysiol*. 10: 371-375.

47. Jensen, O., & Colgin, L.L. (2007). Cross-frequency coupling between neuronal oscillations. *Trends Cogn. Sci.*, *11*(7), 267–269. doi: http://dx.doi.org/10.1016/j.tics.2007.05.003

48. Kalmar, K., & Giacino, J. T. (2005). The JFK coma recovery scale—revised. *Neuropsychological rehabilitation*, *15*(3-4), 454-460.

49. Kaplan, A. Y., Fingelkurts, A. A., Fingelkurts, A. A., Borisov, S. V., & Darkhovsky, B. S. (2005). Nonstationary nature of the brain activity as revealed by EEG/MEG: methodological, practical and conceptual challenges. *Signal processing*, *85*(11), 2190-2212.

50. Kaplan, P. W., & Lesser, R. P. (1990). *Long-term monitoring. Current practice of clinical electroencephalography*, 2, 513-534.

51. Karbe, H. et al. (1998). Brain plasticity in poststroke aphasia: what is the contribution of the right hemisphere?. *Brain and Language*, *64*(2), 215-230.

52. Kessler, R.C., Chiu, W.T., Demler, O., & Walters, E.E. (2005). Prevalence, Severity, and Comorbidity of Twelve-month DSM-IV Disorders in the National Comorbidity Survey Replication (NCS-R). *Archives of General Psychiatry*, *62*(6), 617-27. doi: 10.1001/archpsyc.62.6.617

53. King, J. R., Sitt, J. D., Faugeras, F., Rohaut, B., El Karoui, I., Cohen, L., ... & Dehaene, S. (2013). Information sharing in the brain indexes consciousness in noncommunicative patients. *Current Biology*, *23*(19), 1914-1919.

54. Konig, P., Engel, A. K., Roelfsema, P. R., & Singer, W. (1995). How precise is neuronal synchronization? *Neural Comput.*, *7*(3), 469–485.

55. Kramer, M.A., et al. (2010). Coalescence and fragmentation of cortical networks during focal seizures. *Journal of Neuroscience, 30*(30), 10076-10085. doi: 10.1523/JNEUROSCI.6309-09.2010

56. Lee, H., Mashour, G.A., Noh, G.J., Kim, S., & Lee, U. (2013). Reconfiguration of network hub structure after propofol-induced unconsciousness. *Anesthesiology, 119*(6), 1347-1359. doi: 10.1097/ALN.0b013e3182a8ec8c

57. MacKay, D.G. (1992). *Constraints on theories of inner speech*. Hillsdale, NJ: Lawrence Erlbaum Associates, Inc. 121–149.

58. Maletic, V., Robinson, M., Oakes, T., Iyengar, S., Ball, S. G., & Russell, J. (2007). Neurobiology of depression: an integrated view of key findings. *International Journal of Clinical Practice, 61*(12), 2030–2040. http://doi.org/10.1111/j.1742-1241.2007.01602.x

59. Mani, N., & Plunkett, K. (2010). In the infant's mind's ear: evidence for implicit naming in 18-month-olds. *Psychological Science, 21*(7), 908-913. doi: 10.1177/0956797610373371

60. Marvel, C.L., & Desmond, J.E. (2012). From storage to manipulation: how the neural correlates of verbal working memory reflect varying demands on inner speech. *Brain and Language, 120*, 42-51.

61. Matlis, S., Boric, K., Chu, C.J., & Kramer, M.A. (2015). Robust disruptions in electroencephalogram cortical oscillations and large-scale functional networks in autism. *BMC Neurology*, *15*, 97. doi: 10.1186/s12883-015-0355-8

62. Matthews, P. M., Honey, G. D., and Bullmore, E. T. (2006). Applications of fMRI in translational medicine and clinical practice. Nat. Rev. Neurosci. 7, 732–44.

63. Mayberg, H.S. (1997). Limbic-cortical dysregulation: a proposed model of depression. *J Neuropsychiatry*, *9*(3), 471–481.

64. Mayberg, H.S. (2009). Targeted electrode-based modulation of neural circuits for depression. *Journal of Clinical Investigation*, *119*(4), 717–725. doi: 10.1172/JCI38454

65. Mayberg, H.S. et. al. (2005). Deep brain stimulation for treatment-resistant depression. *Neuron*, *45*(5), 651–660.

66. Mitra, P., & Bokil, H. (2007). *Observed brain dynamics* Oxford University Press.

67. Montgomery, A.A., Graham, A., Evans, P.H., & Fahey, T. (2002). Inter-rater agreement in the scoring of abstracts submitted to a primary care research conference. *BMC Health Services Research*, *2*(1), 8. 10.1186/1472-6963-2-8

68. Nicolo, P., Rizk, S., Magnin, C., Pietro, M.D., Schnider, A., & Guggisberg, A.G. (2015). Coherent neural oscillations predict future motor and language improvement after stroke. *Brain*, *138*(Pt 10), 3048-3060. doi: 10.1093/brain/awv200

69. Nicolo, P., Rizk, S., Magnin, C., Pietro, M.D., Schnider, A., & Guggisberg, A.G. (2015). Coherent neural oscillations predict future motor and language improvement after stroke. *Brain, 138*(Pt 10), 3048-3060. doi: 10.1093/brain/awv200

70. Niedermeyer, E., & da Silva, F. L. (Eds.). (2005). *Electroencephalography: basic principles, clinical applications, and related fields*. Lippincott Williams & Wilkins.

71. Nunez, P.L., & Pilgreen, K.L. (1991). The spline-Laplacian in clinical neurophysiology: a method to improve EEG spatial resolution. *Journal of Clinical Neurophysiology*, *8*(4), 397-413.

72. Nunez, P.L., & Srinivasan, R. (2006). *Electric Fields of the Brain: The Neurophysics of EEG*. Oxford University Press, USA.

73. Nunez, P.L., et al. (1997). EEG coherency: I: statistics, reference electrode, volume conduction, Laplacians, cortical imaging, and interpretation at multiple scales. *Electroencephalography and Clinical Neurophysiology*, *103*(5), 499-515.

74. Oken, B. S., & Chiappa, K. H. (1988). Short-term variability in EEG frequency analysis. *Electroencephalography and clinical Neurophysiology*, *69*(3), 191-198.

75. Özdemir, E., Norton, A., & Schlaug, G. (2006). Shared and distinct neural correlates of singing and speaking. *Neuroimage*, *33*(2), 628-635.

76. Perrone-Bertolotti, M., Rapin, L., Lachaux, J.P., Baciu, M., & Loevenbruck, H. (2014). What is that little voice inside my head? Inner speech phenomenology,

its role in cognitive performance, and its relation to self-monitoring. *Behavioural Brain Research*, *261*, 220-239. doi: 10.1016/j.bbr.2013.12.034

77. Pfurtscheller, G. (2008). 8. EEG (de) synchronisation during covert and overt movement. *Clinical Neurophysiology*, *119*(9), e101.
78. Prerau,M., Brown,E.,Bianchi, M., , Ellenbogen,J., Purdon,P., Sleep Neurophysiological Dynamics Through the Lens of Multitaper Spectral Analysis, *Physiology* 32(1),, 60-92 DOI: 10.1152/physiol.00062.2015
79. Quraan, M. A., Protzner, A. B., Daskalakis, Z. J., Giacobbe, P., Tang, C. W., Kennedy, S. H., ... & McAndrews, M. P. (2014). EEG power asymmetry and functional connectivity as a marker of treatment effectiveness in DBS surgery for depression. Neuropsychopharmacology, 39(5), 1270.
80. Quenouille, M. H. (1949). Approximate tests of correlation in time-series. *Journal of the Royal Statistical Society. Series B (Methodological)*, *11*(1), 68-84.
81. Rajagovindan, R., & Ding, M. (2008). Decomposing neural synchrony: toward an explanation for near-zero phase-lag in cortical oscillatory networks. *PLoS One*, *3*(11), e3649. doi: 10.1371/journal.pone.0003649
82. Rampil, I. J. (1998). A primer for EEG signal processing in anesthesia. *Anesthesiology: The Journal of the American Society of Anesthesiologists*, *89*(4), 980-1002.

83. Rijntjes, M. (2006). Mechanisms of recovery in stroke patients with hemiparesis or aphasia: new insights, old questions and the meaning of therapies. *Current Opinion in Neurology*, *19*(1), 76-83.

84. Riva-Posse, P. et al. (2014). Defining critical white matter pathways mediating successful subcallosal cingulate deep brain stimulation for treatment-resistant depression. *Biological Psychiatry*, *76*(12), 963-969. doi: 10.1016/j.biopsych.2014.03.029

85. Rutter, L., Nadar, S. R., Holroyd, T., Carver, F. W., Apud, J., Weinberger, D. R., & Coppola, R. (2013). Graph theoretical analysis of resting magnetoencephalographic functional connectivity networks. *Frontiers in computational neuroscience*, *7*.

86. Salinsky, M. C., Oken, B. S., & Morehead, L. (1991). Test-retest reliability in EEG frequency analysis. *Electroencephalography and clinical neurophysiology*, *79*(5), 382-392.

87. Salvador, R., Suckling, J., Coleman, M. R., Pickard, J. D., Menon, D., & Bullmore, E. D. (2005). Neurophysiological architecture of functional magnetic resonance images of human brain. *Cerebral cortex*, 15(9), 1332-1342.

88. Schiff, N. D. (2015). Cognitive motor dissociation following severe brain injuries. JAMA neurology, 72(12), 1413-1415.

89. Schiff, N. D., Nauvel, T., & Victor, J. D. (2014). Large-scale brain dynamics in disorders of consciousness. Current opinion in neurobiology, 25, 7-14.

90. Schiff, N.D., et al. (2007). Behavioural improvements with thalamic stimulation after severe traumatic brain injury. *Nature*, *448*(7153), 600-603.

91. Schlaug, G., Marchina, S., & Norton, A. (2009). Evidence for plasticity in white-matter tracts of patients with chronic Broca's aphasia undergoing intense intonation-based speech therapy. *Annals of the New York Academy of Sciences*, *1169*, 385-394. doi: 10.1111/j.1749-6632.2009.04587.x

92. Shah, S.A., & Schiff, N.D. (2010). Central thalamic deep brain stimulation for cognitive neuromodulation–a review of proposed mechanisms and investigational studies. *European Journal of Neuroscience*, *32*(7), 1135-1144. doi: 10.1111/j.1460-9568.2010.07420.x

93. Sitt, J.D. et al. (2014). Large scale screening of neural signatures of consciousness in patients in a vegetative or minimally conscious state. *Brain*, *137*(Pt 8), 2258-2270. doi: 10.1093/brain/awu141

94. Smith, S.M., Brown, H.O., Toman, J.E.P., & Goodman, L.S. (1947). The lack of cerebral effects of d-tubocurarine. *Journal of the American Society of Anesthesiologists*, *8*(1), 1-14.

95. Sporns, O., & Zwi, J. D. (2004). The small world of the cerebral cortex. *Neuroinformatics*, *2*(2), 145-162.

96. Stam, C. J., & Van Dijk, B. W. (2002). Synchronization likelihood: an unbiased measure of generalized synchronization in multivariate data sets. Physica D: Nonlinear Phenomena, 163(3), 236-251.

97. Stam, C. J., Nolte, G., & Daffertshofer, A. (2007). Phase lag index: assessment of functional connectivity from multi channel EEG and MEG with diminished bias from common sources. *Human brain mapping*, *28*(11), 1178-1193.

98. Stam, C.J., & van Straaten, E.C. (2012). The organization of physiological brain networks. *Clinical Neurophysiology*, *123*(6), 1067-1087. doi: 10.1016/j.clinph.2012.01.011

99. Steriade, M., Gloor, P. L. R. R., Llinas, R. R., Da Silva, F. L., & Mesulam, M. M. (1990). *Basic mechanisms of cerebral rhythmic activities. Electroencephalography and clinical neurophysiology*, 76(6), 481-508.

100. Telesford, Q.K. et al. (2010). Reproducibility of graph metrics in fMRI networks. *Frontiers in Neuroinformatics*, *4*, 117. doi: 10.3389/fninf.2010.00117

101. Telesford, Q.K., Burdette, J.H., & Laurienti, P.J. (2013). An exploration of graph metric reproducibility in complex brain networks. *Frontiers in Neuroscience*, *7*, 67. doi: 10.3389/fnins.2013.00067

102. Thengone, D.J., Voss, H.U., Fridman, E.A., & Schiff, N.D. (2016). Local changes in network structure contribute to late communication recovery after severe brain injury. Science Translational Medicine, *8*(368), 368re5.

103. Toga, A. W. and Mazziotta, J. C. *Brain Mapping. The methods*. Academic Press, San Diego, 1996

104. Tomassy, G.S., Dershowitz, L.B., & Arlotta, P. (2016). Diversity Matters: A Revised Guide to Myelination. *Trends in Cell Biology*, *26*(2), 135-147. doi: 10.1016/j.tcb.2015.09.002

105. Tononi, G., & Sporns, O. (2003). Measuring information integration. *BMC neuroscience*, *4*(1), 31.

106. Uhlhaas, P.J., Roux, F., Singer, W., Haenschel, C., Sireteanu, R., & Rodriguez, E. (2009). The development of neural synchrony reflects late maturation and restructuring of functional networks in humans. *Proceedings of the National Academy of Sciences*, *106*(24), 9866-9871. doi: 10.1073/pnas.0900390106

107. Vaessen, M. J., Hofman, P. A. M., Tijssen, H. N., Aldenkamp, A. P., Jansen, J. F., & Backes, W. H. (2010). The effect and reproducibility of different clinical DTI gradient sets on small world brain connectivity measures. *Neuroimage*, *51*(3), 1106-1116.

108. Vicente, R., Gollo, L.L., Mirasso, C.R., Fischer, I., & Pipa, G. (2008). Dynamical relaying can yield zero time lag neuronal synchrony despite long conduction delays. *ceedings of the National Academy of Sciences*, *105*(44), 17157–17162. doi: 10.1073/pnas.0809353105

109. von Stein, A., Rappelsberger, P., Sarnthein, J., & Petsche, H. (1999). Synchronization between temporal and parietal cortex during multimodal object processing in man. *Cerebral Cortex*, *9*(2), 137-150.

110. Voss, H.U. et al. (2006). Possible axonal regrowth in late recovery from the minimally conscious state. *Journal of Clinical Investigation*, *116*(7), 2005-2011.

111. Weiss, S., & Mueller, H. M. (2003). The contribution of EEG coherence to the investigation of language. *Brain and language*, *85*(2), 325-343.

112. Whyte, J. et al. (2014). Zolpidem and restoration of consciousness. *Am J Phys Med Rehabil*, *93*(2), 101-113. doi: 10.1097/PHM.0000000000000069

113. Williams, S.T. et al. (2013). Common resting brain dynamics indicate a possible mechanism underlying zolpidem response in severe brain injury. *Elife*, *2*, e01157. doi: 10.7554/eLife.01157

114. Winter, W. R., Nunez, P. L., Ding, J., & Srinivasan, R. (2007). Comparison of the effect of volume conduction on EEG coherence with the effect of field spread on MEG coherence. *Statistics in medicine*, *26*(21), 3946-3957.

115. Wittchen H. U., Jacobi, F., Rehm, J., Gustavsson, a, Svensson, M., Jönsson, B., Olesen, J.,Allgulander, C., Alonso, J., Faravelli, C., et al. (2011). The size and burden of mental disorders and other disorders of the brain in Europe 2010. *Eur. Neuropsychopharmacol.*21, 655–79.